TECHNISCHE UNIVERSITÄT MÜNCHEN
TUM School of Life Sciences

Physiological and biochemical characterization of a novel insulin-inhibitory receptor in pancreatic β-cells

Fataneh Fathi Far

Vollständiger Abdruck der von der TUM School of Life Sciences der Technischen Universität München zur Erlangung des akademischen Grades einer

Doktorin der Naturwissenschaften

genehmigten Dissertation.

Vorsitz: apl. Prof. Dr. Ralph Kühn

Prüfer*innen der Dissertation:

1. apl. Prof. Dr. Michael W. Pfaffl
2. Prof. Dr. Heiko Lickert

Die Dissertation wurde am 09.09.2022 bei der Technischen Universität München eingereicht und durch die TUM School of Life Sciences am 21.03.2023 angenommen.

Contents

1 List of abbreviations 1
2 Abstract 5
3 Introduction 6
3.1 Diabetes Mellitus 6
3.1.1 Diabetes treatment 6
3.2 The pancreas is an exo-endocrine gland 7
3.3 Development of the pancreas 8
3.3.1 Islet formation 9
3.3.2 Functionality of pancreatic β-cell 10
3.4 Insulin biosynthesis 10
3.4.1 Insulin secretion 11
3.5 Insulin-like growth factor receptor I (IGF-IR) and insulin receptor (IR) signaling 12
3.5.1 The structure of IR, IGF-IR and IGF-IIR and their ligands 13
3.5.2 Signal transduction and function of IR, IGF-IR and IGF-IIR 14
3.5.3 Intracellular Trafficking of Receptor Tyrosine Kinases 16
3.6 Autocrine insulin signaling in pancreatic β-cells 17
3.6.1 Distinct roles of IR and IGF-IR in β-cells 17
3.6.2 The role of PI3K/AKT pathway in β-cell proliferation 18
3.7 Identification and characterization of the insulin-inhibitory receptor (IIR, Inceptor) 19
3.7.1 The Inceptor protein 20
3.8 Aim of the thesis 22
4 Result 23
4.1 Characterization of a novel modulator of the IR/IGF-IR signaling system *in vivo* 23
4.1.1 mRNA expression of *Iir* in *Mus musculus* during development 23
4.1.2 Characterization of inceptor antibodies 24
4.1.3 Generation of $Iir^{-/-}$ full-body KO (ΔEx3) mouse line 32
4.1.4 Gene functional analysis of the insulin inhibitory receptor *in vivo* 35
4.1.5 Analysis of postnatal death of $Iir^{-/-}$ mice 38
4.1.6 Generation of conditional β-cell specific KO (MIP-CreERT; $Iir^{flox/FD}$) mouse line 51
4.1.7 *In vivo* characterization of conditional β-cell specific CKO (MIP-CreERT; $Iir^{flox/FD}$) mouse line 52
4.1.8 Analysis of inceptor in diabetes mellitus 63
5 Discussion 65
5.1 The biological function of inceptor 65

Contents

5.2 Analysis of inceptor function by whole body knock-out 65
5.3 Analysis of inceptor function in insulin producing β-cells 67
5.3.1 Inceptor controls glycemia 68
5.3.2 Inceptor regulates β-cell proliferation 70
5.3.3 Mechanism of action 73
5.4 Function of inceptor in T2D 74
6 Material and methods 76
6.1 Material 76
6.1.1 Equipment 76
6.1.2 Consumables 78
6.1.3 Kits and Mastermix 79
6.1.4 Chemicals 80
6.1.5 Buffers and solutions 82
6.1.6 Enzymes, inhibitors and growth factors 84
6.1.7 Antibodies 84
6.1.8 Mouse lines 86
6.1.9 Primers 86
6.2 Methods 87
6.2.1 General mouse handling 87
6.2.2 Genotyping 87
6.2.3 Analysis of new born mice 88
6.2.4 *in vivo* analysis of adult mice 90
6.2.5 immunohistochemistry and histology 91
6.2.6 Protein biochemistry 93
6.2.7 RNA biochemistry 95
6.2.8 Statistics 96
7 List of figures and tables 97
7.1 Figures 97
7.2 Tables 98
8 References 99
9 Acknowledgments 116
10 List of Publications 117
11 Contributions 118

1 List of abbreviations

5330417C22Rik	KIAA1324, EIG121, Iir
AC-LL	acidic-cluster-dileucine
ADP	Adenosine diphosphate
Adrb2	Beta-2 adrenergic receptor
Agr2	Anterior gradient protein 2 homolog
AgRP	Agouti-related protein
AKT(PKB)	protein kinase B
ANOVA	Analysis of variance
AP1	adaptor protein 1
Ap2	adaptor protein 2
Arx	Aristaless related homeobox
AS160	Akt substrate of 160 kDa
ATF	Activating transcription factors
ATP	Adenosine triphosphate
AUC	Area under the curve
Bmi-1	Polycomb complex protein BMI-1
CAMPS	cAMP-binding protein
Ccl2	Chemokine (C-C motif) ligand 2
CCPs	clathrin-coated pits
CCVs	clathrin-coated vesicles
CD	cation-dependent
CDK	Cyclin-dependent kinases
Cdx2/3	Homeobox protein CDX-2/3
ChgA	chromogranin A
CI	cation-independent
CIE	clathrin-independent endocytosis
CKO	β-cell specific KO (MIP-CreERT+; Iir fl/FD)
CME	clathrin-mediated endocytosis
CRE	Cyclic AMP response element
CREB	cAMP response element binding protein
DAB	3,3′-Diaminobenzidin
DAG	diacylglycerol
DHAP	dihydroxyacetone phosphate
E + no.	Embryonic stage
EdU	Desoxyribonucleotid Ethyl-Uridine
EE	early endosomes
eIF2a	eukaryotic initiation factor2a
Eif2ak3	Eukaryotic translation initiation factor 2-alpha kinase 3

List of abbreviations

EIG121	oestrogen-induced gene 121
ELAPOR1	endosome/lysosome-associated apoptosis and autophagy regulator 1
ELISA	Enzyme-linked immunosorbent assay
ELK1	ETS transcription factor
ER	endoplasmic reticulum
Erbb3	Receptor tyrosine-protein kinase erbB-3
ESC	Embryonic stem cell
Ezh2	Enhancer of zeste homolog 2
FC	Fold change
FD	Flox deleted
Fl	Flox
Foxa1	Forkhead box protein A1
Foxa2	Forkhead box protein A2
FoxM1	Forkhead box protein M1
Foxo1	Forkhead box protein O1
FVF	Foxa2-Venus fusion
G + no.	Gestational stage
G6P	glucose -6-phosphate
GAPDH	Glyceraldehyde 3-phosphate dehydrogenase
Gcg	Glucagon
GCG	glucokinase
GFP	Green fluorescent protein
Gli3	Zinc finger protein GLI3
Glut2	Glucose transporter 2
Glut4	Glucose transporter 4
Gly3P	glycerol-3-phosphate
Grb2	Growth factor receptor-bound protein 2
GSIS	glucose stimulated insulin secretion
GSK3	glycogen synthase kinase 3
GT	Gene trap
GTP	nucleotide guanosine triphosphate
H	Hour
H&E stain	Hematoxylin and eosin stain
hbAP	Human beta act promotor
Hes1	hairy and enhancer of split-1
HFD	High-fat diet
HSP90	heat shock protein 90
IGF	insulin-like growth factor
IGFBP	insulin-like growth factor-binding protein
IGF-I	insulin-like growth factor I
IGF-II	insulin-like growth factor II
IGF-IIR	insulin-like growth factor II receptor

IGF-IR	insulin-like growth factor I receptor
IGFR	insulin-like growth factor receptor
IHC	immunohistochemistry
Ins	Insulin
Ins	Insulin
ipGSIS	in vivo intraperitoneal glucose stimulated insulin secretion
ipGTT	intraperitoneal glucose tolerance test
IR	insulin receptor
IR-A	insulin receptor type A
IR-B	insulin receptor type B
IRES	Internal ribosome entry-site
IRS	insulin receptor substrate
IRS-1	insulin receptor substrate 1
IRS-2	insulin receptor substrate 2
ITT	insulin tolerance test
KATP channels	ATP-sensitive potassium channels
Klk1b	Kallikrein 1-related peptidase b
KO	knock-out
LE	late endosomes
LRH-1	liver receptor homolog-1
M6P/IGF-IIR	mannose 6-phosphate/ insulin-like growth factor II receptor
MAPK	RAS-mitogen-activated protein kinase
MEK	Mitogen-activated protein kinase kinase
MODY	Maturity onset of diabetes of the young
MPCs	progenitor cells
mRNA	messenger ribonucleic acid
mTOR	mechanistic target of rapamycin
MVBs	multivesicular bodies
MyoD	myoblast determination protein
NAD	Nicotinamide adenine dinucleotide
NeuroD1	Neurogenic differentiation 1
Ngn3	Neurogenin3
Nkx6.1	Nk6 homeobox 1
Nkx6.2	Nk6 homeobox 2
NPY	Neuropeptide Y
NR5A2	nuclear receptor subfamily 5, group A, member 2
P + no.	Postnatal day
PACS-1	Phosphofurin acidic cluster sorting protein 1
PAS	periodic acid-schift reaction
Pax4	Paired box gene 4
Pax6	Paired box gene 6
Pb	Base pare

List of abbreviations

PCA	Principal component analysis
PCR	Polymerase chain reaction
Pcsk1/3	Proprotein convertase 1
Pdx1	pancreatic and duodenal homeobox 1
Pepck	Phosphoenolpyruvate carboxykinase
PI3K	phosphatidylinositol 3-kinase
PIP3	phosphatidylinositol-3,4,5-triphosphate
POMC	Pro-opiomelanocortin
PP	pancreatic polypeptide
Prox1	Prospero homeobox protein 1
Ptf1a	Pancreas transcription factor 1 subunit alpha
Rab9	Ras-related protein Rab 9
Rbp-j1	Recombination signal binding protein for immunoglobulin kappa J region1
RE	recycling endosomes
Rfx6	Regulatory factor X, 6
RTK	Receptor tyrosine kinase
RT-qPCR	Real Time Quantitative PCR
s.e.m.	Standard error of the mean
SDS-PAGE	sodium dodecyl sulphate–polyacrylamide gel electrophoresis
SE	sorting endosomes
Shc	src-homology domain containing proteins
SNAP-25	Synaptosomal-Associated Protein, 25kDa
SRP	cytosolic ribonucleoprotein signal recognition particles
βIGF-IR	β-cell-specific KO of IGF-IR
βIRKO	β-cell-specific KO of IR
Sst	Somatostatin
T1D	Type 1 diabetes
T2D	Type 2 diabetes
Tcf2	transcription factor 2
TGN	trans-Golgi network
TIP47	Mannose-6-phosphate receptor binding protein 1
Ucn3	Urocortin-3
VAMP-2	Vesicle-associated membrane protein 2
WB	Western Blot
WT	wildtype
ΔEx3	delta exon

2 Abstract

In the past two decades, it has become more apparent that dysfunction or failure of the pancreatic β-cell is an essential defect in the pathogenesis of type 2 diabetes. Intensive efforts have been aimed at finding strategies to restore β-cell mass to provide better glycemic control and to slow diabetes progression. Identifying novel molecules important for β-cell regeneration and/or function is essential to identify molecular pathways that can be used for anti-diabetic drug targets.

Pancreatic β-cells express insulin receptors that are exposed to the highest amounts of insulin concentration. Insulin (INS)/ Insulin-like growth factor (IGF) signaling is known to be essential for all β-cell function, including β-cell survival and compensatory proliferation; thus, is a promising target for diabetes therapy. We identified a novel insulin inhibitory receptor (IIR, inceptor), that counter regulates INS/IGF signalling in pancreatic β-cells.

In the first part of the study, we demonstrated that inceptor is expressed in insulin-producing β-cells and regulates insulin receptor (IR) and IGF1 receptor (IGF-1R) desensitization. Additionally, we proposed a role of inceptor as a target to promote β-cell function. Molecular and cellular analyses of embryonic and postnatal pancreases from *Iir*$^{-/-}$ showed an increase in the activation of IR/IGF1-R and increased proliferation of β-cells. Further, we demonstrated, that the *Iir*$^{-/-}$ newborn pups die due to hypoglycemia due to hyperinsulinemia.

IR and IGF-1R are major regulators of growth and metabolism. In the second part of this study, we started to unravel the involvement of inceptor in regulating metabolism and proliferation of the endocrine pancreas via the INS/IGF1 pathway. Tissue-specific and conditional knock-out (CKO) of inceptor in β-cells displayed improved glucose tolerance and increased first-phase insulin secretion. Moreover, the CKO mice of the inceptor led to an increase of the INS/IGF-1 signaling pathway resulting in increased β-cell proliferation and mass. Overall, based on these results, we propose inceptor as a negative regulator of IR/IGF-1R signalling that prevents constitutive insulin pathway activation in pancreatic β-cells.

In summary, the physiological function of inceptor is likely to shield the pancreas at the source of the ligand from overactivation of the INS/IGF1 pathway. Taken together, the identification of inceptor as a target to increase β-cell function and proliferation may have important implications in the field of β-cell regeneration therapies.

3 Introduction

3.1 Diabetes Mellitus

According to the International Diabetes Federation, more than 463 million people worldwide were diagnosed with diabetes in 2019, and this number is expected to increase to 700 million in the next three decades.

Patients with diabetes mellitus fail to maintain blood glucose homeostasis resulting in hyperglycemia (Alberti and Zimmet, 1998). Several types of diabetes have been described and characterized by the pathology and etiology. Type 1 diabetes (T1D) is caused by autoimmune destruction of pancreatic β-cells by cytotoxic T-cells like CD8+ (Pan and Wright, 2011). Type 2 diabetes (T2D), which is the most common form, is often a consequence of modern life style, in particular obesity, which triggers insulin resistance. Chronic insulin resistance leads to β-cell compensation, but eventually β-cells fail and the gradual loss leads to insulin deficiency causing diabetes (Kahn et al., 2006). In case of impaired glucose tolerance, T2D progresses as β-cells are unable to secrete enough insulin to overcome insulin resistance (Kahn et al., 2008; Reaven, 1988). Overweight, obesity, reduced secretion of the incretin glucagon-like peptide (GLP-1), hyperglucagonemia and increased concentration of other counter-regulatory hormones are main contributors to insulin resistance and reduced insulin secretion (Burcelin et al., 2008; Cooper and Stewart, 2009; Drucker and Nauck, 2006; Mulder and Ling, 2009).

Gestational diabetes is developed during pregnancy by some woman due to an inappropriate response to the metabolic demands (Klara Feldman et al., 2016) and it is mostly reverted after birth. However, the mother and the children show an increased risk for T2D during their later life (Dabelea, 2007; Damm, 2009; Petitt et al., 1985). Another form of diabetes is maturity-onset diabetes of the young (MODY) which is a monogenetic disease caused by mutations in genes involved in β-cell development, glucose sensing and insulin secretion. Several MODY genes, including hepatocyte nuclear factor 1, 1β or 4α, glucokinase, pancreatic duodenal homeobox 1 (PDX1) and insulin, have already been identified (Anik et al., 2015; Reis et al., 2000; Weng et al., 2001).

3.1.1 Diabetes treatment

The discovery of insulin 100 years ago improved the care of T1D patients and enabled children with diabetes to survive. Although several studies showed that girls live 18 years and boys 11-12 years shorter when diagnosed with T1D, most of the patients with T1D who get insulin therapy and are in good glycemic control can expect a lifespan comparable to general population. Since in 70-90% of T1D cases, β-cells are destroyed, insulin injection is necessary to replace the β-cell function and to maintain blood sugar in a normal range.

In contrast to T1D, the variable and progressive pathophysiological changes associated with T2D require different pharmacological compounds at different stages of the disease and there are some limitations in pharmacological treatments of T2D. Due to ongoing loss and dysfunction of β-cell in T2D, neither insulin nor other anti-diabetic drug Metformin are able to treat the root cause of this disease but only its symptoms particularly insulin resistance and hyperglycemia. In

addition, these treatments are often accompanied by side effects such as hypoglycemia, weight gain, gastrointestinal problems, peripheral, oedema and an increased risk for cardiovascular events (Black et al., 2007). To maintain glycemic control and reverse or stop the decline of β-cell function, new treatments must be developed. The new treatment may also help to enhance insulin action, aid weight loss and prevent hypoglycemia and have a positive impact on cardiovascular disease.

Beside other drugs targeting β-cell dysfunction, many patients with T2D need lifelong insulin administration. Insulin is needed in advanced β-cell failure to compensate this dysfunction and to reverse severe insulin resistance. Additionally, for having higher portal than peripheral insulin concentrations, approaches have been developed to activate insulin receptor or post-receptor signaling intermediators. In the last years compounds such as TLK16998 have been developed to potentiate insulin action by prolonging phosphorylation of the β subunit or the insulin receptor (Manchem et al., 2001).

Although the current treatments with insulin or combination of more glucose-lowering drugs succeeded to improve the life quality of patients, they require self-monitoring of glucose level and they failed to alleviate long-term complications such as weight gain, hypoglycemia, vascular complications, neuropathy, retinopathy or kidney damage (Garber, 2010; Jamiolkowski et al., 2012). Therefore, intensive efforts in the field of regenerative medicine have been developed to restore and replace loss of β-cell mass that can be transplanted into patients to provide a better glycemic control and potentially cure diabetes. In order to do this, three different approaches have been followed to replace or regenerate β-cells: using stem cell-derived β-cells, transdifferentiation from other cell types (α or δ- cells) towards β-cells and the self-replication capacity of β-cells. To generate β-cells artificially, we need to understand how β-cells are formed during development, how β-cell homeostasis and function is maintained and what happens when β-cells experience autoimmune T1D or gluco-/lipotoxic T2D stress. Blocking this stress may protect β-cells. An understanding how β-cells are generated may allow to regenerate them.

3.2 The pancreas is an exo-endocrine gland

On cellular level, the pancreas is an endocrine (hormones) and exocrine (digestive enzymes) producing and secreting gland that is important to regulate the glucose metabolism and digestion. In mice, the bulk of the pancreas is comprised of acinar cells, which comprises 95-99% of it and produces digestive enzymes to secrete through the ductal system into the duodenum. The endocrine pancreas composes of β (65-80%), α (15-20%), δ (3-10%), PP (3-5%) and Ɛ (<1%) cells organized in structures called the islets of Langerhans. These cells secrete insulin, glucagon, somatostatin, pancreatic polypeptide and ghrelin, respectively. These hormones are secreted into the blood to maintain glucose homeostasis. In addition, β-cells are placed in the core of islets, meanwhile the other cell types are arranged around in the so called mantel. The development, differentiation and morphogenesis of pancreas is regulated by signal factors and transcription factors, which is well described in mice (Pan and Wright, 2011).

Anatomically, pancreas is composed of four different parts. The head is the biggest component and sits within the curvature of the duodenum. The neck, which is about 2 cm long, connects the head to the body. The 10 cm long body is the largest part of the pancreas. This flat part is located

behind the stomachs and below the peritoneum. The last part is the 2.5 cm long tail, which sits between the spleen and the left kidney. The pancreas comprises, anatomically, of dorsal and ventral lobes which are named in human as tail and head.

3.3 Development of the pancreas

At the beginning of the pancreas development, ventral and dorsal pancreatic buds are formed at Embryonic stage (E) 8.5-9.5, then this buds fuse. All cells of the multilayered pancreatic primordium are multipotent and capable of contributing to both endocrine and exocrine cells. During primary transition (from E9-11.5) the first wave on endocrine cells are formed, which are mainly α-cells. At the beginning of secondary transition (E12.5-15.5), mainly β and δ-cells are formed (Zhou et al., 2007). The tip which expresses crucial transcription factors such as Pancreas transcription factor 1 subunit alpha (Ptf1a) and c-Myc and enzymes like Cpa1 becomes exocrine, whereas the trunk domain that expresses NK6 homeobox1 (Nkx6.1), NK6 homeobox2 (Nkx6.2) and Sox9 becomes ductal and endocrine (Schaffer et al., 2010; Zhou et al., 2007).

At E15.5, almost all tip cells have been differentiated to the acinar cells. The following expansion of these cell populations is provided by cell proliferation (Pan et al., 2013; Zhou et al., 2007). Acinar cell differentiation is identified by the transcription factors Ptf1a, Mist1, Recombination signal binding protein for immunoglobulin kappa J region1 (Rbp-j1) and nuclear receptor subfamily 5, group A, member1/ liver receptor homolog-1 (Nr5a2/LRH-1) (Rose et al., 2001; Zhou et al., 2007).

At E12.5 the cells of the trunk domain change their morphogenesis to build a 3D structure of branched tubules. The epithelial cells of tubules are described as progenitor cords (Hick et al., 2009; Kopp et al., 2011). During the secondary transition, the cells in the progenitor cord express Neurogenin3 (Ngn3), which is important for the differentiation of endocrine cells (Gradwohl et al., 2000; Gu et al., 2002; Johansson et al., 2007) Epithelial cells, which do not express Ngn3, give rise to the ductal tree, suggesting that the Ngn3 is a key factor balancing the endocrine against ductal cells (Beucher et al., 2012; Magenheim et al., 2011; Wang et al., 2010). However, other transcription factors like Sox9, transcription factor2 (Tcf2), Onecu-1, Hairy and enhancer of split-1 (Hes1), Prospero homeobox protein1 (Prox1) and Zinc finger protein GLI3 (Gli3) are restricted to the ducts and play a role in ductal cell differentiation, morphology and architecture of the ductal tree (Delous et al., 2012; Kang et al., 2009).

Pancreatic duodenal homeobox 1 (Pdx1) is first expressed at E8.5 in the pre-pancreatic region of the foregut. During early pancreas development, pancreatic progenitor cells move out of the epithelium to commit to the endocrine lineage (Jensen et al., 2000). Low expression of Pdx1 remain in acinar and ductal cells (Guz et al., 1995), whereas endocrine cells, which begin to differentiate into insulin-positive β-cells show increased expression of Pdx1 (Marshak et al., 1996).

In addition to Pdx1, the Ptf1a is also essential for early specification of pancreatic progenitor cells. Ptf1a is first expressed at E9.5, when the cells of the foregut give rise to the dorsal and ventral pancreas (Burlison et al., 2008; Krapp et al., 1998). In the later stage of development, the expression of Ptf1a continues in the epithelium and in acinar cells, whereas its expression is decreased in endocrine cells (Chiang and Melton, 2003; Kawaguchi et al., 2002).

Ngn3 is the master regulatory transcription factor in the pancreatic endocrine lineage and absolutely necessary for endocrine differentiation. The first expression of Ngn3 appears at E9.0 during the so called primary transition and then then is strongly upregulated during to the peak of endocrinogenesis (Gradwohl et al., 2000). The Ngn3 positive endocrine progenitor cells will give rise to post-mitotic hormone-producing cells, which expresses islet cell transcription factors, such as NeuroD1, Nkx6-1 and Pax6 (Jensen et al., 2000).

3.3.1 Islet formation

As soon as Ngn3 expression is activated in pancreatic progenitors these cells delaminate from the progenitor epithelium and form endocrine progenitors (Bastidas-Ponce et al., 2017; Desgraz and Herrera, 2009; Gouzi et al., 2011) and finally find together in clusters named as islets of Langerhans. Desgraz and Herrera (Desgraz and Herrera, 2009) have shown that the endocrine progenitors are unipotent. Depending on when during development Ngn3 is induced (primary or secondary transition) the five main endocrine cells are induced: glucagon-producing α-cells, insulin-producing β-cells, somatostatin-producing δ-cells, pancreatic polypeptide-producing PP-cells and ghrelin-producing Ɛ-cells (Figure 3.1). In this context, the decision of endocrine precursors for differentiating into which kind of endocrine cells is known to be temporally controlled. This means that the α and Ɛ-cells differentiate at first and β and δ-cell differentiate later (Murtaugh, 2007). The gene expression of Ngn3 is transient in endocrine progenitors and is downregulated as soon as the endocrine cells express the hormones. Endocrine cell fate is determined by combination of different transcription factors downstream of Ngn3, such as Paired box gene4 (Pax4), Aristaless related homeobox (Arx), Regulatory factor X, 6 (Rfx6), Neurogenic differentiation (NeuroD) and Paired box gene6 (Pax6) (Figure 3.1). Studies have revealed that these factors control cell differentiation, but also, cell maintenance, islet cell identity and function (Bastidas-Ponce et al., 2017; Mastracci and Sussel, 2012; Pan and Wright, 2011).

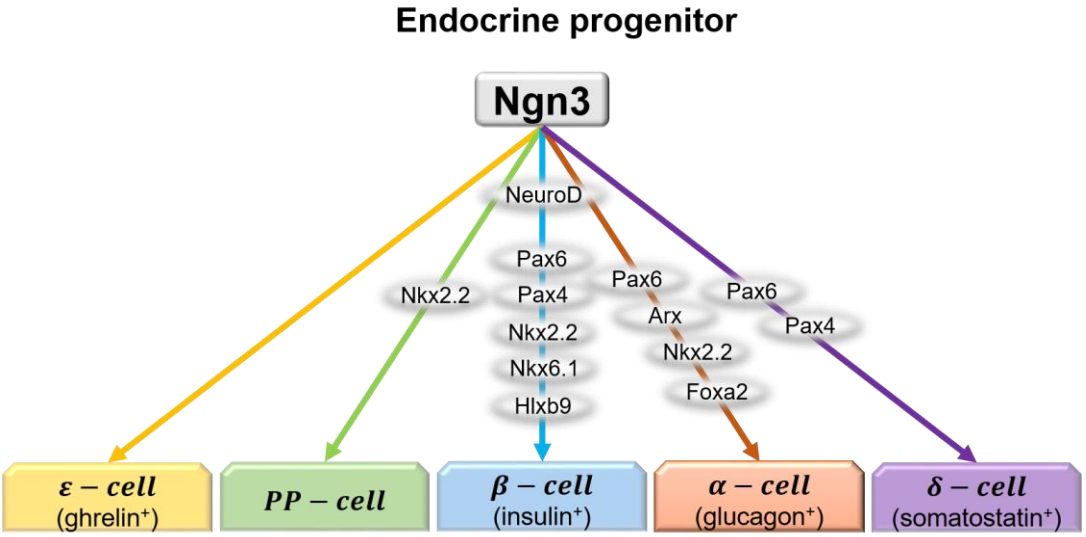

Figure 3.1: Pathways of islet-subtype specification.

Ngn3 expressing endocrine progenitors give rise to all islet cell types (glucagon-producing α-cells, insulin-producing β-cells, somatostatin-producing δ-cells, pancreatic polypeptide-producing PP-cells and ghrelin-producing Ɛ-cells.

3.3.2 Functionality of pancreatic β-cell

As described above, Ngn3 positive endocrine progenitor cells differentiate into β-cells. However, generation of functional β-cells, which respond to glucose by insulin secretion, are regulated by additional transcription factors. Among these factors, Pdx1 is one of the most crucial transcription factor, which activates a number of β-cell specific genes (Carty et al., 1997; Chakrabarti et al., 2002). Moreover, NeuroD and MafA belong to transcription factors, that regulate β-cell insulin gene transcription (Zhang et al., 2005) by binding to the regulatory elements of the insulin promotor (Kataoka et al., 2002; Matsuoka et al., 2003; Olbrot et al., 2002). The forkhead transcription factor Foxa1 and Foxa2 are essential for glucose-stimulated insulin secretion, but not for insulin gene expression (Vatamaniuk et al., 2006).

3.3.2.1 β-cell maturation and proliferation

Mature β-cells are defined by responding to the glucose and secreting proper level of insulin. At E13.5 during the secondary transition, the β-cells generate insulin positive cells. However, these cells have restricted capability to synthesize insulin and do not properly respond to glucose (Asplund, 1973; Boschero et al., 1990; Rozzo et al., 2009). Only after birth, by switching to an autonomous energy sources, the newborn β-cells rapidly mature. Additionally, immature β-cells are not capable of increasing their oxidative metabolism to secrete insulin by high glucose exposure. Hence, the insulin secretion is lower in immature β-cells compared to mature adult β-cells (Freinkel et al., 1984; Hole et al., 1988). The physiology of β-cell maturation changes by expression of different marker including adenylate cyclase, which has been identified to enhance β-cell GSIS (Whim, 2011). Moreover, it is known that Pdx1, NeuroD and MafA are important transcription factors, which regulate β-cell maturation, and their expression is increased after birth (Aguayo-Mazzucato et al., 2011). Loss-of-function studies have shown that the lack of MafA resulted in an impairment of insulin secretion. In addition, MafA has also been identified to be involved in insulin synthesis and secretion (Wang et al., 2007; Zhang et al., 2005)

Immature β-cells have still the potential to proliferate in neonatal stages in mice and human. Several regulators like, cyclin dependent kinase (Kushner, 2006; Rane et al., 1999), CDK inhibitors (Uchida et al., 2005) and the Forkhead box protein M1 (FoxM1) transcription factor are known to be involved in β-cell proliferation and maintenance. Moreover, the mRNA levels of the cyclin-dependent kinase inhibitors, including $p16^{INK4a}$ and $p19^{Arf}$, are increased in neonatal mice and drop in adult β-cells (Ramsey et al., 2007). Additional studies have shown that upon metabolic demand β-cells have the capacity to proliferate and compensate for the demand. In mice, β-cells are supposed to be the source of new β-cells in adult animals (Dor et al., 2004; Teta et al., 2007). Thus, older animals show a decreased β-cell expansion capacity, suggesting that the age plays an important role in the proliferative capacity of β-cells (Georgia and Bhushan, 2004; Teta et al., 2005; Tschen et al., 2009).

3.4 Insulin biosynthesis

Proinsulin has 110 amino acids and consist of an N-terminal signal peptide. Proinsulin undergoes folding which depends on two critical disulfide bonds before it is transported from the endoplasmic reticulum (ER) to the Golgi apparatus (Huang and Arvan, 1995). Subsequently, proinsulin is

cleaved to insulin and C-peptide in the trans-Golgi network and is stored in secretory granules (Peterson et al., 1972). Several factors, including glucose stimulation, trigger the gene transcription and mRNA translation of insulin (Poitout et al., 2006). In spite of high amount of insulin granules in β-cell, which contains about 200.000 insulin molecules (Howell and Tyhurst, 1984), the insulin content is dynamic and depend on the nutrient condition. In response to nutrients, the protein translation of insulin is increased in β-cell (Wicksteed et al., 2007). In addition, since the stability of insulin mRNA is uncoupled to nutrient changes, the stability of insulin mRNA plays an important role to influence the synthesis of the protein (Giddings et al., 1982). Taken together, β-cells have developed mechanisms to regulate insulin transcription and translation independently and upon need. Insulin is then further stored in secretory granules and secreted upon nutrient, glucose and insulin stimulation.

3.4.1 Insulin secretion

Diabetes mellitus is defined by impairment of glucose homeostasis. Insulin, which is a 51-amino-acid peptide, is the key player for regulation of glucose homeostasis postprandial after a meal. Therefore, a peripheral insulin resistance causing overload and dysfunction of β-cells are characteristic for T2D. The small blood vessels in the dense structure of islets enable the nutrient exchange between blood circulation and the islet cells. In addition, the small pores in these blood vessels called fenestration, allow insulin diffusion from the β-cells to the blood (Suckale and Solimena, 2008). Besides glucose, β-cells respond to other nutrient in the blood stream, including monosaccharides, amino acid, fatty acid and incretin hormones from the gut.

β-cells secrete insulin respectively to the blood glucose concentration to regulate the glucose uptake in muscle and fat cells as well as to regulate gluconeogenesis in the liver. Since β-cells do not contain membrane-bound glucose receptors, glucose enters the β-cell via glucose transporters-mediated diffusion. In mice glucose transporter2 (Glut2) is only express in β-cells, whereas glucose transporter4 (Glut4) is express in muscle and fat cells. After entering the β-cell, glucose is phosphorylated to glucose -6-phosphate (G6P) by glucokinase, which is an essential glucose sensor (Suckale and Solimena, 2008). Subsequently, glucose is metabolized to pyruvate, which is oxidized by citrate cycle in mitochondria to produce Adenosine triphosphate (ATP). As a result, there is a change in ATP/ adenosine diphosphate (ADP) ratio in the cytoplasm, which trigger closure of the ATP-sensitive potassium channels (KATP channels). In addition, the cell membrane depolarizes, which results in action of voltage-dependent Ca^{2+} pumps. While opening the Ca^{2+} channels the cytoplasmic concentration of Ca^{2+} increases leading to activation of exocytosis of insulin-containing granules (Figure 3.2).

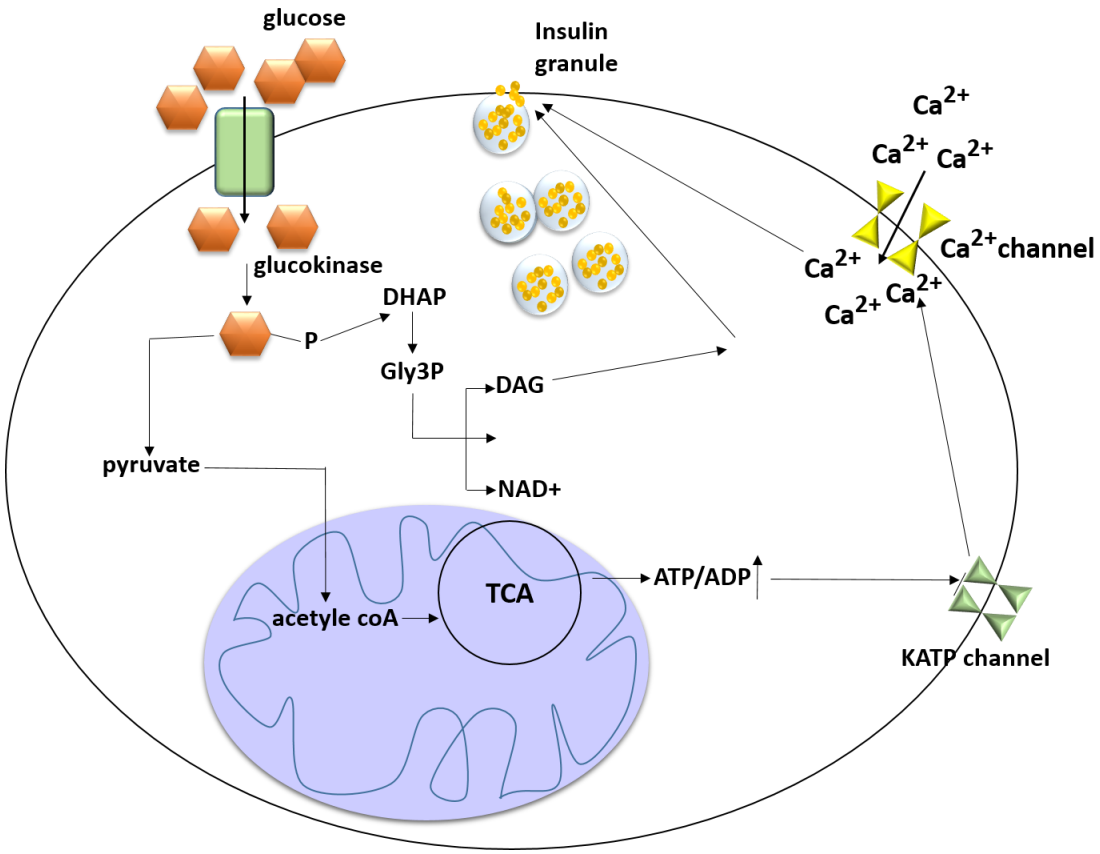

Figure 3.2: Schematic illustration of Glucose-regulated insulin secretion

The secretion of insulin is occurred by both K^+ATP channel-dependent or mitochondrial-independent process.

The process of insulin secretion consists of two steps: fusion of insulin granules with the plasma membrane and their subsequent exocytosis. The secretion of insulin is defined by a transient first phase followed by a sustained second phase. While first phase insulin secretion and exocytosis can happen in absence of glucose or other stimulus, second phase can occur in respond to the nutrients (Olofsson et al., 2002).

3.5 Insulin-like growth factor receptor I (IGF-IR) and insulin receptor (IR) signaling

IGF and insulin regulate growth, proliferation and metabolism. Since insulin resistance causes diabetes and IGF-I overactivation is linked to cancer, the understanding of the underlying INS/IGF system is of utmost importance. The insulin and IGF signaling pathways comprises of three ligands (IGF-I, IGF-II and insulin) as well as six high affinity binding proteins (IGFBP-1 to 6) and their proteases (Federici et al., 1997; Le Roith, 2003). In addition, this family includes the IGF-I receptor (IGF-IR), the mannose 6-phosphate/IGF-II receptor (M6P/IGF-IIR), the insulin receptor (IR) and the hybrid IR/IGF-IR (Figure 3.3). These receptors are expressed ubiquitously and

transduce signals that control growth, proliferation and metabolism as well as cellular processes including, cell migration and differentiation in nearly all mammalian tissues (Figure 3.3).

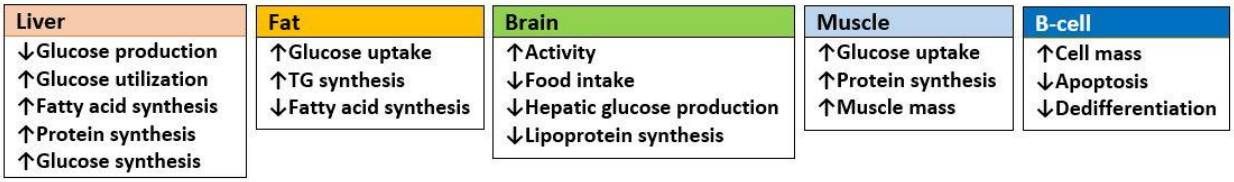

Figure 3.3: Effect of IR/IGF-IR signaling in various tissues and cell types.

The predominant effects of IR/IGF-IR signaling in different tissues and cell types are summarized by (Haeusler et al., 2018).

3.5.1 The structure of IR, IGF-IR and IGF-IIR and their ligands

Many years ago, it was discovered that insulin can bind to both IRs in the liver (Freychet et al., 1971) and endocrine pancreas (Verspohl and Ammon, 1980). The IR consist of α and β subunit, which are covalently linked (Adams et al., 2000; De Meyts and Whittaker, 2002). Further studies have revealed that alternative splicing in exon 11 of the IR transcript results in two different insulin receptor isoforms: type A (IR-A) and type B (IR-B). Even though insulin has the same binding affinity to both isoforms, IGFs have higher affinity to bind to IR-A (Seino et al., 1989). The ectodomain of IR extends to the extracellular space to initiate ligand-binding leading to signal transduction. The two half-receptors locate anti-parallel to surround a ligand-binding pocket. Since an individual ligand, which interact with receptor can change the extend, duration and nature of the receptor activation, the regions regulating the ligand specificity, have the most significant structural differences between IR and IGFRs. This explains the predominantly metabolic effect of IR in contrast to the mainly proliferative effect of IGF-IR (Pandini et al., 2002).

Since IGF-I and IGF-II exhibit close homology with insulin and their effect on growth is more pronounced than the effect on metabolism, they were named insulin-like growth factors (Daughaday et al., 1989). Although most circulation IGF-I is derived from the liver, IGF-I is synthesized in other organs, suggesting autocrine and paracrine effects. IGF-I is a 70-amino acid peptide, which is cross-linked by disulfide bonds (Rotwein, 1986). Despite sharing 48% amino acid homology with insulin and similar tertiary structure, IGFs remain the C-peptide, which is cleaved in proinsulin (Blundell et al., 1978; Rinderknecht and Humbel, 1978). The second difference is the existing specific amino acid in IGFs, which are not present in insulin. This amino acid enables in IGFs molecule the binding to the high affinity binding proteins (IGFBPs) (Clemmons, 1997; Firth and Baxter, 2002). IGFBPs modulate the activity of IGFs by increasing the IGF-IR activation by prolonging IGFs half-life. Although IGF-I, IGF-II and insulin bind to IGF-IR, the affinity binding of IGF-II and insulin are much lower than IGF-I (Federici et al., 1997; Le Roith, 2003). The α-subunits of IGF-IR have the IGF binding site, whereas β-subunits span the membrane and has tyrosine kinase domain (Steele-Perkins et al., 1988).

In addition, both receptors are able to build homodimers of two α and β subunit with each other (

Figure 3.4) (heterotetramer α2β2) as well as heterodimers by linking a αβ dimer of each receptor. Hybrids binds IGFs with similar affinity to IGFR. However, the binding affinity of hybrids receptors to bind insulin is lower than to IR (Belfiore et al., 2009).

IGF-II has the similar hepatic and extrahepatic expression pattern like IGF-I and resembles the structure of IGF-I but with 67 amino acids (Rotwein, 1986). In addition, of IGF-IR, IGF-II binds to another receptor, the IGF-IIR. IGF-IIR belongs to type-1 integral membrane glycoproteins. The extracellular region of IGF-IIR contains 15 homologous repeat domains (mannose 6-phosphate domains) and IGF-II binding site (Hancock et al., 2002; Marron-Terada et al., 2000). IGF-IIR tends to dimerize at the plasma membrane that enable the receptor a high affinity binding to the ligands. Although IGF-IIR binds IGF-II and IGF-I with high affinity, it does not bind to insulin. In contrast to IR and IGF-IR, IGF-IIR lacks a tyrosine kinase domain and activity.

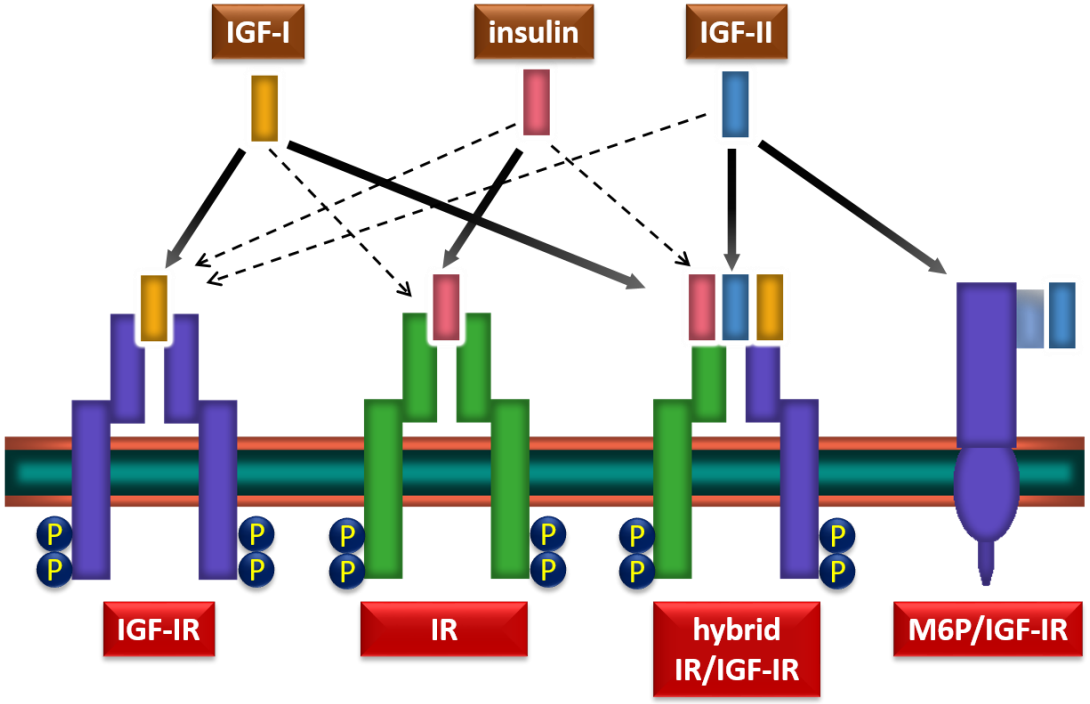

Figure 3.4: Schematic representation of the insulin-like growth factor system

The IGF system consist of three ligands (IGF-I, insulin and IGF-II), their receptors (IGF-IR, IR; the hybrid IR/IGF-IR and M6P/IGF-IIR).

3.5.2 Signal transduction and function of IR, IGF-IR and IGF-IIR

Ligand binding induces autophosphorylation of specific tyrosine kinase enzymes, which act as docking sites for signaling proteins, such as insulin receptor substrate (IRS), including the four IRS proteins (IRS-1 to -4) and Src-homology domain containing proteins (Shc). IRS has been identified to link to the activation of two main signaling pathway. The first one is phosphatidylinositol 3-kinase (PI3K)-AKT/protein kinase B (PKB) pathway, which plays a role in metabolic regulation of insulin. The second pathway is the RAS-mitogen-activated protein kinase

(MAPK), which is responsible for gene expression and with cooperation with PI3K regulates the cell growth and differentiation (Figure 3.5) (Avruch, 1998).

The phosphorylation of IRS enables their interaction to the p85 subunit of the key regulator PI3K, thereby facilitating the conversation of PIP_2 to phosphatidylinositol-3,4,5-triphosphate (PIP_3). PIP_3 triggers the activation of serine/threonine kinase Akt/PKB. Akt/PKB mediates most of the PI3K-mediated metabolic action of insulin, e.g. regulation of glucose uptake by phosphorylating the RAB-GTPase-activating protein AS160 (Akt substrate of 160 kDa), resulting in translocation of GLUT4 to the plasma membrane (Figure 3.5) (Sano, H.et al. 2003). Akt/PKB also stimulate mTOR (mammalian target of rapamycin) by inhibiting tuberin (tuberous sclerosis complex-2) (Harris T.E et al. 2003) and inhibit pro-apoptotic factors Bad (Vasudevan and Garraway, 2010). In addition, AKT/PBK-mediated phosphorylation of FoxO1 prevents its transcriptional activity, which is required for activation of gluconeogenenic genes in the liver (Puigserver et al., 2003).

In common with other receptor tyrosine kinases, the IR and IGF-IR regulate the gene transcription, which are involved in cell proliferation and survival using the Ras/MAP kinase pathway (Katz et al., 2007). The pathway activation is triggered by the interaction of IRSs and Shc proteins with the adaptor guanine nucleotide exchange factor complex Grb2/Sos, which subsequently phosphorylates the small G-protein Ras. Activated (GTP-bound) Ras stimulates a signaling cascade including proto-oncogene-Raf (Raf), the dual specificity kinase MEK and ERK, a kinase of the MAPK family (Figure 3.5) (Ramos, 2008). MEK/ERK translocate to the nucleus and phosphorylate a number of mitogenic transcription factors including cellular oncogene c-Fos and ETS transcription factor (ELK1) (Roskoski, 2012; Sturgill, 2008).

In contrast to IR and IGF-IR, the IGF-IIR does not activate signaling cascades due to the lacks of enzymatic activity in the cytoplasmic domain and the mitogenic activity of IGF-II has been reported to be regulated by IGF-IR (Dahms et al., 1996) and IR isoform A (Frasca et al., 1999). Rather, IGF-IIR has scavenging function by transporting the IGF-II ligand to the lysosome for degradation. To fulfill this function, IGF-IIR binds and internalize IGF-II at the plasma membrane and delivers enzymes from the Golgi network to the endosomal-lysosomal system. Therefore, IGF-IIR has a role in regulating cell growth and motility by modulating extracellular levels of this mitogenic polypeptide hormone. Despite of established role of IGF-IIR in IGF-II clearance, several studies indicate a function of IGF-IIR in IGFII signaling through a G-protein-coupled pathway that leads to activation of MAPK (Groskopf et al., 1997; McKinnon et al., 2001).

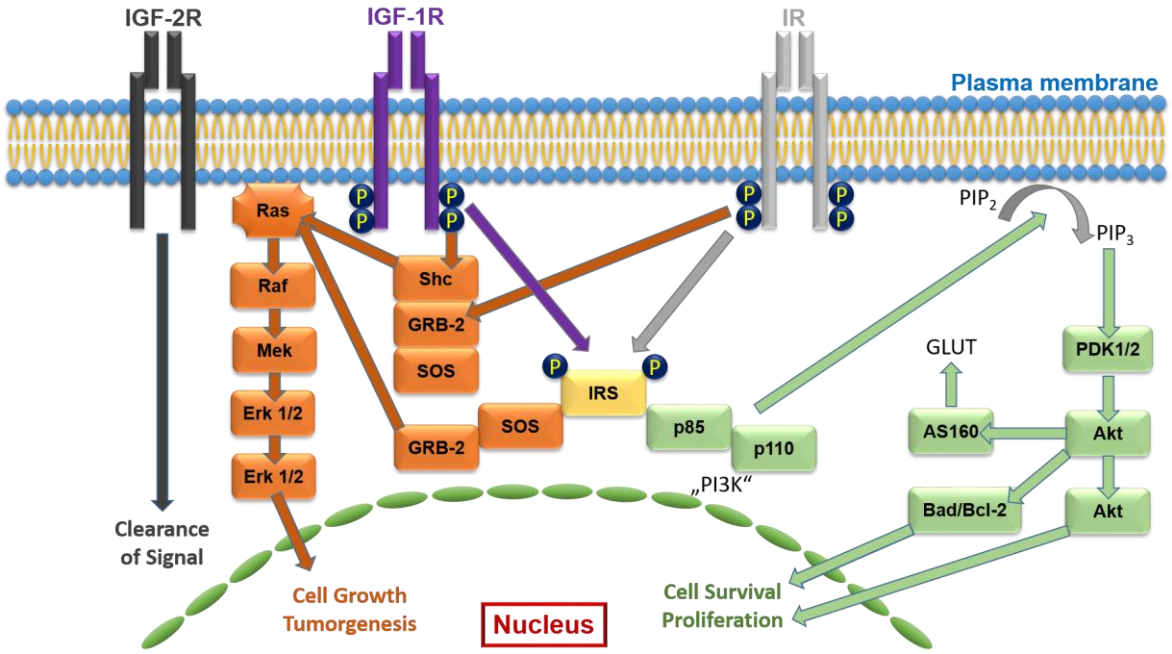

Figure 3.5: The IR/IGF-IR signaling system

IR and IGF-IR organize a complex signaling network regulating metabolic processes and growth. Key pathways act via PI3K/Akt and Ras/MAP kinases. IGF-IIR controls mechanism involved in lysosomal function and growth factor/cytokine signaling.

3.5.3 Intracellular Trafficking of Receptor Tyrosine Kinases

Receptor tyrosine kinases (RTKs) are folded and processed to dimers in the endoplasmic reticulum (ER) by the chaperones calnexin and calreticulin. After they transport to the trans-Golgi network (TGN) they undergo further post-translation modifications including disulfide bridge formation or glycosylation. From the TGN they are routed to different organelles but especially to the plasma membrane, where they bind to their ligands. Therefore, intracellular trafficking controls the functional activities of RTKs.

First, at the cell surface, the ligand binding induces a conformational change of the receptor resulting in autophosphorylation of the dimeric cytoplasmic domains. The RTKs including IR and IGF-IR interact with epsin, which has an ubiquitin-binding domain and interact with clathrin or adaptor protein 2 (Ap2). Subsequently IR/IGF-IR segregate in membrane areas, where clathrin-coated pits (CCPs) are formed so that ligand-receptor complex endocytosed via clathrin-mediated endocytosis (CME) (Goh and Sorkin, 2013a).

In addition to the RTK ubiquitination, the binding of CCPs to the transmembrane protein is also facilitated by sequence motifs in the cytoplasmic domain of receptor. For instance, IR binds to the clathrin adaptor protein complex AP2 uses the dileucine D(E) xxxLL (I) (“LL”) internalization motif (Haft et al., 1994). Subsequently after internalization, the vesicles of CCPs fuse with early endosomes (EE), where the acidic environment leads to release of some ligands. However, both unoccupied receptors and ligand-receptor complexes are capable to recycle to the cell membrane through back fusion of EE or retro-endocytosis. Another recycling pathway occur by maturation

of EE into sorting endosomes (SE) or multivesicular bodies (MVBs). Additional transformation of SE/MVBs into late endosomes (LE) leads to the fusion of LE with lysosome, which degrade RTKs via its proteolytic enzymes.

In addition, IGF-IIR binds to the AP1 uses an acidic-cluster-dileucine (AC-LL) motif of its cytoplasmic tail (Hong Jung Chen et al., 1993; Johnson and Kornfeld, 1992). After receptor internalized via AP2-containing clathrin-coated vesicles (CCVs), it delivers to the EE, where the low pH facilitates the release of acid hydrolases. Furthermore, IGF-IIRs recycles from early endosomes to the TGN by PACS-1/AP1-CCVs and from late endosomes via TIP47/Rab9. From TGM the IGF-IIRs go to the cell membrane either via recycling endosomes (RE) or from TGN cisternae.

In contrast to CME, which is the major and fastest pathway of IR/IGF-IR, internalization via clathrin-independent pathways (CIE) occurs especially under high, rather unphysiological ligand concentrations. It is associated with caveolin and cholesterol but with actin cytoskeleton (macropinoyctosis) (Boothe et al., 2016).

3.6 Autocrine insulin signaling in pancreatic β-cells

The possible direct physiological effect of insulin on β-cells is controversially discussed (Rhodes et al., 2013a). However, there are several evidences supporting the clear contribution of down-stream elements of β-cells. These are autocrine insulin signaling in glucose and lipid metabolism, ion flux, insulin biosynthesis, insulin secretion, β-cell mass, cell proliferation, cell size and apoptosis (Goldfine and Kulkarni, 2012; Leibiger et al., 2000, 2008a; Rhodes et al., 2013b; Uchizono et al., 2007a).

The question of what concentration of insulin are islets exposed could be answered by two possibilities. Either the β-cells are used to be in a very high concentration of secreted insulin or the high concentration of insulin desensitized the IRS signaling pathway downstream of the receptor as well as downregulate the IR expression (Zick, 2005). The insulin binding to the IR triggers its internalization into an endosomal compartment, which contributes to receptor desensitization resulting in a reduction of the receptor binding capacity or plasma membrane levels (Carpentier et al., 1985; Zick, 2005). This feedback inhibition mechanism is provided to control the activity of IR signaling in β-cells and would be only deactivated upon absence of insulin to restore insulin signal transduction (Heaton and Gelehrter, 1981). Some studies have claimed that the hyperinsulinemia in obesity-linked T2D could contributes to the insulin-resistance by this desensitization mechanism (Zick, 2005).

An alternative to the inhibition-mechanism is the β-cell→α-cell→δ-cell communication, which is involved to coordinate insulin and glucagon downregulation by preventing the accumulation of somatostatin (Bonner-Weir and Orci, 1982). Additionally, somatostatin secreted from δ-cells inhibits insulin and glucagon secretion from β- and α-cells, respectively.

3.6.1 Distinct roles of IR and IGF-IR in β-cells

Mouse and human β-cell express both the IR and IGF-IR and most components involving in their signaling pathways (Kulkarni et al., 2002a; Muller et al., 2006; Petyuk et al., 2008). However, the

IR expression depends on its isoform (Giddings and Carnaghi, 1992). While both IR-A and IR-B are expressed in β-cells (Seino and Bell, 1989), the expression of IR-B is more pronounced in peripheral tissues including liver, fat and muscle. Mice with global mutation for the IR as well as β-cell-specific KO of IR (βIRKO) show a slight growth retardation at birth suggesting that IR does not contribute to embryonic development (Accili et al., 1996; Kulkarni et al., 1999). However, early after birth they develop hyperglycemia and ketoacidosis (Kitamura et al., 2003). βIRKO mice born with a normal complement of β-cell but display decrease in glucose-induced insulin release and impaired glucose tolerance. Moreover, due to the loss of proliferative activity they develop an insulin deficiency during aging (Brüning et al., 1997). Although diet-induced insulin resistance causes adaptive enhancement of β-cell mass, βIRKO mice show an age-dependent decrease in β-cell mass (Kulkarni et al., 1999; Otani et al., 2004a), which suggest an important role of IR, but also IGF-IR signaling in β-cell mass and hyperplasia regulation in adult mice (Ueki et al., 2006a).

In contrast to βIRKO mice, β-cell-specific KO for IGF-IR mice (βIGF-IR) show unaffected β-cell mass during aging. Moreover, they do not tend to develop overt diabetes (Kulkarni et al., 1999; Otani et al., 2004b). However, they exhibit impaired glucose tolerance and reduced first phase of GSIS. Interestingly, βIGF-IR mice have shown to develop hyperinsulinemia phenotype under fasting condition, suggesting a role of IGF-IR in the negative feedback on basal insulin secretion. In addition, mice lacking both IR and IGF-IR in β-cells are born with normal number of mature β-cells but several weeks after birth, they develop diabetes (Ueki et al., 2006b). Beside *in vivo* studies, it has been shown that reduction of IR or IGF-IR expression in Min6 cell leads to inhibition of GSIS but does not affect KCl-mediated hyperpolarization and insulin release (da SILVA XAVIER et al., 2004).

IGF-IIR deficient mice die soon after birth due to a heart failure causing by cardiac hyperplasia. Additionally, they show overgrowth, due to excessive IGF-II and failure of IGF-IIR, scavenging the growth and proliferation effect of IGF-II (Lau et al., 1994; Ludwig et al., 1996; Wang et al., 1994).

In summary, these finding demonstrate that both IR and IGF-IR are not essential for development of β-cells, but transmit signals for differentiation, proliferation and regulation of insulin secretion.

3.6.2 The role of PI3K/AKT pathway in β-cell proliferation

It has been reported that IRSs and AKT, which are the downstream signaling molecules of IR/IGF-IR signaling pathways are involved in β-cell growth. *In vivo* studies from β-cell-specific IRS-1 and IRS-2 knock out suggest the role of IRS-1 in regulation of insulin secretion. Whereas, IRS-2 seems to be a positive regulator for β-cell mass and compensation (Choudhury et al., 2005; Kubota et al., 2004; Lin et al., 2004). In addition, inactivation of IRS-2 leads to reduced β-cell mass, probably duo to the lack of neogenesis or elevation in apoptosis (Withers et al., 1999). Moreover, β-cell-specific transgenic mice that express constitutively active AKT1 exhibit islet hyperplasia, β-cell hypertrophy, hyperinsulinemia and improved glucose tolerance (Bernal-Mizrachi et al., 2001a; Tuttle et al., 2001). Furthermore, AKT regulates β-cell proliferation by phosphorylation and inactivation of one of its downstream molecules named as glycogen synthase kinase 3 (GSK3) (Manning and Cantley, 2007). Since GSK3 known to promote the degradation of cyclin D1 (Diehl et al., 1998), constitutively activation of Akt1 *in vivo* leads to increase in cyclin D1 level in islets resulting in improvement of β-cell cycle progression (Figure

3.6) (Fatrai et al., 2006a). FoxO is another downstream molecule of AKT that is known to regulate β-cell proliferation. AKT phosphorylate FoxO1 leading in its translocation from the nucleus to cytoplasm where it is inactive and unable to regulate expression of Pdx-1 (Rena et al., 1999)(Ahlgren et al., 1996). In addition, ablation von $p70^{s6k1}$, which is the substrate of AKT resulted in decreased cell size and hypoinsulinemia (Figure 3.6)(Assmann et al., 2009a).

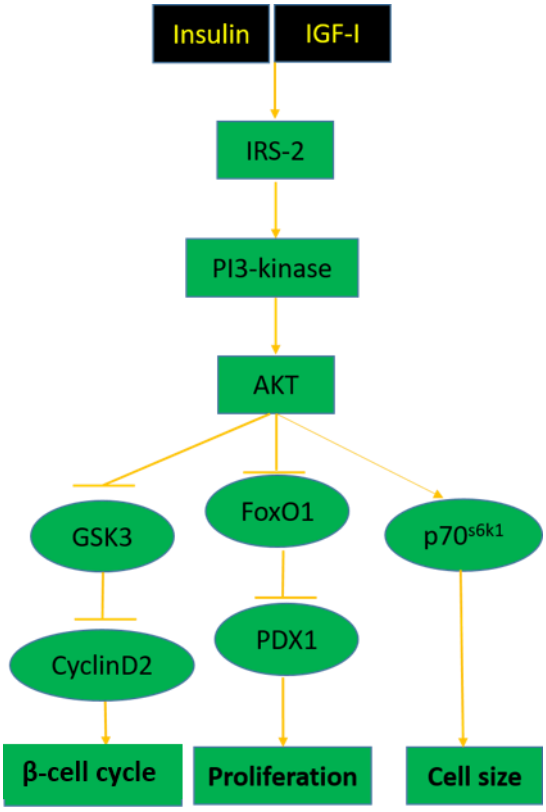

Figure 3.6: Schematic representation of the IR/IGF-IR signaling in β-cell

Autocrine or paracrine activation of the IR/IGF-IR leads to signaling via the downstream effectors, PI3-kinase, AKT with effect on growth and survival of the β-cell.

3.7 Identification and characterization of the insulin-inhibitory receptor (IIR, Inceptor)

In screens to identify novel pancreatic regulators, we identified *5330417C22Rik* as a pancreas specific expressed gene during development. Despite unknown murine gene function, the humane gene (*KIAA1324)* was identified as oestrogen-induced gene (EIG121) in endometrial cancer (Deng et al., 2005). The murine gene is located on chromosome 3 and comprises of 22 exons (Figure 3.7), a similar gene structure when compared to the IR or IGF-IR gene. *5330417C22Rik* encodes for seven alternative splice isoforms of which only three are predicted to be transcribed (one long isoform and two shorter ones). The longest alternative splice variant (*5330417C22RIK-202*), which is translated to a single-pass type I transmembrane protein consist of 1013 amino acids. *5330417C22RIK-201* is the second longest transcript and translates into a

protein with 911 amino acids. The shortest transcript is called *5330417C22RIK-203* and the synthesized protein contains 939 amino acids (Figure 3.7).

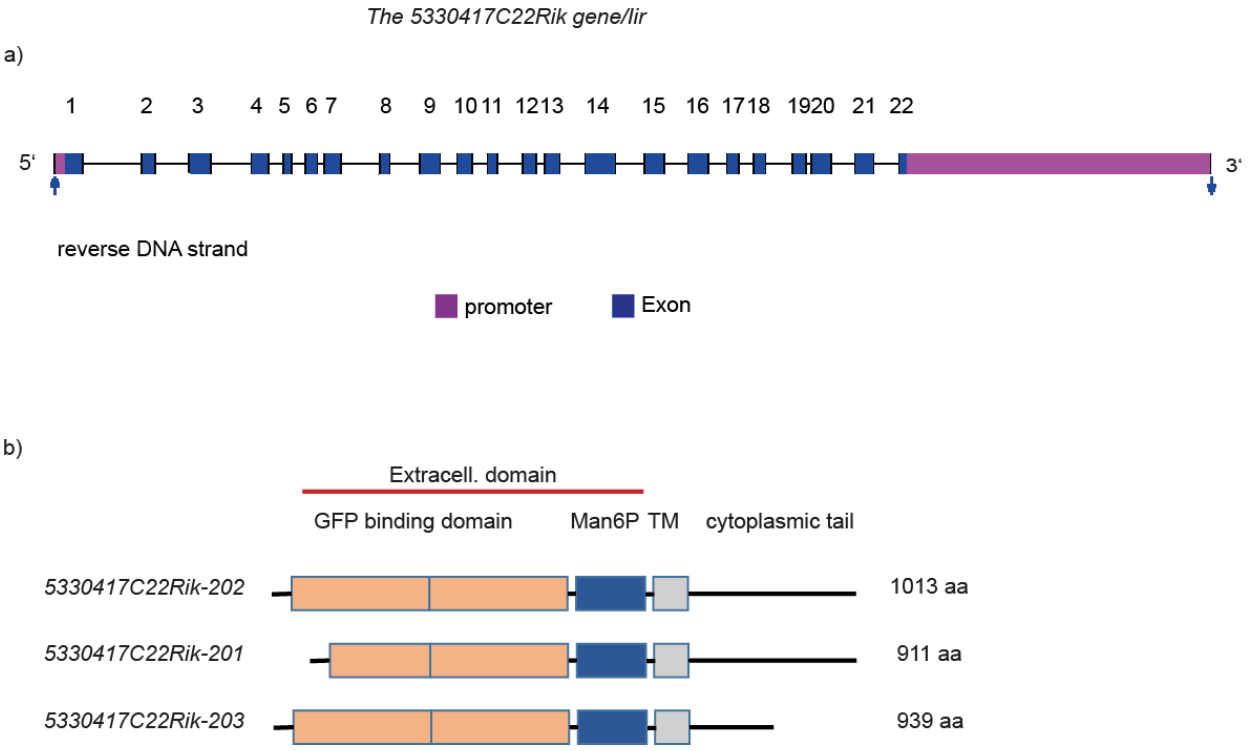

Figure 3.7: Schematic representation of gene *5330417C22Rik/lir* and its predicted alternative protein coding splice variants

a. The gene contains 22 exons and its predicted exon-intron sequences. Promotor and exons are represented in colored boxes. (Modified from ensembl.org)
b. Beside a cytoplasmic tail, there are three predicted functional protein regions for the *5330417C22RIK/lir* receptor, a growth factor receptor domain, a mannose-6-phosphate receptor binding domain and a transmembrane domain. (Modified from the Ensemble database).

3.7.1 The Inceptor protein

The mouse protein has a molecular weight of 110 kDa and its expression is highly conserved in evolution as it shows 90% homology between rodents and human proteins, suggesting an important cellular function. Mammalian orthologs of 5330417C22Rik can be found in human (*Homo sapiens*; KIAA1324), in *C. lupus* (dog), *B. taurus* (cow) and in *G. gallus* (chicken). Orthologs in other species are present in model organisms such as the *X. tropicalis* (frog) and the *D. rerio* (zebrafish).

The human homologue belongs to the UPF0577 protein family and its high expression has been identified across a range of cancers for instance, in endometrial, ovarian, pancreatic and gastric cancer (Deng et al., 2005; Estrella et al., 2014; Kang et al., 2015; Schlumbrecht et al., 2011a). KIAA1324 expression has been found to be differentially regulated in endometrial carcinoma. Due to increased expression of KIAA1324 in the estrogen-proliferative phase of premenopausal

endometrium and in endometrial carcinoma, KIAA1324 is known to be induced by estrogen and therefore named as estrogen-induced gene 121 (EIG121) (Deng et al., 2005). Aligned with this, it has been shown that elevated expression of estrogen receptor (ER) and EIG121 links to shorter overall survival and could be used as a suitable biomarker to predict responsiveness to hormone treatment in women with advanced stage ovarian/primary peritoneal high-grade serous carcinoma after surgery (Schlumbrecht et al., 2011b). *In vitro* the KIAA1324 protein is associated with the plasma membrane of different organelles such as the trans-Golgi apparatus, late endosome-lysosome compartments, endoplasmic reticulum. Along these lines, *in vitro* studies have shown that the overexpression of KIAA1324 inhibits cellular proliferation, invasiveness, and decrease apoptosis induced by drugs. Moreover, KIAA1324 has been described to regulate autophagy and promotes cell survival. Furthermore, it has been published that the overexpression of KIAA1324 in cancer xenografts causes decreased tumour size (Kang et al., 2015).

To understand the predicted function of 5330417C22Rik/*Iir*, we carried out bioinformatics analysis using *the ENSEMBL database (transcript ID ENST00000369939.8)* (Data shown in PhD thesis Felizitas Schmitz). This information gave us a better overview of the localization of the *5330417C22Rik/Iir* gene. Furthermore, the bioinformatics studies predicted potential interaction partners or the involvement of this protein in signaling pathways. In addition, these studies revealed that the 5330417C22Rik protein is a transmembrane receptor, which contains four predicted domains. The N-terminus region is composed of signal sequences and followed by an extracellular region, a transmembrane helix and a cytoplasmic tail. Two potential and functional regions were identified by the extracellular domain, comprising of mannose-6-phosphate receptor binding domain and a growth factor receptor cysteine-rich domain (Figure 3.8).

The growth factor receptor cysteine-rich domain exists in receptor tyrosine kinases like type-1 insulin-like growth-factor receptor (IGF-IR) which plays a part in binding the IGF-I receptor to its ligand IGF-I and IGF-II to trigger the receptor dimerization and shows similarities to the cysteine-rich domain of the 5330417C22Rik protein. Furthermore, bioinformatics analysis demonstrated that the mannose-6-phosphate receptor-binding domain is involved in the cation-dependent (CD-M6PR) and cation-independent (CI-M6PR, IGF-IIR) reveals similarities to the mannose-6-phosphate receptor-binding domain of the 5330417C22Rik protein. The short cytoplasmic C-terminus of 5330417C22Rik protein shows potential phosphorylation sites but unlike IR and IGF-IR lacks kinase activity (Figure 3.8). In addition, 5330417C22Rik protein consist of a potential binding motif for the adaptor protein 2 (AP2). AP2 is a heterotetrameric protein complex, which is involved in clathrin-mediated endocytosis (CME).

Based on the similarities of these domains in the extracellular region to IR, IGF-IR and IGF-IIR, we named the protein insulin inhibitory receptor, or short inceptor (gene name: *IIR* (human) or *Iir* (mouse).

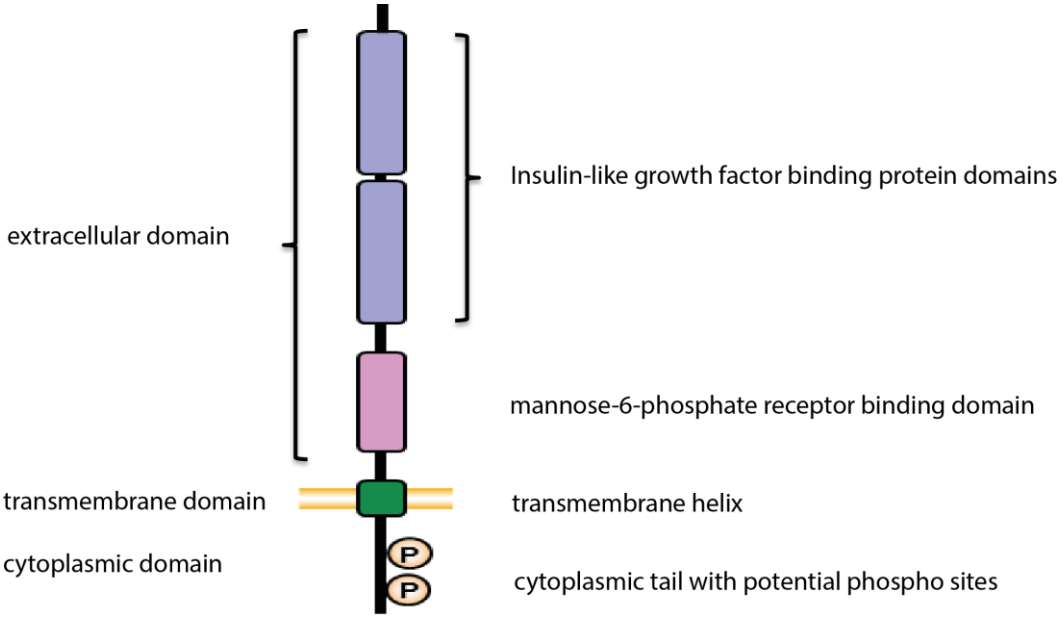

Figure 3.8: Predicted domain structures of the inceptor protein

The inceptor protein contains a large extracellular region, a short transmembrane domain and a short cytoplasmic tail.

3.8 Aim of the thesis

The high expression of inceptor in the embryonic pancreas and its structural similarities to IR, IGF-IR and IGF-IIR, suggested a functional role of inceptor in regulating insulin and IGF signaling in the pancreas. Therefore, the first part of this project was to assess the *in vivo* function of inceptor using inceptor knock-out mice. As we hypothesize that we identified a novel regulator of the Ins/IGF system, our aim was to investigate the potential role of inceptor in the regulation of growth, proliferation and metabolism.

Due to the perinatal lethality of inceptor knock-out animals, the second part focused on addressing the potential function of inceptor in adult β-cells in the context of glucose regulation and insulin signaling activation. For this purpose, we generated a tamoxifen-inducible conditional β-cell specific KO (MIP-CreERT^{+}; *Iir* $^{fl/FD}$). In addition, to determine whether the expression of inceptor is altered in diabetic conditions, we investigate the biological significance of inceptor in diabetic mice and human islets.

4 Result

4.1 Characterization of a novel modulator of the IR/IGF-IR signaling system *in vivo*

4.1.1 mRNA expression of *Iir* in *Mus musculus* during development

To systematically address the function of the insulin inhibitory receptor (*Iir*), we analyzed the expression of the *Iir* mRNA and inceptor protein levels in different mouse tissues during mouse development. First, we searched several available mRNA expression databases such as EMBL-EBL expression atlas (Figure 4.1a). We found *Iir* mRNA to be mainly expressed in secretory cells including endocrine and exocrine glands (e.g. adrenal gland, pituitary and pancreas), sex-related tissues (e.g. ovary and testis), as well as in the brain, suggesting a function of inceptor in the hypothalamic-pituitary-gonadal axis.

To confirm these bioinformatics predictions, we next performed a quantitative real time PCR (qPCR) in different tissues from WT mice to confirm the database predictions and better profile the mRNA expression of *Iir*. qPCR results from P0 mice revealed high expression in gastro-intestinal tract including spleen, pancreas, colon, duodenum and stomach tissues and weak expression, in lung, liver, muscle, testis and brain (Figure 4.1b), which was in line with the database results (Figure 4.1a). The fact that *Iir* mRNA is highly enriched in the gastrointestinal system, as well as secretory cells of endocrine and exocrine glands, suggests a function in digestion, endocrine regulation or systemic metabolism.

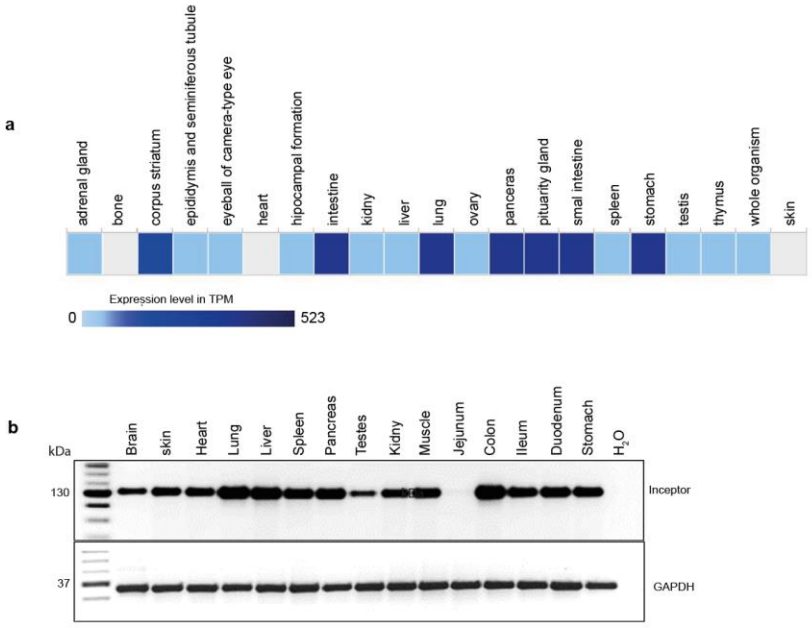

Figure 4.1: mRNA expression profile of *Iir* in various mouse tissues.

a. Gene expression of *Iir* in neonate mouse tissues (modified from Ensemble expression atlas, release 38-Feb 2022). The normalization method for RNA-seq: Transcript per Million (TMP), expression value is 0.5, expression level (0-523). Array Express: experiment E-MTAB-3579.
b. Qualitative PCR results using 5' and 3' primers (localized e.g.exon 19-22 spanning intron xγ) to detect *Iir* mRNA in a variety of postnatal day 0 (P0) mouse tissues. H_2O is the non-cDNA template negative control.

4.1.2 Characterization of inceptor antibodies

To understand the protein expression and intracellular localization pattern of inceptor, we next generated a series of mono- and polyclonal antibodies directed against the intra- and extracellular domains of the inceptor protein.

The human and mouse inceptor amino acid sequence show high similarity, hence we generated several polyclonal anti-rabbit antibodies against a conserved cytoplasmic peptide (see material and method, Tab 6-4).

In addition to the polyclonal rabbit antibodies, we generated mouse and rat monoclonal inceptor antibodies against the peptide sequence of the cytoplasmic tail of the inceptor protein (antibody core facility of Helmholtz Munich). First, these antibodies were tested for their specificity on cell lysates from Min6 insulinoma cells (data not shown). Antibodies that recognized the inceptor protein in Western blot analysis and were highly specific as they did not show any reactivity in lysates of Min6 *Iir* KO cells were further characterized in immunocytochemistry (data shown in PhD thesis from Felizitas Schmitz). Next, I tested some of these antibodies to show specificity in WT an KO tissues and to analyze the *in vivo* expression pattern and localization of the inceptor protein.

Since we can prove that an antibody is specific if it does not detect anything in KO tissues, I first characterized these antibodies using Western blot. The inceptor protein was detected at 130 kDa in SDS-PAGE using mouse pancreas lysates, whereas the *Iir*$^{-/-}$ lysates showed no band (Figure 4.1b). Another good indication for specificity of an antibody is also if antibodies directed against different epitopes of the same protein show perfect colocalization.

To further prove the specificity of our newly generated mono- and polyclonal antibodies we co-stained tissues and compared the expression pattern. Therefore, we analyzed inceptor antibodies by immunohistochemistry using rat monoclonal anti-inceptor (16F6) and rabbit anti-inceptor (1692) and their co-expression was quantified. Localization of the inceptor protein is clearly detectable in the endocrine and ductal/exocrine pancreas. Furthermore, the mono- and polyclonal antibody expression pattern perfectly overlaps (right panel) as proven by a co-staining for these two antibodies (Figure 4.2). Taken together, the absence of immunoreactivity in knock-out WB and tissue staining as well as the perfect overlap of antibody staining patterns proofs that our newly generated antibodies are highly specific for the inceptor protein and do not show any cross-reactivity.

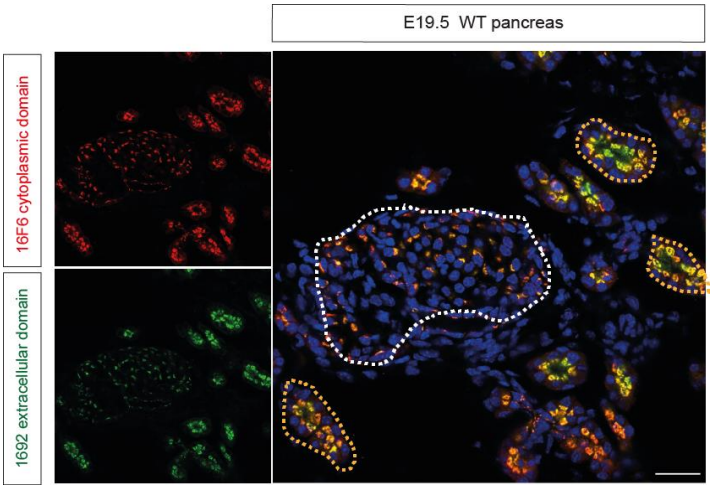

Figure 4.2: Inceptor antibody specificity in immunocytochemistry in WT pancreas.

Immunostaining for inceptor expression from WT mouse pancreata of E19.5 embryo using rat (16F6-cytoplasmic) anti-inceptor (red) and rabbit (1692 - extracellular) anti-inceptor (green) antibodies in endocrine region (white outline) and ductal regions (orange outline). The upper left panel shows localization of monoclonal rat anti-inceptor antibody, which binds to the cytoplasmic domain of the inceptor. The lower panel shows antibody staining for a rabbit polyclonal anti-inceptor antibody, which recognizes the extra-cellular domain of inceptor.

4.1.2.1 The protein expression of inceptor is detectable in different organs of P0 mice

After we confirmed the specificity, we next investigated the tissue specific expression and subcellular localization pattern of the inceptor protein. As little is known about the expression of inceptor in *M. musculus* and *Iir* mRNA was detected in gastro-intestinal tract, lung, liver, muscle, testis and brain similar to the database information. For protein expression, different organs were

isolated from WT CD1 animals and analyzed by WB. High expression of inceptor (130 kDa) could be found in the pancreas, stomach and lung, whereas, brain, uterus liver, adrenal gland and testis expressed lower protein levels (Figure 4.3a).

To further investigate the expression of inceptor, monoclonal inceptor antibody was used on murine P0 tissue sections. Inceptor was expressed specifically in islet and exocrine cells of pancreas. In colon inceptor could be found in mesenchymal cells but not epithelial cells. Inceptor was also weakly found in glomeruli of the kidney. In liver, inceptor was found in endothelial and hepatocytes around the portal and/or central vein. Additionally, inceptor was broadly expressed in bronchioles of the lung. In the spleen, inceptor expressing cells are close to the red pulp and therefore we assume that there are the trabecular artery cells, which express inceptor. In addition, we could show inceptor expressing cells in zona reticularis of the adrenal gland. These cells are responsible to release androgens hormones. In the testis, inceptor expression seems to be in intertubular cells surrounding the seminiferous tubules. The thymus consists of several thymic Hassall's corpuscles, which are surrounded by epitheliorecular cells and we assume that inceptor is expressed in these cells. In the uterus, inceptor seems to be found in the ciliated epithelium surrounding the gland of the uterus. In the bladder, transitional epithelium, which is found in part of bladder supposed to be expressed inceptor (Figure 4.3b).

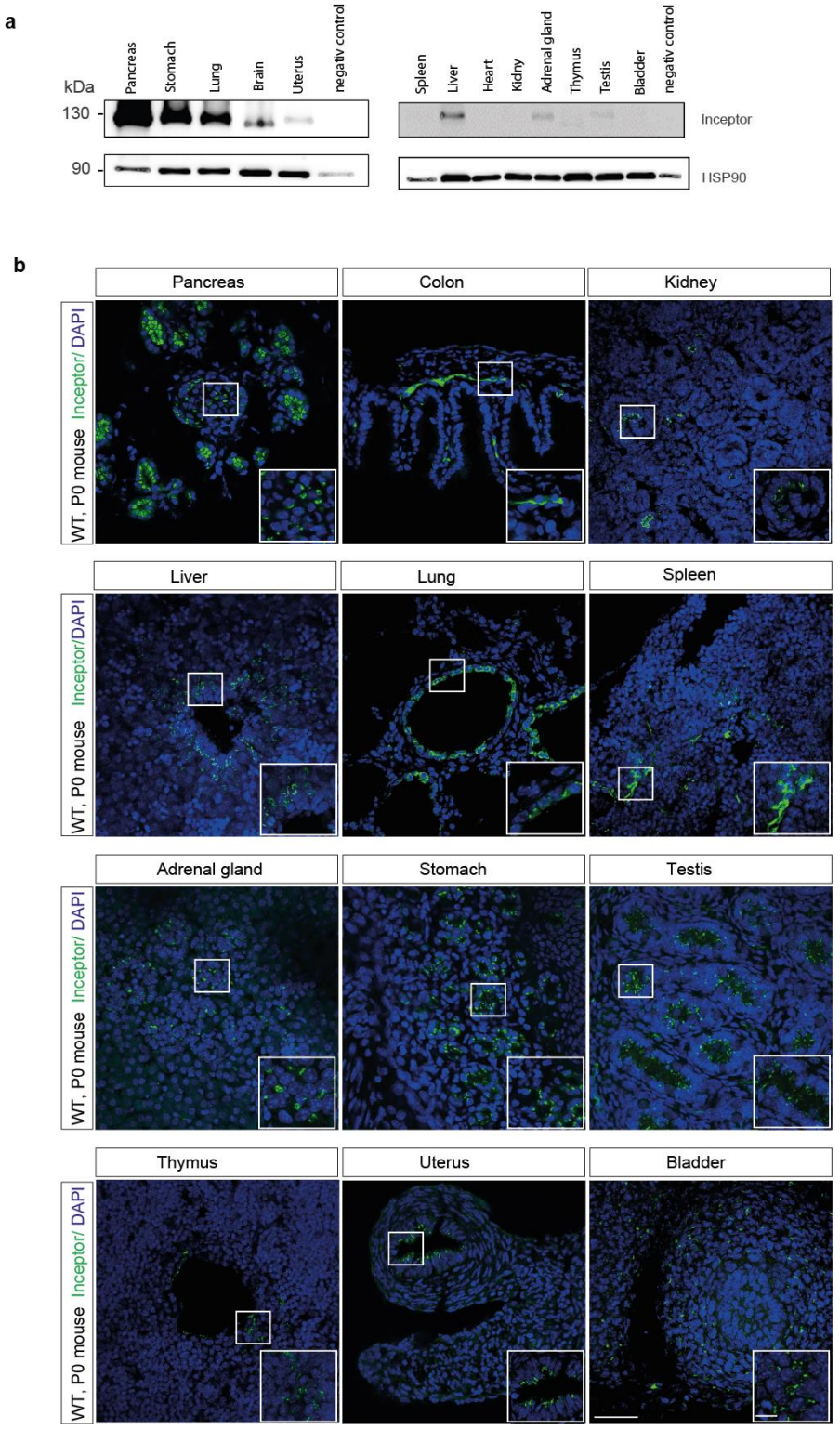

Figure 4.3: Inceptor is widely expressed in mouse tissues

a. Western blot analysis of lysates of different organs of P0 CD1 WT animals using monoclonal rat antibody (14F1).
b. Images from P0 CD1 mice organs immunostained with monoclonal inceptor antibody;16F6 (green). Scale bar, 50 µm.

To understand which brain cell types express inceptor, we performed immunostaining for inceptor expression from P0 mice brains. Interestingly, inceptor positive cells could be detected in different brain region, such as the hypothalamus, cortex, anterior pituitary, hippocampus and amygdala (Figure 4.4), suggesting a potential function of inceptor in the brain.

Amygdala consist of basolateral complex, the cortical nucleus, the medial nucleus, the central nucleus, and the intercalated cell clusters. Since the amygdala is a tiny region in the brain, it is difficult to recognize the divided regions or the morphology of amygdala with a DAPI staining. Therefore, we are not able to assume in which region of amygdala the inceptor is express. The developing cortex in mouse at P0 is divided by marginal zone (MZ), cortical plate (CP), intermediate zone (IZ) and Ependymal layer (EP). Inceptor is modestly expressed between CP and IZ suggest inceptor expression by migrating neurons (Figure 4.4). The hippocampus, including the dentate gyrus, has the shape of a curved tube, which consist among other of *Cornu Ammonis.* Its abbreviation CA is used in naming the hippocampal subfields CA1, CA2 and CA3 It can be distinguished as an area where the cortex narrows into a single layer of densely packed pyramidal neurons. Inceptor seems to be expressed in all regions CA1-3 and dentate gyrus. In addition, in pituitary gland inceptor is in the adenohypophysis (anterior pituitary gland) expressed (Figure 4.4).

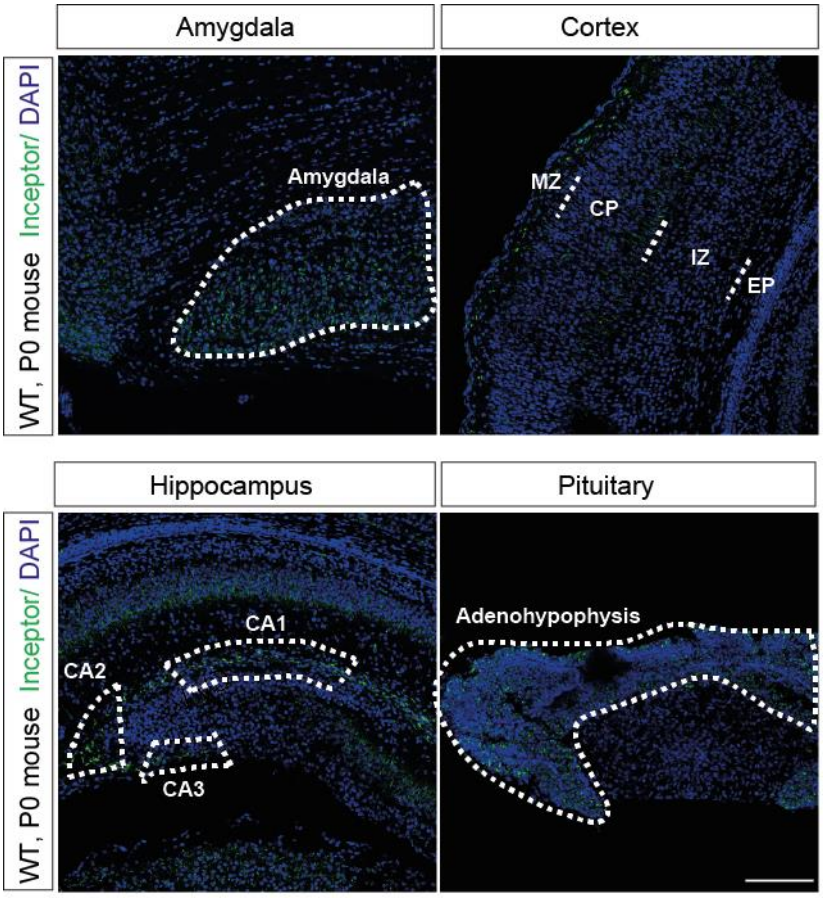

Figure 4.4: Inceptor is highly expressed in brain.

Images from P0 CD1 mice organs immunostained with monoclonal inceptor antibody;16F6 (green). Scale bar, 50 µm.

Taken together, we show that endogenous inceptor protein detected by monoclonal antibody is expressed mainly in different regions of the brain, gastrointestinal tract as well as sex-specific organs. However, identity of the cells types of the described organs which express inceptor has to be investigated by specific cell type markers. In summary, inceptor is primarily expressed in secretory and endocrine cells of different organs.

4.1.2.2 Expression of inceptor in pancreatic compartment during embryonic development

We initially identified inceptor to be highly expressed in the endo- and exocrine pancreas. In order to characterize the temporal expression profile of inceptor, we carried out immunostaining of pancreas from stage E11.5, E14.5, E16.5 and E18.5. Inceptor expression was not detected at E11.5 (data not shown) and was first expressed E14.5 onwards. At E14.5 stage, inceptor was co-expressed with endocrine cells stained with the pan-endocrine marker chromogranin A (ChgA) at low levels. However, the staining intensity of inceptor was stronger at E16.5 and seems to be increased at E18.5, suggesting an age dependent inceptor expression in the endocrine compartment (Figure 4.5a). Next, we could detect inceptor in ductal cells marked by Sox9 at E14.5 in the pancreas. Reduced levels of ductal cells correlated with weak staining signal intensity of inceptor in ductal cells at E16.5, which is more reduced at E18.5 (Figure 4.5b). Additionally, inceptor could be detected in acinar cells stained with Amylase at E14.5. At E16.5 as well as E18.5 the staining signal intensity is comparable with detected inceptor signal intensity in acinar cells at E14.5 (Figure 4.5c).

Taken together, the expression of inceptor seems to be evenly strong in all pancreatic epithelial compartments (ductal, acinar and endocrine). However, from E16.5 onwards, the staining signal intensity of inceptor is more pronounced in endocrine cells. Particularly, at E18.5 there are many inceptor positive cells, which were co-positive for ChgA (Figure 4.5a).

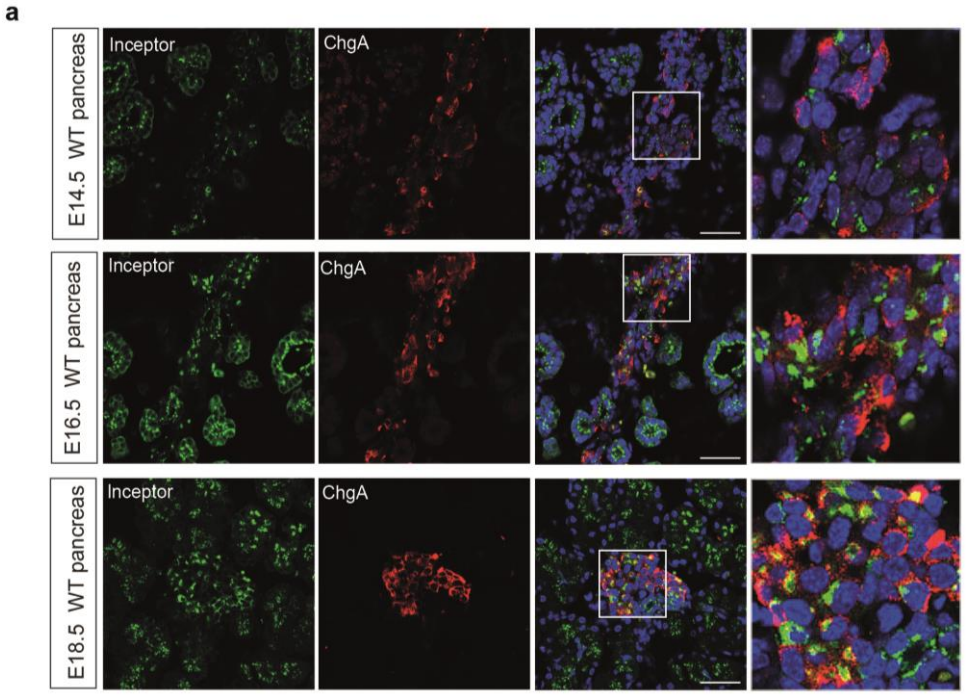

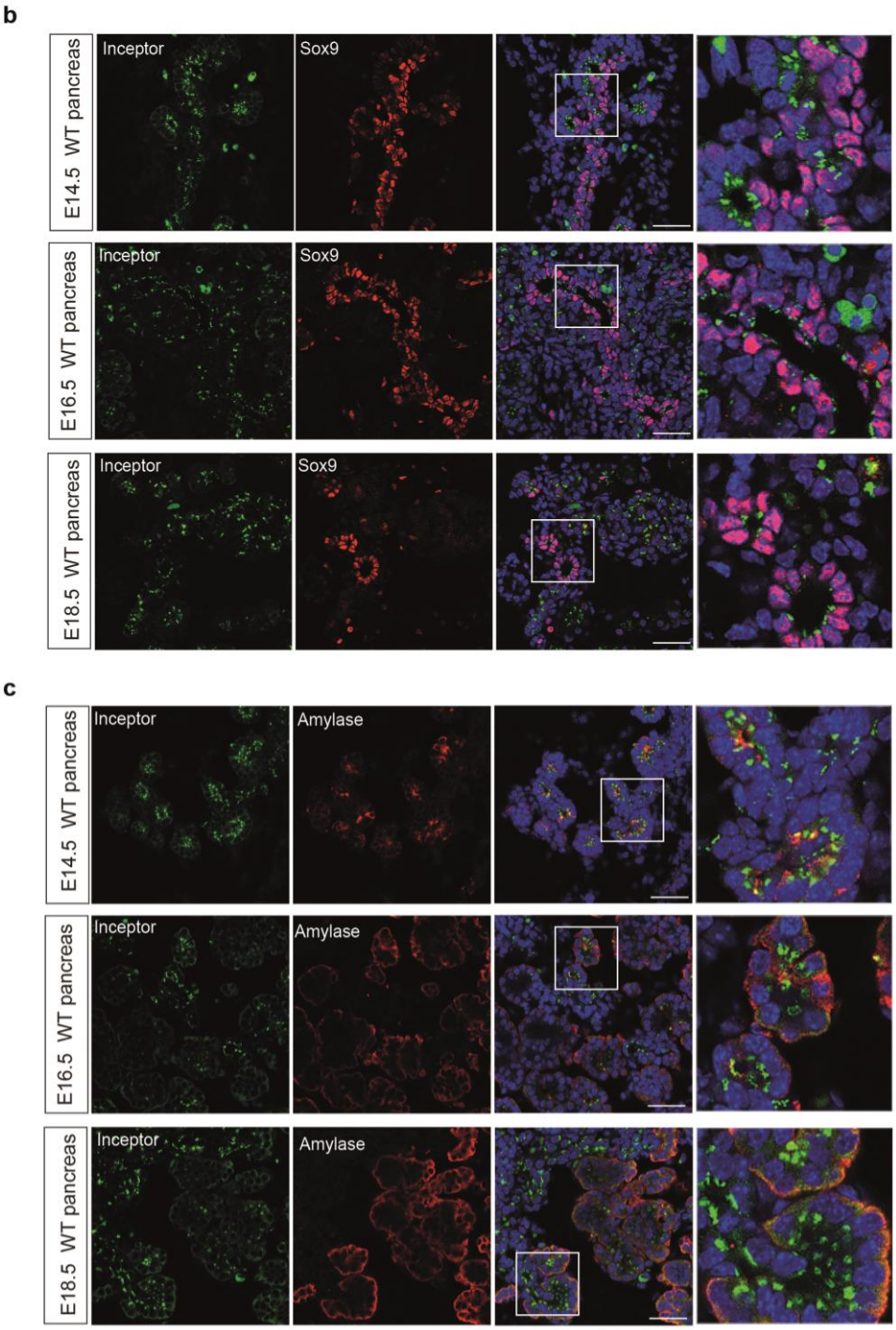

Figure 4.5: Inceptor expression during pancreas development

a. Representative immunostaining showing co-localization of inceptor (green) with endocrine (ChgA, red) cells at different embryonic stages (E14.5, E16.5 and E18.5).
b. Confocal images of showing expression of inceptor (green) in ductal cells (Sox9, red) in E14.5, E16.5 and E18.5.
c. Immunostaining showing the expression of inceptor (green) in exocrine cells (Amylase, red) cells in the embryonic pancreas at E14.5, E16.5 and E18.5. Scale bar, 50µm.

4.1.2.3 Inceptor expression in endocrine hormone-producing cells

While inceptor was expressed in ductal, exocrine and endocrine cells, we next wanted to analyze the endocrine cell type specific expression in the forming islets of Langerhans. Therefore, we performed immunohistochemical studies using adult WT mouse islets to determine the expression of inceptor in glucagon-expressing α cells, insulin-expressing β cells and somatostatin-expressing δ cells. Inceptor was clearly expressed in both α, β cells and δ cells (Figure 4.6). Interestingly, we observed that inceptor is closely localized to the nucleus, in the ER-Golgi-lysosomal region, as known from proteins containing M6PR domains (Ansarullah et al., 2021).

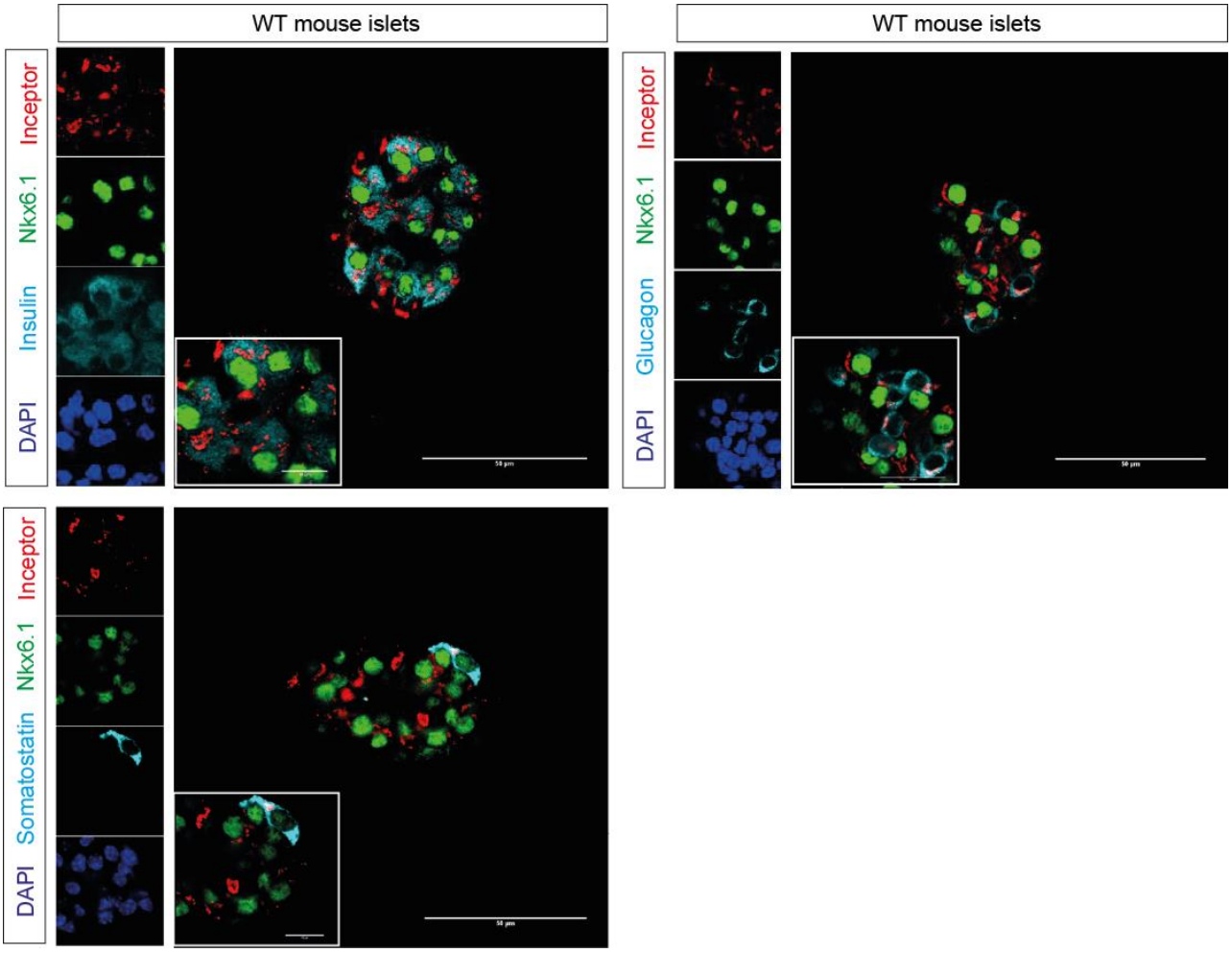

Figure 4.6: Inceptor expression in different endocrine cell types.

Confocal images showing expression of inceptor (green) in the β, α and δ cells in adult (6 months old) islets of WT mice. Insulin, Glucagon and somatostatin positive cells (Cyan). Scale bar, 50µm.

4.1.3 Generation of *Iir*$^{-/-}$ full-body KO (ΔEx3) mouse line

Due to domain structure similarities of inceptor to IR/IGF-R as well as high expression of inceptor in the pancreas where insulin is synthesized, we hypothesized that inceptor might be a regulator of Insulin/IGF signaling. To test this idea, we generated a full-body ko (*Iir*$^{-/-}$) using embryonic stem cell (ESC) clones derived from the European Conditional Mouse Mutagenesis Program (EUCOMM, http://www.mousephenotype.org/).

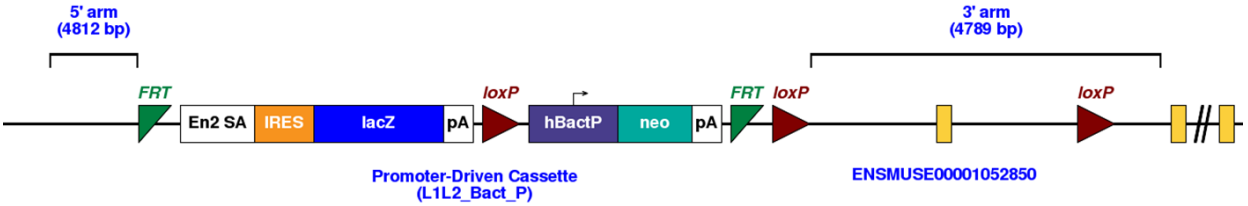

Figure 4.7: Gene trap allele with the *LacZ* reporter and NeoR cassette as well as LoxP and FRTsites.

(Abbreviations: En2 SA= splice acceptor of mouse exon 2; IRES= internal ribosome entry-site; *lacZ*=β-galactosidase; pA= SV40 large T gen; hbAP= human beta act promoter; neo=neomycin).

4.1.3.1 Design and generation of *Iir* targeting vector

To generate a full-body ko (*Iir* $^{-/-}$) mice, we use the EUCOMM strategy. The targeting vector was designed to target the critical exon-3 in the *Iir* gene. Deletion of exon 3 leads to frame-shift and a premature stop, when the upstream exon-2 splices into the downstream exon-4. The *Iir*-targeted KO allele consisted of an inserted internal ribosome entry-site (IRES)/*LacZ*-promoter driven Neo targeting cassette. Insertion was located upstream of the critical exon by recombination in the 5´-and 3´-homology arms. The *lacZ*-cassette comprised of a splice acceptor of mouse exon 3 (En3SA) next to the IRES. Both these elements together with *lacZ* gene were fused to a polyadenylation site from the SV40 large T gene (PA). The *lacZ*-gene is needed for β-galactosidase activity, whereas PA site terminate the transcription of the reporter gene. A human β actin promotor (hbAP), which is *loxP* flanked acts as a promotor for the neomycin resistance.

The knockout-first strategy to produce a knockout targeting of the *5330417C22RIK/Iir* locus in ESC was achieved by the European Mouse Mutagenesis consortium (EUCOMM). Aβgeo cassette (including the genes encoding β-galactosidase and neomycin) flanked by *FRT* sites was inserted into intron 2 of the intact *5330417C22RIK/Iir* gene. Additionally, exon-3 was flanked by *loxP* sites for optimal deletion of the targeted locus. The EUCOMM clone *5330417C22RIK/Iir* $^{tm1a(EUCOMM)Hmgu}$ (clone number HO3) ESC were aggregated with CD1 morula to generate chimeric mice. To delete the critical exon, gene-trap mice were crossed with *Rosa26R-Cre* to generate *Iir*$^{+/-}$ mice used for intercrosses to obtain *Iir*$^{-/-}$.

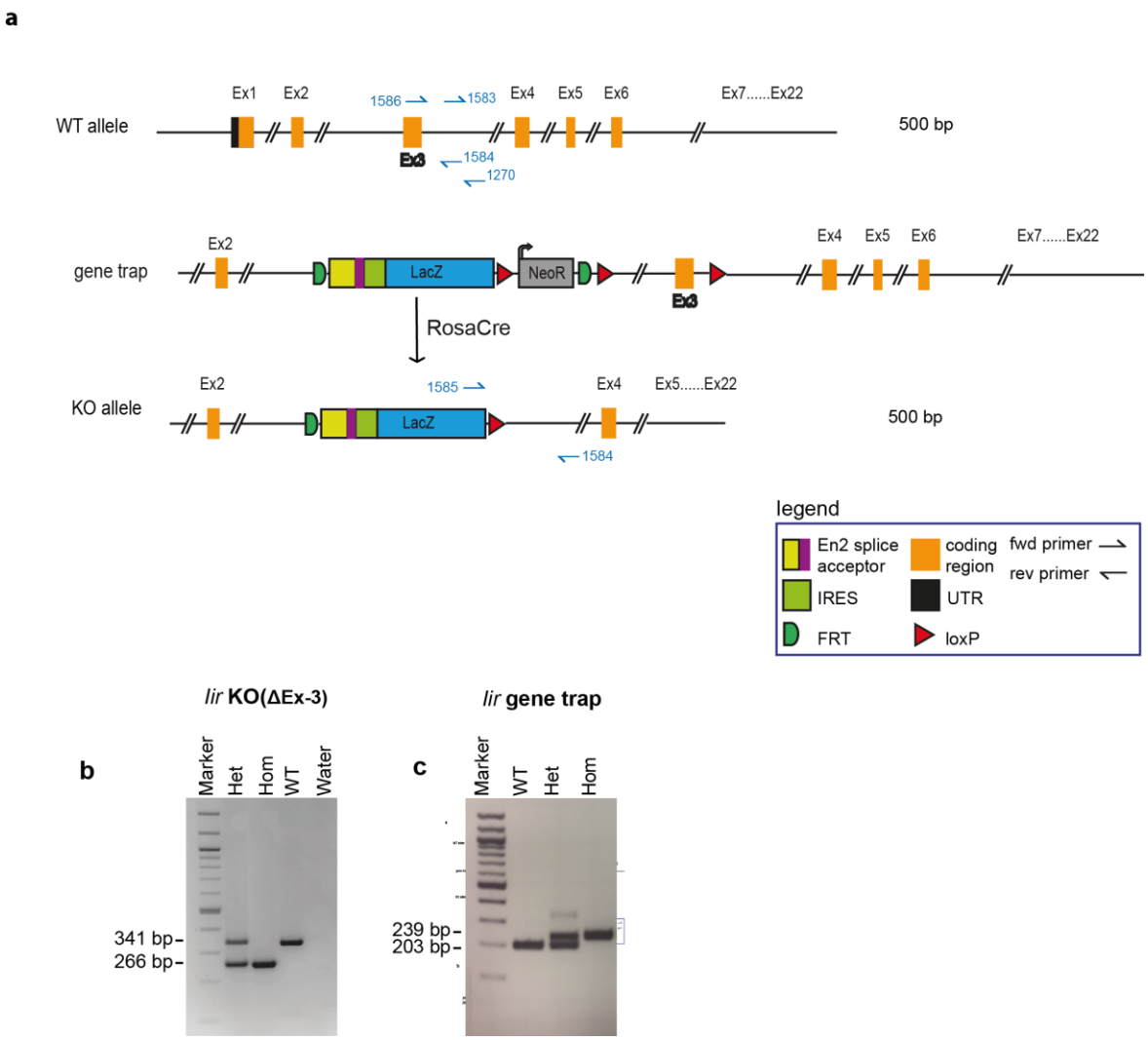

Figure 4.8: Generation and genotyping of full body *Iir*$^{-/-}$ mice.

a. WT allele comprises of 22 exons. The targeted allele can be distinguished between the WT allele by genotyping using the Primer EP 1584 and 1583.The exons are marked by orange boxes. Site-specific recombinase Cre (loxP sites, red arrow) and Flp-e will achieve conditional knockout. The figure is on scale. **b.** Genotyping of full body (*Iir*$^{+/+}$, *Iir*$^{+/-}$ and *Iir*$^{-/-}$). Cre mediated intercrosses *Iir*$^{-/-}$ were genotyped with specific primer for *Iir*$^{-/-}$ allele. The PCR product resulted in a WT band of 341 bp and the KO allele *Iir*$^{-/-}$ of 266 bp. **c.** Gene-trap (WT, *Iir*$^{+/GT}$, *Iir*$^{GT/GT}$) animals. To distinguish between WT and *Iir*$^{GT/GT}$ allele, genotyping was carried out with specific primers, resulting in a PCR product for the WT allele of 203 bp and 239 bp for the targeted *Iir*$^{GT/GT}$ allele.

Western blot analysis of pancreas lysate from the genotypes *Iir*$^{GT/GT}$, *Iir*$^{GT/+}$ and WT showed one predicted band in WT mouse which is attenuated in *Iir*$^{GT/GT}$ (data not shown). The different protein expression level of inceptor indicated a hypomorphic allele for *Iir*$^{GT/GT}$. As this might complicate *in vivo* analysis, we crossed the *Iir*$^{GT/GT}$ mouse with Rosa26 Cre reporter line (Figure 4.8a). The Rosa Cre mediates excision of the loxp-flanked neo cassette and critical exon 3.

To test whether the β-galactosidase (*lacZ*) reporter could be used to detect tissues and cells that express inceptor, we performed β-galactosidase stainings in whole organs and tissue sections of *Iir*$^{+/GT}$ and *Iir*$^{GT/GT}$ animals. Next, we analyzed the offspring of intercrossing of gene-trap allele into the Rosa26 Cre reporter line. Next, we observed *Iir* reporter gene expression in the embryo at E14.5. At this stage *β-gal* activity appears to be actively transcribed. In different pancreatic regions the cells showed weak expression, while the endocrine cells seemed to exhibit a strong pattern of the *lacZ* reporter gene (Figure 4.9). In the lung, the *lacZ* reporter gene activity could be observed in the trachea and large bronchioles in a dose-dependent manner, i.e. one vs two reporter alleles. Moreover, the *lacZ* expression pattern was identical in *Iir*$^{+/GT}$ and *Iir*$^{GT/GT}$ lungs indicating that lung epithelial development occurred normal upon inceptor knock-out.

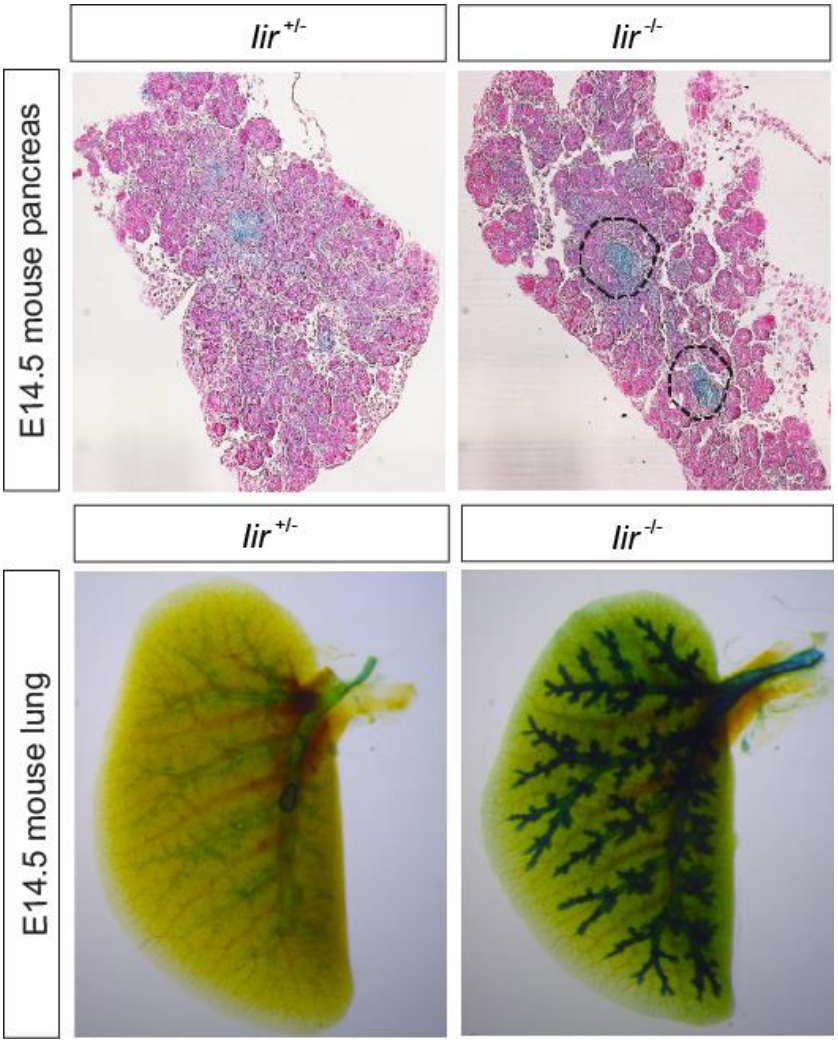

Figure 4.9: Schematic reperesentation of *lacZ*-reporter analysis

β-gal activity starts in the pancreas and lung at E14.5. *lacZ* reporter activity is visible in the pancreas of both *Iir*$^{+/-}$ and *Iir*$^{-/-}$ (upper panels). The expression of *lacZ* in the lung of *Iir*$^{+/-}$ and *Iir*$^{-/-}$ shows dose-dependency and seems restricted to the lung epithelium.

4.1.4 Gene functional analysis of the insulin inhibitory receptor *in vivo*

4.1.4.1 Validation of deletion efficiency of full-body KO (ΔEx3) mouse line

To confirm the deletion efficiency of inceptor protein in *Iir*$^{-/-}$ mice, we performed immunostaining and Western blot using polyclonal anti-inceptor antibodies. As expected, inceptor expression was undetected in *Iir*$^{-/-}$ mice (Figure 4.10a).

In SDS-PAGE in WT pancreas lysates the generated rabbit antibody recognizes specifically protein at ~130kDa, whereas the lysate from *Iir*$^{-/-}$ mice showed no band in expected protein size, which that deletion of exon 3 leads to a loss-of-function allele (Figure 4.10b).

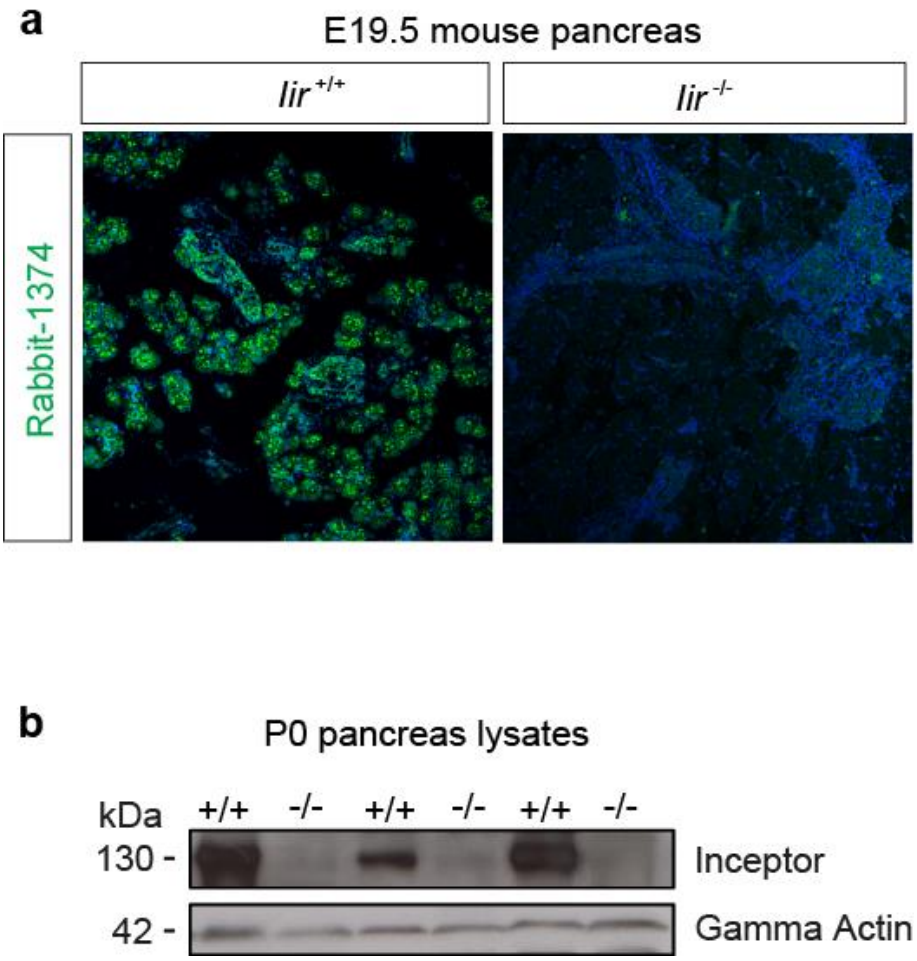

Figure 4.10: Confirmation of KO efficiency in *vivo*.

a. Immunofluorescence images of the detection of inceptor in the pancreas of E19.5 embryos from *Iir*$^{+/+}$ and *Iir*$^{-/-}$ mice using rabbit (1374) anti-inceptor antibody (only background staining visible).
b. Detection of inceptor in pancreas lysate of E19.5 *Iir*$^{-/-}$ and *Iir*$^{+/+}$ animals by Western blot analysis. Antibody: Pineda (Clone # Animal-3) rabbit polyclonal.

4.1.4.2 *Iir*$^{-/-}$ embryos show normal morphology

Histological analysis showed normal tissue morphology between *Iir*$^{+/+}$ and *Iir*$^{-/-}$ embryos using C-section at E19.5. The pancreas anatomy of both *Iir*$^{+/+}$ and *Iir*$^{-/-}$ mice showed microscopically normal pancreatic tissue architecture which has a lobular structure. The majority of the lobule is composed of acinar tissue. Islets of Langerhans (arrowhead) are distributed throughout the pancreas. A branched pancreatic ductal system (arrow) is also present in WT and KO (Figure 4.11). The kidney also did not show any cross morphological differences between WT and KO mice at E19.5. The outer region called renal cortex contains many small, round renal corpuscles, much of the tubule system and blood vessels. The renal medulla (arrowhead), the region internal to the cortex that contains parallel tubules (nephron loops, collecting tubules and collecting ducts) and blood vessels. The absence of renal corpuscles distinguishes the medulla. The liver Hematoxylin and eosin stain (H&E) images illustrate a similar anatomy of both image of both WT and KO liver sections. The hepatocellular cords (HC) are mostly one or two layers thick and are divided into three zones: acinus, and periportal, mid-, and centrilobular zones of the lobule. Blood flows from the portal tract (PT) to the central vein (CV), also referred to as terminal hepatic venule. In the lung tissue images, we could identify tubular branches called respiratory bronchiole (RB). The bronchioles eventually end up in clusters of microscopic air sacs called alveoli, which have extremely large surface area and make up the major part of the lung. Each alveolus is a small air space surrounded by an epithelium.

In conclusion, we could not observe any cross morphological differences between the *Iir*$^{+/+}$ and *Iir*$^{-/-}$ pancreas, kidney, liver and lung in terms of size, anatomy and morphology in tissue sections at E19.5 (Figure 4.11).

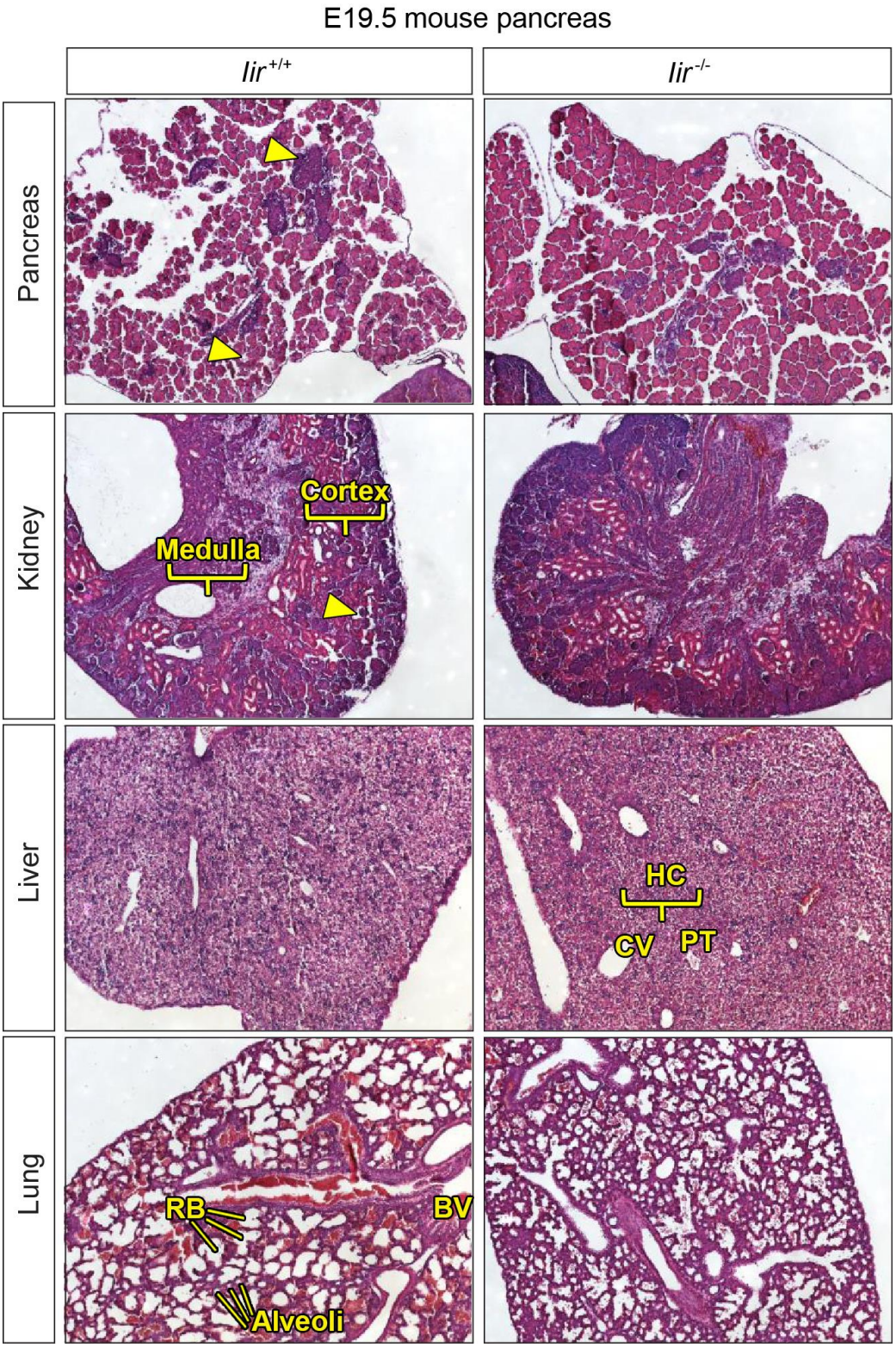

Figure 4.11: No morphological differences in *lir*$^{-/-}$ organs in E19.5 animals.

Paraffin fixed and H&E stained histological images from *lir*$^{+/+}$ (left panels) and *lir*$^{-/-}$ (right panels) E19.5 mouse tissues. Cell nuclei (blue), red blood cells (red), extracellular material (pink) and airspaces (white). The sections were under the microscope at 40x magnification.

4.1.5 Analysis of postnatal death of *Iir*$^{-/-}$ mice

Phenotypically *Iir*$^{-/-}$ mutants were born without any developmental defects and died within 2-5 h postpartum displaying signs of lethargy, respiratory distress and cyanotic episodes. Between hours after birth at P0, absence of the milk in the stomach were noticed in *Iir*$^{-/-}$ pups, whereas *Iir*$^{+/+}$ pups did not exhibit this phenotype (Figure 4.12a).

To analyze the effects of inceptor deletion on lethality, mendelian ratio of embryos and pups between E14.5 and P7 was calculated. The observed mendelian ratio for KO was 30% (25% expected using heterozygous intercrosses) until E19.5, however, after birth, there was a decline to 19% and after postnatal day 1 only 6% mutant animals were recorded (Figure 4.12c). This suggested that on the given background (mixed C57BI6/J and N), inceptor KO leads to perinatal or early postnatal lethality.

We next measured the body weight of neonate's animals at E19.5. Body weight of E19.5 pups showed no significant differences (Figure 4.12b), suggesting that inceptor does neither regulate embryonic development, nor growth or proliferation.

a

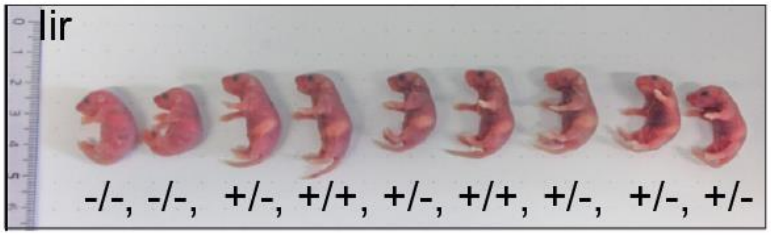

b

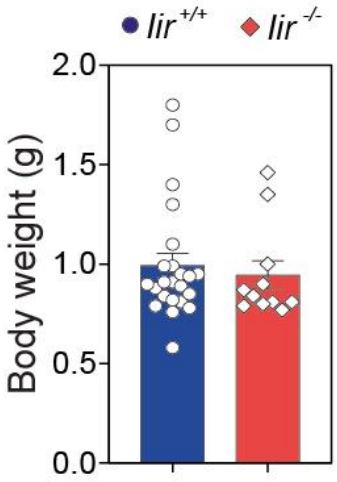

c

Age	n	Iir +/+	Iir +/-	Iir -/-
prenatal	280	27%	54%	19%
E19.5	312	27%	43%	30%
P0	336	30%	51%	19%
postnatal	179	37%	57%	6%

Figure 4.12: Morphology, body weight and mendelian ratio of *Iir*$^{-/-}$ mice

a. Look of neonates at P0, which were obtained from an *Iir*$^{+/-}$ intercross with their genotype.
b. Monitoring of body weight of neonates at E19.5 from *Iir*$^{+/-}$ intercross.
c. Mendelian ratio indicating embryonic stages E7.5-E19.5 or 1-7 days after birth (P1-7). Percentages of *Iir*$^{+/+}$, *Iir*$^{+/-}$ and *Iir*$^{-/-}$ embryos and total number of analyzed embryos (n) (Ansarullah et al., 2021).

4.1.5.1 *Iir*$^{-/-}$ mice shows hyperinsulinemia and hypoglycemia

Since *Iir*$^{-/-}$ newborn pups showed absence of milk in the stomach, we measured blood glucose levels from newborn mice immediately after birth. However, we could not observe any significant changes in blood glucose level immediately after birth. Due to the fact that *Iir*$^{-/-}$ newborn mice die within hours after birth, we fasted the *Iir*$^{-/-}$ mice for 5 h. After 5 h starvation, the blood was collected and the fasting blood glucose was measured by Mutarotase-GOD method. Surprisingly, blood glucose levels were drastically reduced in *Iir*$^{-/-}$ mice (Figure 4.13a), and the *Iir*$^{-/-}$ newborn pups were hypoglycemic.

To investigate if the hypoglycemia in *Iir*$^{-/-}$ newborn mice was because of excessive insulin secretion, we quantified serum insulin levels by an enzyme-linked immunosorbent assay (ELISA). Interestingly, we observed that the insulin concentration in *Iir*$^{-/-}$ E19.5 pups was significantly elevated compared to *Iir*$^{+/+}$ pups (Figure 4.13b).

Hyperinsulinemia can be caused by a hypersecretion of insulin from β-cell due to increased insulin content. We next examined the insulin content in pancreas, from mice, which were fasted for 2h and quantified insulin content. As expected, pancreatic insulin concentration in *Iir*$^{-/-}$ E19.5 pups was significantly increased as compared to the *Iir*$^{+/+}$ pups (Figure 4.13c).

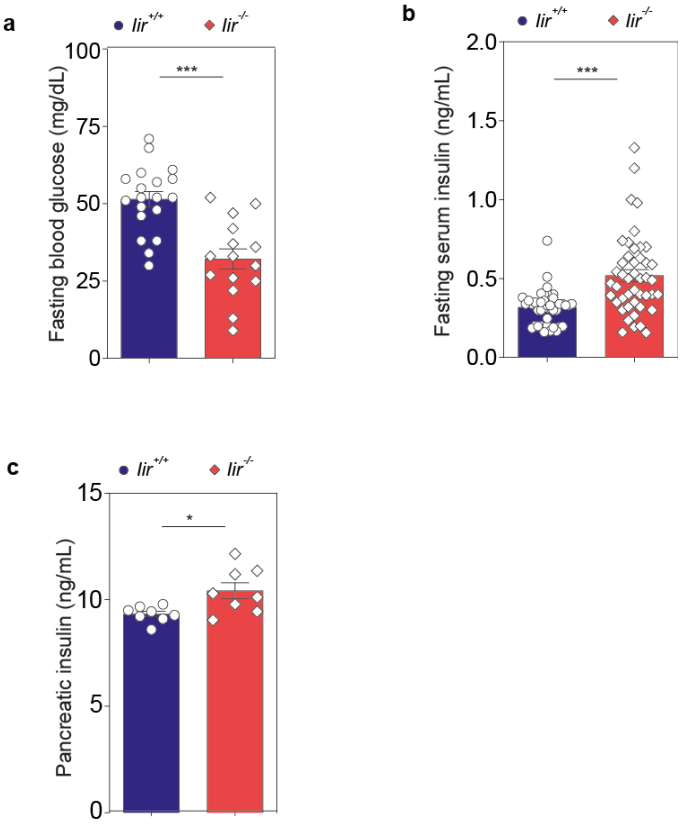

Figure 4.13: *Iir*$^{-/-}$ new born mice show hypoglycemia and hyperinsulinemia phenotype.

a. Measurement of fasting blood glucose levels of pups at E19.5 (n=19, *Iir*$^{+/+}$; n=15, *Iir*$^{-/-}$; P<0.0001).
b. Analysis of fasting serum insulin levels of E19.5 pups (n=44, *Iir*$^{+/+}$; n=45, *Iir*$^{-/-}$; P<0.0001).
c. Total insulin content of pancreas isolated from *Iir*$^{+/+}$ and *Iir*$^{-/-}$ mice at E19.5 (n=8; P<0.05).
Data are mean ± s.e.m. Significance was calculated using unpaired t-test. (Ansarullah et al., 2021).

4.1.5.2 β-cell area was increased in *Iir*$^{-/-}$ pups

While *Iir* $^{-/-}$ revealed increased in pancreatic and serum insulin levels, we next investigated whether or not there was an increase in β-cell area. We carried out morphometric immunohistochemistry from the entire pancreas to quantify the β-cell area (in collaboration Analytical Pathology Unit). Interestingly, we found a significant increase in the β-cell area at E19.5 in *Iir*$^{-/-}$ compared to the *Iir*$^{+/+}$ pancreas (Figure 4.14a). To examine contributions from α-cells, we also performed morphometric quantifications for α-cell area as well as quantified circulating serum glucagon levels. Quantifications revealed that there was no difference in the α-cell area and serum glucagon levels in *Iir*$^{+/+}$ and *Iir*$^{-/-}$ E19.5 pups (Figure 4.14b-c).

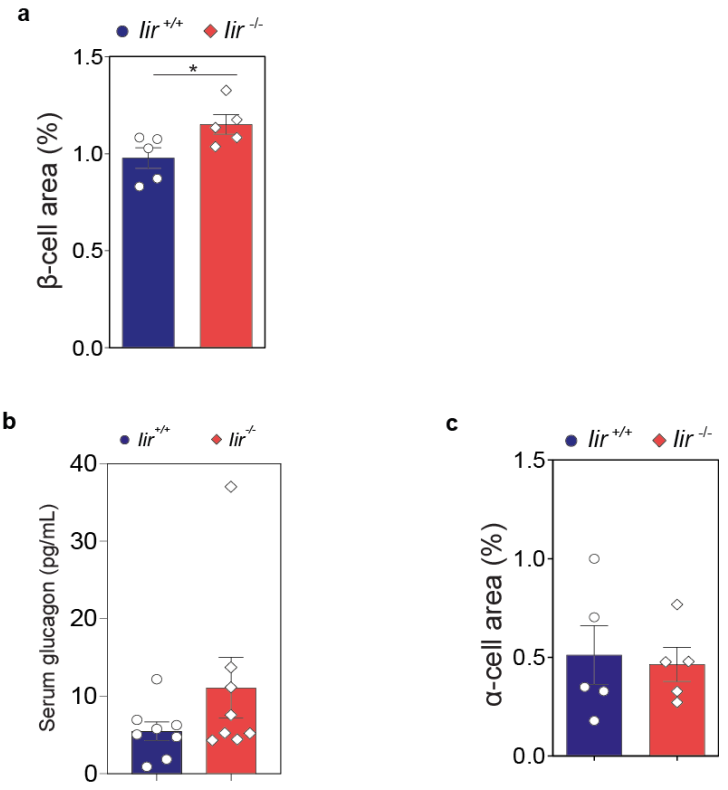

Figure 4.14: Elevated β-cell area in *Iir*$^{-/-}$ pups.

a. Quantification of β-cell area using immunofluorescence images of *Iir*$^{+/+}$ and *Iir*$^{-/-}$ pancreatic sections at E19.5 mice (n=5; data are mean ± s.e.m.; P=0.0438). Significance was calculated using unpaired t-test.
b. Analysis of serum glucagon levels after 2-5 h starvation at E19.5 (*Iir*$^{+/+}$, n =8; *Iir*$^{-/-}$, n = 8, Data are mean ± s.e.m.; P=0.20,).
c. Quantification of α-cell area using immunofluorescence images of *Iir*$^{+/+}$ and *Iir*$^{-/-}$ pancreatic sections at E19.5 mice (n=5; data are mean ± s.e.m.; P=0.7906). (Ansarullah et al., 2021).

4.1.5.3 Inceptor knock out pups exhibit increased endocrine proliferation

We reasoned the increase in β-cell area and next sought to quantify endocrine cell proliferation using EdU/Chromogranin-A co-immunostaining. To label the proliferating cells we injected 5-ethynyl-2'-deoxyuridine (EdU) to the pregnant dams during gestation periods- G14.5, G16.5 and G18.5. After 2h of EdU injection, the pancreases were dissected, fixed and processed for paraffin immunohistochemistry. Sections were immunostained for ChgA to assess proliferation in endocrine (ChgA+) and non-endocrine (ChgA-) cells. To analyze the EdU positive cells, Click iT EdU detection kit Alexa flour 647 was used. All images were scanned and quantified as detailed in the methods section (the percentage was estimated by dividing EdU/ChgA co-positive cells over total ChgA positive area).

Interestingly, the *Iir*$^{-/-}$ pups exhibited significant increase in endocrine proliferation at E16.5 stage and a modest increase during E14.5 and E18.5 – yet did not reach statistical significance. (Figure 4.15). Overall, increase in β-cell area corroborate with the increase in endocrine proliferation and specifically β-cell proliferation as α-cell area remained unchanged.

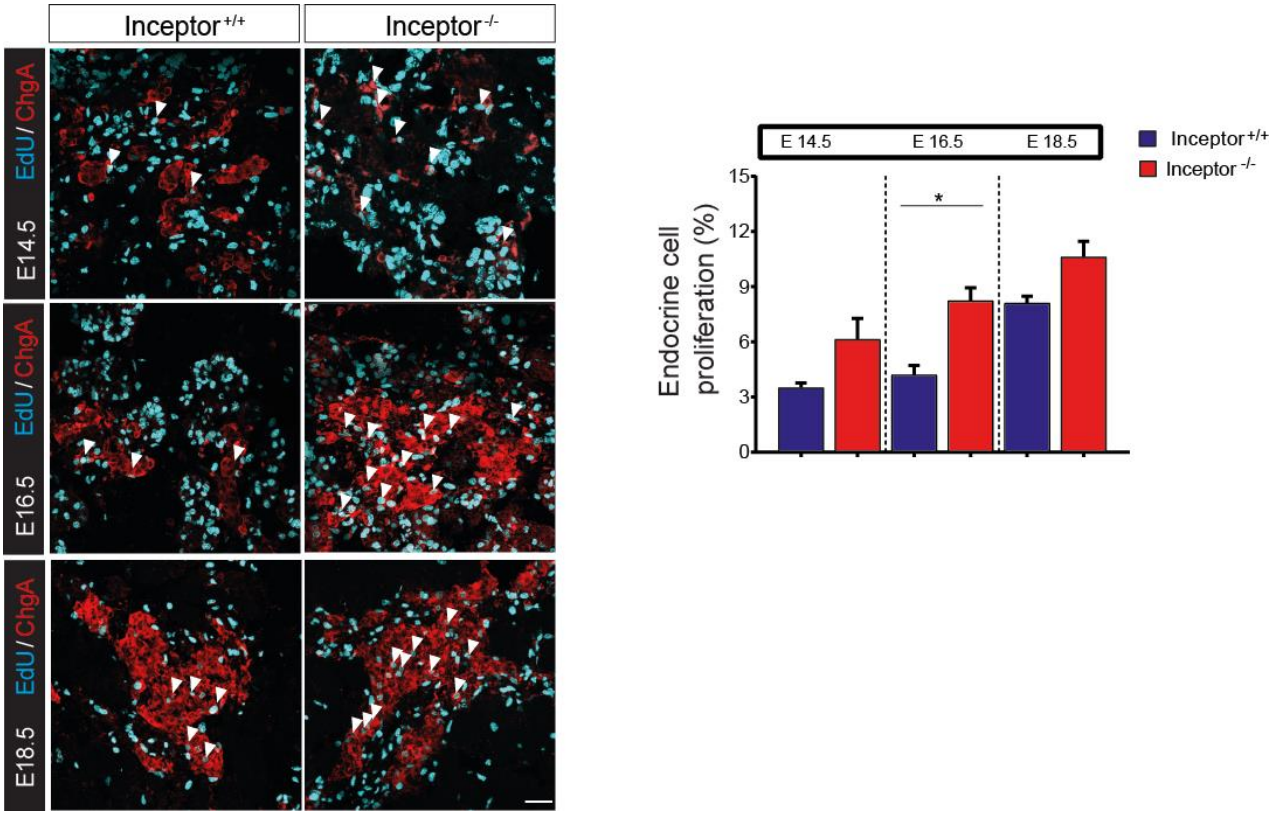

Figure 4.15: Increased in endocrine cell proliferation in *Iir*$^{-/-}$ mice.

Representative confocal images of EdU positive cells (cyan) and ChgA positive cells (red) in *Iir*$^{+/+}$ and *Iir*$^{-/-}$ pancreata from E14.4, E16.5 and E16.5 (n=3 animals and 4-8 sections per animal). Double positive EdU and ChgA cells were normalized to total Chr-A positive cell. Scale bar, 60 µm. For quantification, see right panel.

Inceptor is expressed in all endocrine cell types (Figure 4.16). Therefore, we next analyzed the proliferation in β-, α-, δ- and PP-cells cell types using immunohistochemistry at E16.5 and E18.5. Analyzing the proliferation of endocrine subpopulations (β-, α-, δ- and PP-cells) was intended to identify the source of the increased ChgA+ endocrine proliferative cells. To do this, EdU was injected intra peritoneal (i.p.) at G16.5 and G18.5 into pregnant mothers. After 2 h of EdU administration, the pregnant mothers were sacrificed and the pancreas of E16.5 and E18.5 embryos were sectioned and stained for Ins, Gcg, Sst and PP antibodies. The quantification of EdU^{+} β-cells confirmed an elevated proliferation rate in *Iir*$^{-/-}$ compared to *Iir*$^{+/+}$ animals in both E16.5 and E18.5 (Figure 4.16e). A higher sample size was needed to analyze the significant of this observation. Therefore, we performed a systematic immunohistochemistry from entire pancreas to quantify β-cell area (Chapter 4.1.5.2). The amounts of PP-cell, which incorporated EdU were

slightly increased in *Iir*$^{-/-}$ E16.5 and E18.5 pancreas in comparison with *Iir*$^{+/+}$ (Figure 4.16c). However, the analysis of Edu incorporation with both α- and δ-cells revealed an unaffected Proliferation rate in both E16.5 and E18.5 *Iir*$^{-/-}$ pancreas (Figure 4.16b and Figure 4.16e).

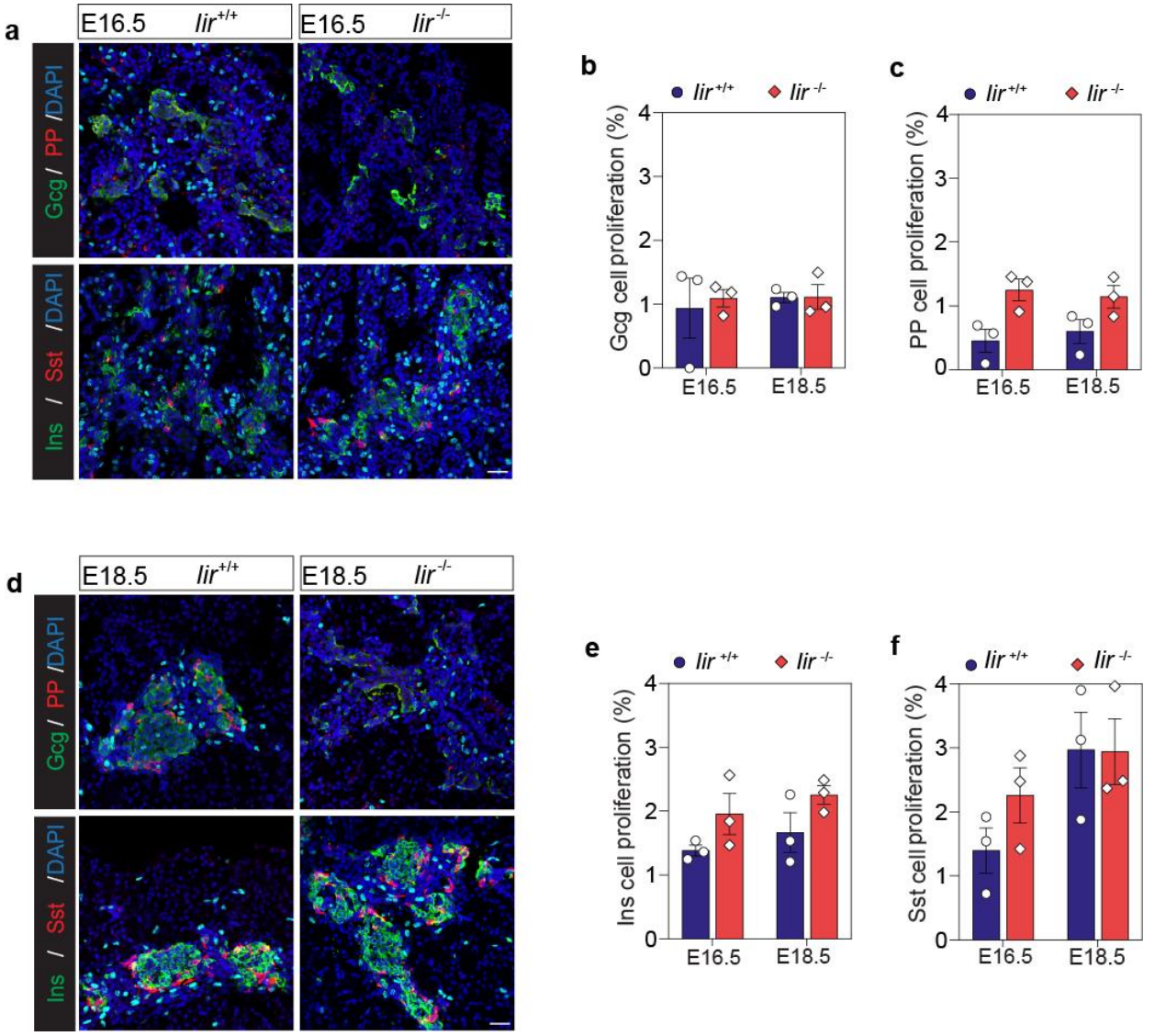

Figure 4.16: Effect of Inceptor deletion on proliferation of β-, α-, δ- and PP-cells.

a. Images from *Iir*$^{+/+}$ (n = 3) and *Iir*$^{-/-}$ (n = 3) embryos at E16.5 immunostained with Gcg (green), PP (red), DAPI (blue) and EdU (white) in upper panels; Ins (green), Sst (red), DAPI (blue) and EdU (white) in lower panels. Scale bar, 100 µm.
b. Quantification of α-cell proliferation in EdU^{+}/Gcg^{+} double-positive cells in *Iir*$^{+/+}$ and *Iir*$^{-/-}$ at E16.5 (*P* = 0.7433 and E18.5 (*P* =0.9280; unpaired *t*-test).
c. Quantification of PP-cell proliferation in EdU^{+}/PP^{+} double-positive cells in *Iir*$^{+/+}$ and *Iir*$^{-/-}$ at E16.5 (*P* = 0.6036) and E18.5 (*P* = 0.6938; unpaired *t*-test).
d. Images from *Iir*$^{+/+}$ (*n* = 3) and *Iir*$^{-/-}$ (*n* = 3) embryos at E18.5 immunostained with Gcg (green), PP (red), DAPI (blue) and EdU (white) in upper panels; Ins (green), Sst (red), DAPI (blue) and EdU (white) in lower panels. Scale bar, 100 µm.
e. Quantification of β-cell proliferation in EdU^{+}/Ins^{+} double-positive cells in *Iir*$^{+/+}$ and *Iir*$^{-/-}$ at E16.5 (*P* = 0.42820) and E18.5 (*P* = 0.4522; unpaired *t*-test).
f. Quantification of δ-cell proliferation in EdU^{+}/Sst^{+} double-positive cells in *Iir*$^{+/+}$ and *Iir*$^{-/-}$ at E16.5 (*P* = 0.1021) and E18.5 (*P* = 0.3679; unpaired *t*-test).
For Quantifications 3-6 sections were used per animal. Proliferative Ins, Gcg, Sst ad PP cells were normalized to all hormone positive cells. Data are mean ± s.e.m.

4.1.5.4 Inceptor negatively regulates Insulin/IGF signaling

All together our studies revealed a marked increase in β-cell mass resulting from enhanced proliferation parallel with increased circulating and pancreatic insulin content. To unravel signaling mechanisms governing these results, we examined the role of inceptor protein in regulation of the IR/IGF-IR signaling pathway. Whole pancreas lysate from E19.5 pups (5h starvation) were processed for Western blot analysis. As expected, inceptor expression was absent in *Iir*$^{-/-}$ pancreata lysate, hence confirming the successful knock-out strategy. In addition, *Iir*$^{-/-}$ pups triggered an increased upregulation of IR/IGF-IR phosphorylation relative to *Iir*$^{+/+}$ pups (Figure 4.17a-b). Furthermore, IR levels were significantly reduced, while the levels of IGF-IR remained unchanged (Figure 4.17), implying the role of inceptor in calibrating IGF-IR signaling pathway in *Iir*$^{-/-}$ β-cells.

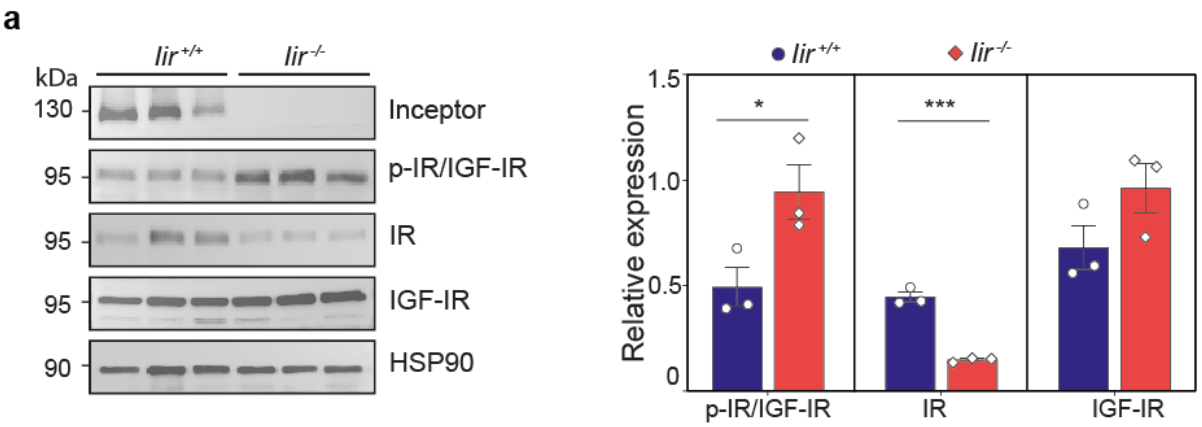

Figure 4.17: *Iir*$^{-/-}$ activates IR/IGF-IR signaling during nutritional starvation.

a. Representative Western blot images of E19.5 *Iir*$^{+/+}$ and *Iir*$^{-/-}$ pancreas. Pups were starved for 5 h before sacrificing. Quantification of insulin signaling in pancreata of 4-5 h starved pups at E18.5. p-IR/IGF-IR were normalized on the loading control heat shock protein-90 (HSP90) and total IR and IGF-IR (n=3 mice; p-IR/IGF-IR P=0.002; IR, P=0.0002; IGF-IR, P=0.1464). Significance was calculated using unpaired t-test. Data are mean ± s.e.m (Ansarullah et al., 2021).

Finally, to assess the impact of high glucose induction in Ins/IGF-I signaling pathway, we performed immunostaining using p-AKT antibody in *Iir*$^{-/-}$ pups with or without glucose induction. The phosphorylation levels of AKT were quite low in pancreata section of non-treated E19.5 pups but after 30 min of glucose injection, we observed a general increase in AKT phosphorylation. Interestingly, the qualitative analysis revealed that the AKT phosphorylation in *Iir*$^{-/-}$ section displayed an increase after 30 min of glucose induction when compared to *Iir*$^{+/+}$ section (Figure 4.18), which warrants further quantitative investigations. In summary, knock-out of inceptor leads to an upregulation of IR/IGF-IR signaling, suggesting that inceptor is a negative regulator of Ins/IGF signaling.

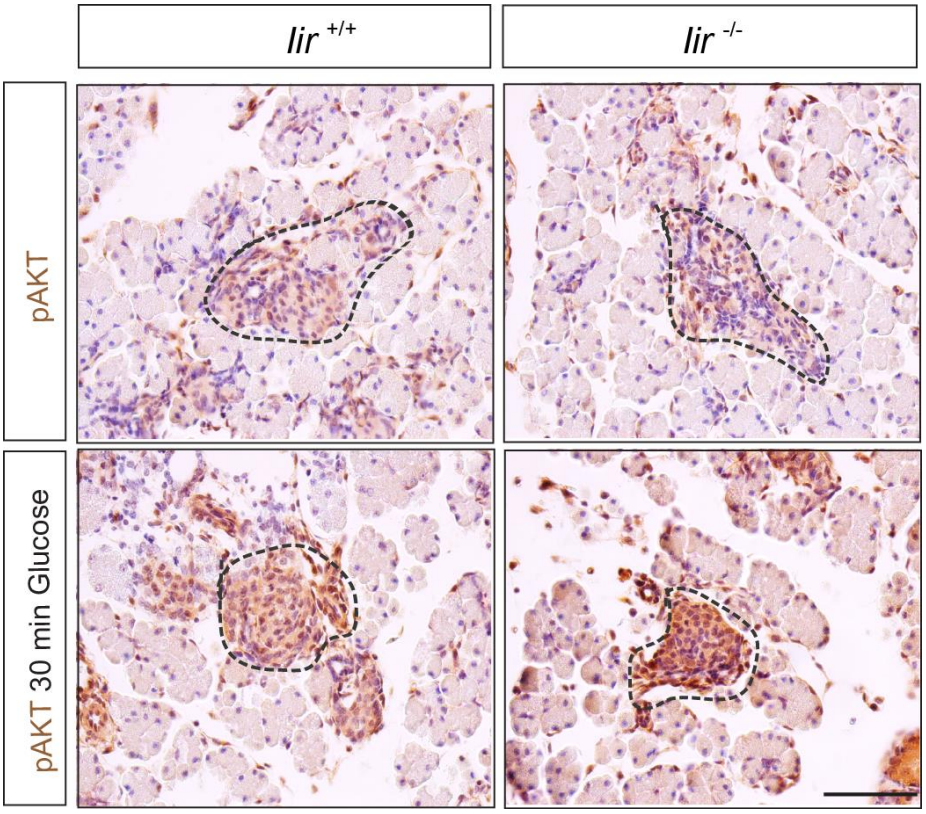

Figure 4.18: *lir*$^{-/-}$ activates phosphorylation of AKT upon glucose induction.

Representative immunohistochemical staining (DAB) images of E19.5 WT and *lir*$^{-/-}$ pancreas. The E19.5 pups were either injected or not with 10% glucose 30 min before analysis. Cell nuclei (blue), phosphorylated AKT (brown) and empty tissue spaces (white). Scale bar, 50 µm.

4.1.5.5 *lir*$^{-/-}$ new born pups could be rescued by glucose

To provide a hypothesis about the potential cause of death of *lir*$^{-/-}$ pups, we set up two different sets of experiments, which were carried out in P0 pups. As mentioned above, the *lir*$^{-/-}$ pups likely die due to hypoglycemia. As pancreatic islets regulate blood glucose regulation and the new born pubs presented with hypoglycemia and hyperinsulinemia, we wondered whether hypoglycemia could be the reason of postnatal lethality. To rescue the newborn pups from postnatal lethality, we injected 10% glucose every 6 h for 24 h into E19.5 pups. We have shown that 50% of the *lir*$^{-/-}$ pups could be rescued with glucose (Figure 4.19c), suggesting postnatal lethality due to hypoglycemia.

Furthermore, we designed a glucose tolerance test to evaluate the glucose elevation and rate of glucose disposal. Immediately after birth, individual P0 pups received 10% glucose (50 µl) and were sacrificed at 0, 15, 30, 60 and 120 min (Figure 4.19a). A significant decrease in the rate of glucose elevation were observed at time point 30 min in *lir*$^{-/-}$ pups (Figure 4.19b), suggesting an increased insulin secretion or sensitivity in *lir*$^{-/-}$ pups. Furthermore, these data support that the glucose clearance remain unaffected in *lir*$^{-/-}$ animals. Altogether, these experiments provided evidence that the *lir*$^{-/-}$ pups primarily die due to hypoglycemia.

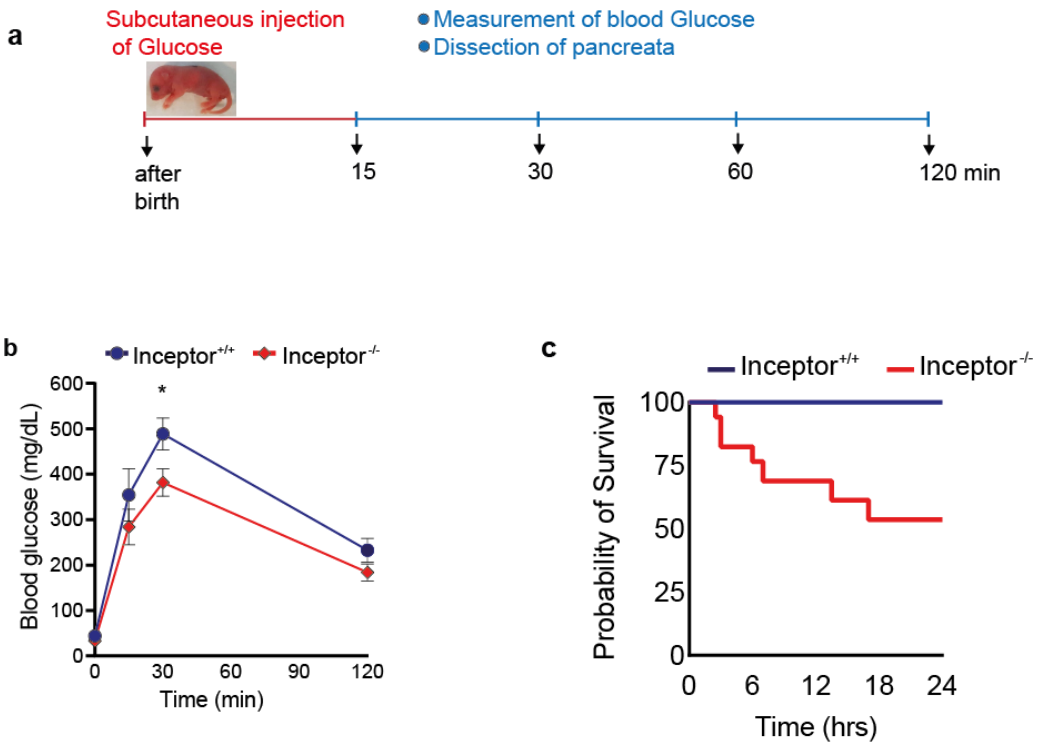

Figure 4.19: *Iir*$^{-/-}$ newborn mice could be rescued from death by glucose injection

a. Experimental design for the glucose tolerance test (GTT) in newborn mice.
b. Analysis of blood glucose levels during glucose tolerance test in *Iir*$^{+/+}$ and *Iir*$^{-/-}$ P0 pups (*Iir*$^{+/+}$, n = 6-12 each time point; *Iir*$^{-/-}$, n = 4-12 each time point). Data are mean ± s.e.m; * P≤0.05.
c. Kaplan Meier curve was used to estimate survival ratio of *Iir*$^{+/+}$ and *Iir*$^{-/-}$ P0 pups after glucose injection. Log rank (Mantel-Cox) test with Welch's t test compared the differences between the survival curves of *Iir*$^{+/+}$ and *Iir*$^{-/-}$ P0 pups (*** P ≤ 0.001) (*Iir*$^{+/+}$, n = 6; *Iir*$^{-/-}$, n = 12). (Ansarullah et al., 2021).

4.1.5.6 Inceptor knock-out islets show enhanced insulin secretion

Hyperinsulinemia can be caused by a hypersecretion of insulin from β-cells due to increased insulin content or an insulin secretion defect and can result in an enlarged β-cell mass in the pancreas. To identify a reason for hyperinsulinemia or any functional endocrine defects in *Iir*$^{-/-}$ mice, we analyzed insulin secretion of whole pancreas in E19.5 *Iir*$^{-/-}$ and *Iir*$^{+/+}$ pups in response to low, high glucose and KCl over 75 minutes. To assess glucose stimulated insulin secretion, we loaded pancreata on a nylon filter in a plastic perfusion chamber containing acrylamide-based microbead slurry using the BioRep perfusion system (Biorep Technologies, Miami, USA). Glucose, which is added to the KRBH buffer, triggers the first and second phase insulin secretion in a time-resolved manner. *Iir*$^{+/+}$ and *Iir*$^{-/-}$ E19.5 animals were starved for 2 h before sacrificing. Whole pancreas from *Iir*$^{-/-}$ E19.5 animals were then sequentially perfused with low-glucose (0.5, 1.5 and 2.8 mM) for 24 min, followed by high-glucose (20 mM) for 8 min. Both, *Iir*$^{+/+}$ and *Iir*$^{-/-}$ pancreas secreted insulin upon glucose induction, representing the first and second phase of insulin secretion. However, upon both high glucose and KCL induction, *Iir*$^{-/-}$ pancreata demonstrated slightly elevated amount of insulin secretion (Figure 4.20). This was further

supported by the Area Under Curve (Figure 4.20b); AUC (high glucose) =71.86 ± 33.93 (s.e.m.); P=0.1016; AUC (KCL)=98.90 ± 34.80 (s.e.m.); P=0.0468.

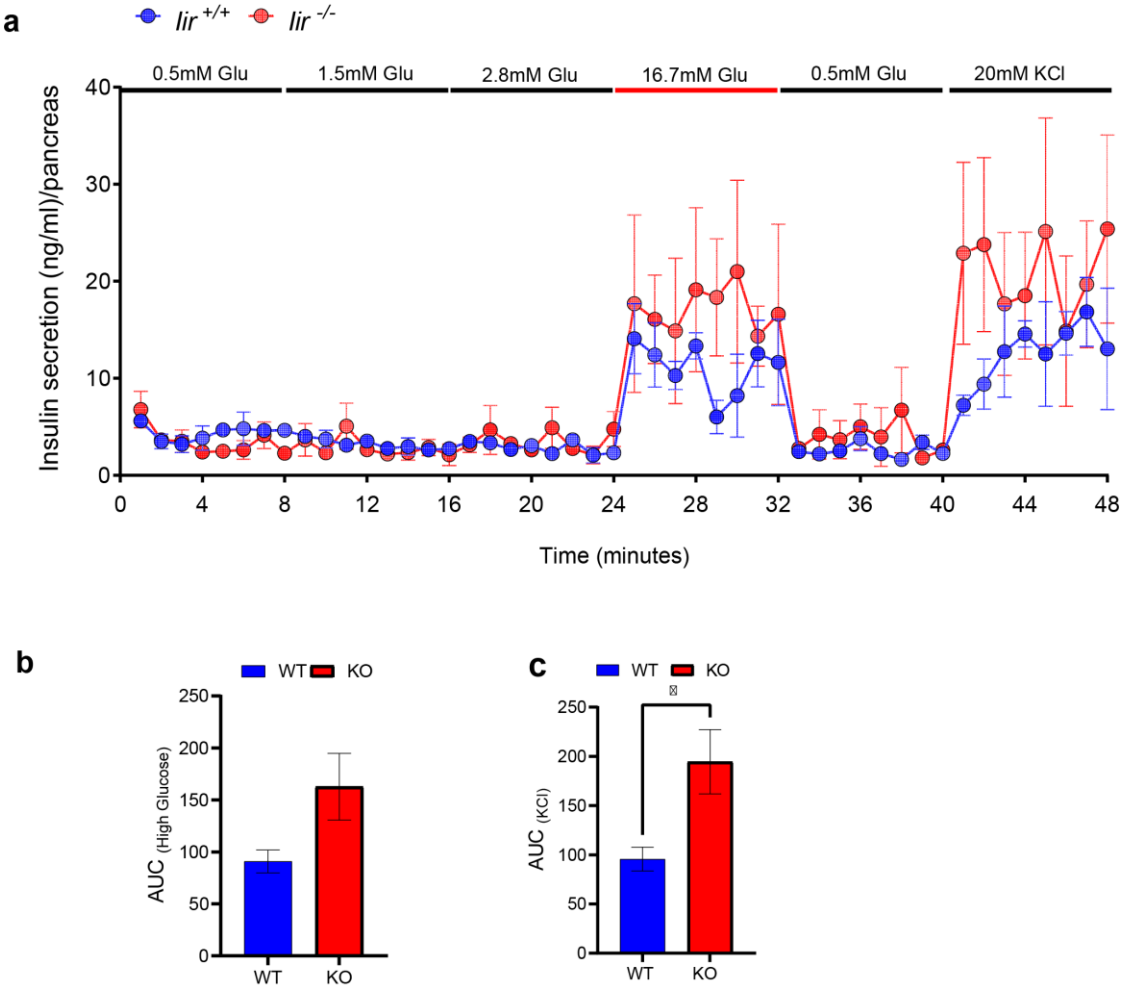

Figure 4.20: Dynamic glucose induced insulin secretion in E19.5 pancreata

a, Time-resolved glucose induced insulin secretion (GSIS). Insulin secreted from dissected pancreata of control and *Iir*$^{-/-}$ E19.5 animals. Whole pancreata were cultured in 0.5, 1.5 and 2.8mM glucose, followed by a 16.7 mM glucose solution. After, pancreata were recovered with 0.5 mM glucose culture buffer, they were induced with 20 mM KCl. Secreted insulin concentrations were measured in the buffer supernatant. Insulin secretion was normalized by the weight of pancreas. (*Iir*$^{+/+}$, n = 4; *Iir*$^{-/-}$, n = 4). Data are mean ± s.e.m).
b, Area under curve (AUC) of GSIS after high glucose induction. Significance was calculated by unpaired t-test.
c, Area under curve (AUC) of GSIS after KCL induction. Significance was calculated by unpaired t-test. Data are mean ± s.e.m; *P≤0.05, **P≤0.01, ***P≤0.001.

4.1.5.7 *Iir*$^{-/-}$ mice indicated higher hepatic glycogen content

The liver occupies a central position in metabolic adaptation after birth like gluconeogenesis. We investigated whether the death of *Iir*$^{-/-}$ newborn mice is a consequence of an impairment of gluconeogenesis. To address this, we performed a periodic acid-schiff reaction (PAS) staining of *Iir*$^{+/+}$ and *Iir*$^{-/-}$ liver sections. Paraffin fixed sections were stained with Schiff reagent (data not

shown). In addition, we measured liver glycogen levels in *Iir*$^{+/+}$ and *Iir*$^{-/-}$ E19.5 animals using Glycogen Assay kit. Interestingly, *Iir*$^{-/-}$ showed a significantly increased hepatic glycogen content (Figure 4.21b).

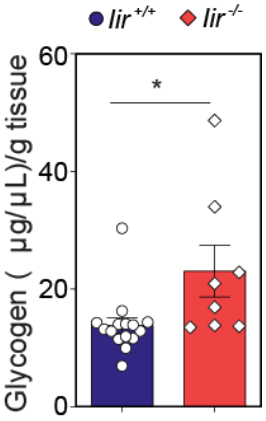

Figure 4.21: Increased glycogen accumulation in liver of *Iir*$^{-/-}$ mice.

b, Measurement of Glycogen levels in E19.5 control and *Iir*$^{-/-}$ animals. Pups were starved for 5 h before sacrificing (n=15, *Iir*$^{+/+}$; n=8, *Iir*$^{-/-}$; P<0.194). Data are mean ± s.e.m. Significance was calculated using unpaired t-test. (Ansarullah et al., 2021).

4.1.5.8 Global gene expression analysis of *Iir*$^{-/-}$ pancreata

To analyze the effect of inceptor in the pancreas on a molecular level, we compared mRNA expression profiles of *Iir*$^{+/+}$ and *Iir*$^{-/-}$ pups using global gene expression analysis at E18.5 and P0 (in collaboration with M. Irmler from Institute of Developmental Genetics -Helmholtz Zentrum München). The principal component analysis of the micro-array data analysis showed that *Iir*$^{+/+}$ and *Iir*$^{-/-}$ embryos at E18.5 are clustered together. In contrast, after birth *Iir*$^{+/+}$ and *Iir*$^{-/-}$ pups during starvation clustered in independent groups (Figure 4.22a). This indicate strong gene expression changes when neonates switched from maternal to autonomous metabolic control when placental nutrient supply is interrupted (PC1: 30.7% variance). Taken together, at E18.5 the gene expression is not affected, however after birth at P0 (PC2: 9.3% variance) several genes are up- or downregulated.

The analysis of the microarray reveals 516 significantly regulated genes (>1.5 fold, p<0.05, av>30) between *Iir*$^{+/+}$ and *Iir*$^{-/-}$ P0 pups. The p-value of the Iimma t-test was used to define sets of regulated genes (p<0.05/0.01). For further analysis, we restricted to genes with a FDR <10% and a fold change (FC) of >1.5x (ko vs. wt) to focus on significant changes. From these genes 75 were downregulated and 132 genes upregulated in *Iir*$^{-/-}$ P0 pups. Further analysis of the transcriptional signature of *Iir*$^{-/-}$ revealed a distinct expression of the genes involved in IGFR, PI3K-AKT and FoxO signaling pathways. In detail, *Iir*$^{-/-}$ pancreata express elevated levels of Klk1b (Kallikrein 1-related peptidase b) genes involved in IGF-IR signaling pathway. Of note, the GO-term Regulation of IGFR, PI3K-AKT and FoxO together with the elevated expression of gene Irs-2 and Insr involved in insulin secretion in the *Iir* $^{-/-}$ pancreata might suggest an improved insulin secretion in the *Iir*$^{-/-}$ compared to the *Iir*$^{+/+}$ pancreata. Furthermore, *Iir*$^{-/-}$ pancreata is enriched of GO-terms for pathways such as autophagy, mitophagy and ER-stress. Besides the GO-term analysis, the microarray reveals that the *Iir* $^{-/-}$ pancreata are expressing different levels of genes such as Eif2ak3 (Eukaryotic translation initiation factor 2-alpha kinase 3) (Figure 4.22b). In addition, *Iir*$^{-/-}$ pancreata

show a diminution of pathways related to metabolism, mitochondrion function, oxidative phosphorylation and pancreatic exocrine secretion (Figure 4.22b).

To validate the result of the microarray, we performed a real-time quantitative polymerase chain reaction (RT-qPCR) using RNA isolated from pancreata at postnatal day zero (P0). We analyzed 96 genes. In line with the analysis of the microarrays, the *Iir*$^{-/-}$ pancreata exhibit an increase in the expression of genes that are involved in Ins/IGF-I signaling or Insulin secretion (Igfbp3, Insr, Irs2 and Foxo3). Furthermore, we validated genes, which are important for cholesterol and fatty acid metabolism (Idi1). Some of the selected genes, which are significantly increased, encode chemokines, kinases, peptidases, receptor, channels and transporter (*Adrb2*, *Erbb3*, *Agr2*, *Ccl2*, *Slc38a5* and *Clp11*). Strikingly, after birth many of these genes were either slightly or significantly differentially expressed (Figure 4.22c)

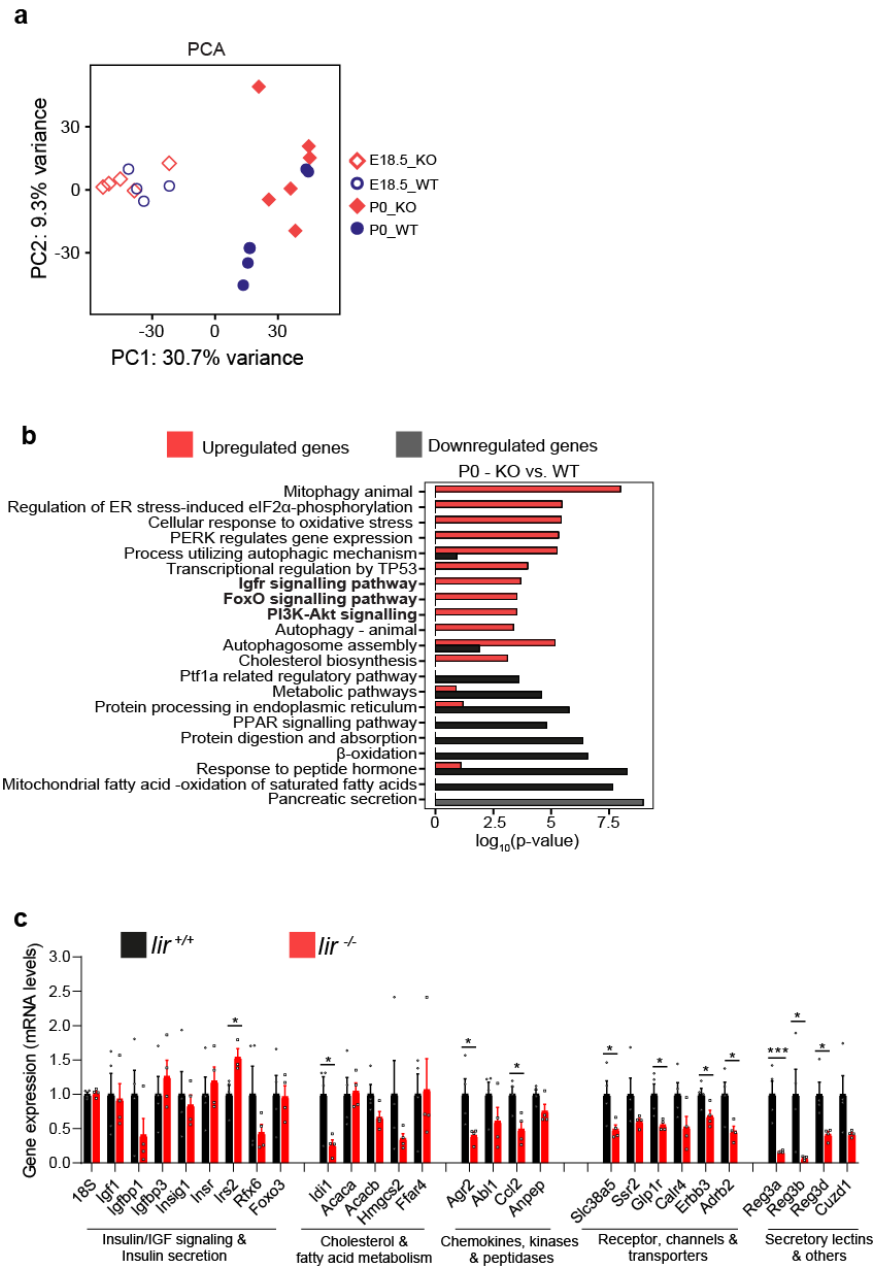

Figure 4.22: Differential gene expression changes in control vs *Iir*$^{-/-}$ P0 pups.

a. Principal component analysis showed clustering of mRNA expression arrays from pancreata of 5 h starved pups before (n=5, *Iir*$^{+/+}$; n=4 *Iir*$^{-/-}$) and after birth (n=5, *Iir*$^{+/+}$; n=6, *Iir*$^{-/-}$).
b. Functional enrichment analysis was performed on of differentially expressed genes (P0 *Iir*$^{-/-}$ vs *Iir*$^{+/+}$, p<0.01, fold change >1.5) using Homer (v.4.10).
c. q-PCR analysis of *Iir*$^{+/+}$ and *Iir*$^{-/-}$ pancreata selected from top up/ down regulated genes for microarray validation. Multiple t-test was used to calculate the significance of *Iir*$^{+/+}$ and *Iir*$^{-/-}$ groups (n = 4 pups). Data are mean ± s.e.m; * P≤0.05, ** P≤0.01. (Ansarullah et al., 2021).

4.1.6 Generation of conditional β-cell specific KO (MIP-CreERT; *Iir*$^{flox/FD}$) mouse line

To ablate *Iir* gene from pancreatic β-cell, we used a transgenic mouse line Tg (Ins1-Cre/ERT) 1Lphi (Wicksteed et al., 2010), also termed MIP1-CreERT.To trigger Cre-mediated recombination, Cre recombinase is fused to modified the human estrogen receptor (CreERT) under control of mouse insulin 1 gene promotor (Ins1, MIP1), which can be activated by the synthetic estrogen receptor ligand 4-hydroxytamoxifen (tamoxifen). Tamoxifen binds the estrogen receptor, Cre translocate to the nucleus and can excised the loxP flanked target gene (*Iir*).

MIP-CreERT line is already characterized (Tamarina et al., 2014a). They have shown that in a cross of MIP1-CreERT with a ROSA26/*LacZ* reporter strain, β-galactosidase expression, which is triggered by tamoxifen induction; occur within pancreatic β-cell but not in other organ systems. In addition, they have shown that intra-peritoneal glucose tolerance test was not adversely affected in adult MIP1-CreERT.

As shown in Figure 4.23a, our conditional allele is based on the 'knockout-first' design (Testa et al., 2004). This strategy is a combination of both a reporter-tagged and a conditional mutation. The 'knockout-first' allele (*Iir*$^{+/GT}$) contains a *lacZ* trapping cassette and a floxed promoter-driven *neo* cassette inserted into the intron of a gene of interest. Flp converts the 'knockout-first' allele to a conditional allele (*Iir*$^{+/fl}$) to restore gene activity. In this line, the exon of interest was flanked by two loxp sites between exon 2 and 4. In following step Cre deletes the floxed exon of the *Iir*$^{+/fl}$ allele to generate a frameshift mutation (*Iir*$^{+/FD}$). By crossing of MIP-CreERT+ with *Iir*$^{+/FD}$ we took advantage of the Cre-loxp system to ablate *Iir* in a specific tissue and at a chosen time point; we called this line CKO (MIP-CreERT+; *Iir*$^{fl/FD}$).

To distinguish WT and MIP-CreERT2; *Iir*$^{flox/FD}$ mice, we used three PCR strategies with primers flanking the integrated T2A-CreERT sequence and within the sequence. Ep: 1486 and Ep:1487 resulting in a PCR product for CreERT^{+} allele of 280 bp.

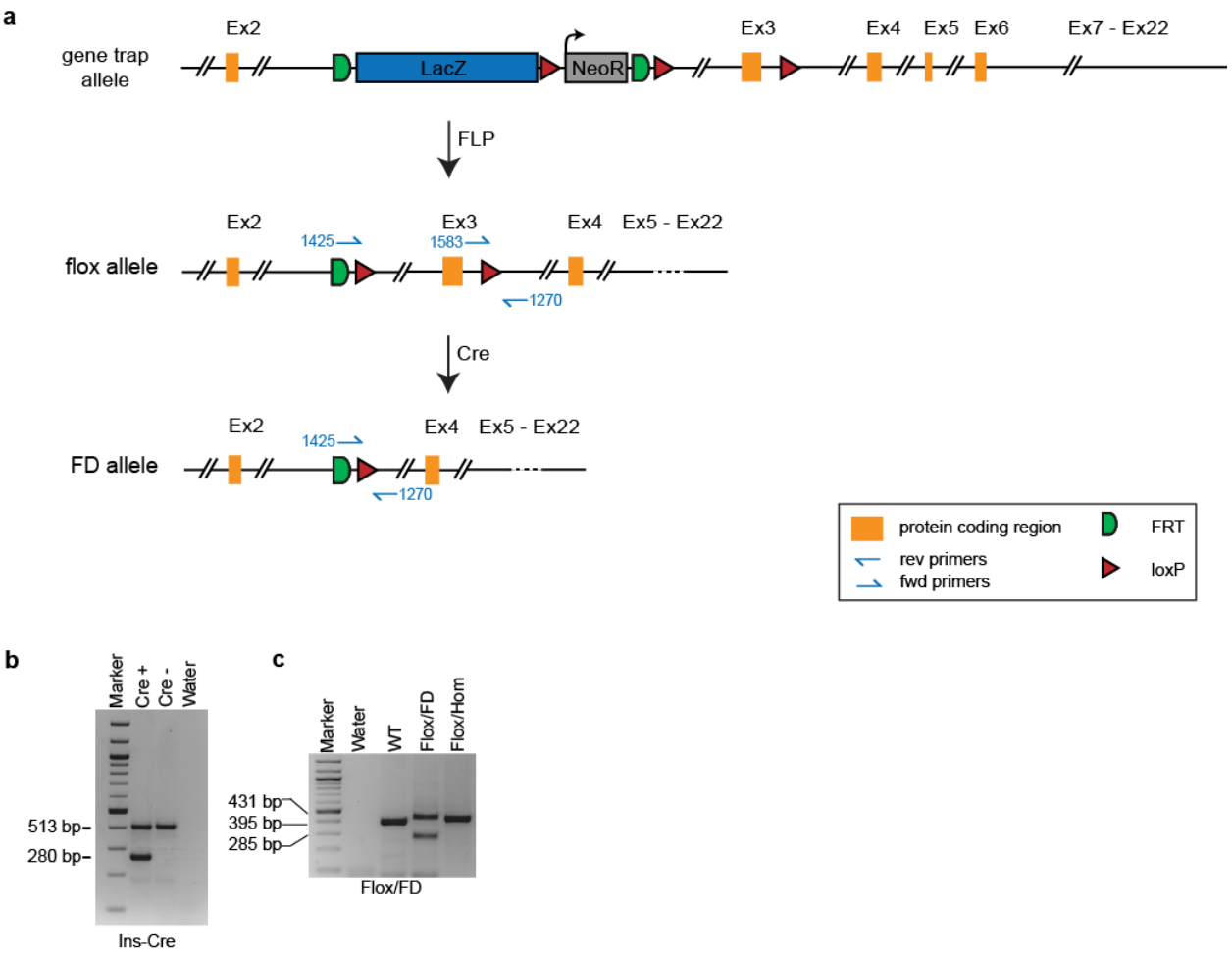

Figure 4.23: Generation and genotyping of MIP-CreERT; *Iir*$^{flox/FD}$ Mice.

a. Schematic illustration of the *Iir* allele. Targeted *Iir* allele was used to generate CKO (MIP-CreERT+;*Iir*$^{flox/FD}$) mice.The FRT-flanked *Lac-Z* with neomycin resistance cassette (NeoR) was removed by Flp-mediated excision. The protein coding regions are depicted in orange, and the FRT sites in green and the loxP sites in red. Site-specific recombinase Cre (loxP sites) and Flp-e will achieve conditional knockout. The figure is on scale.
b. Genotyping of Ins-Cre (Ins-Cre^{+} and Ins-Cre^{-}) c, flox (WT, *Iir*$^{+/fox}$ and *Iir*$^{flo/flox}$) and, FD (WT, *Iir*$^{flox/FD}$) animals.

4.1.7 *In vivo* characterization of conditional β-cell specific CKO (MIP-CreERT; *Iir*$^{flox/FD}$) mouse line

Based on our previous results with whole body KO (*Iir*$^{-/-}$) mice predominantly owing to hypoglycemia and hyperinsulinemia phenotype, we next investigated the role of inceptor deletion in adult β-cell. Moreover, conditional deletion of allele permits the functional characterization of inceptor in a tissue-specific and/or temporal manner during postnatal development.

As we have mentioned, inceptor plays a role in glucose homeostasis. Furthermore, *Iir*$^{-/-}$ E19.5 pups showed hyperinsulinemia and hypoglycemia phenotype in immature β-cell, which need to be confirmed in adult mice. Since the MIP1-CreERT mouse line is a powerful tool for conditional

manipulation of gene expression in β-cell by generating a MIP-CreERT; *Iir*$^{flox/FD}$ mouse line, metabolic phenotype like ipGTT, ipGSIS and dynamic GSIS, can be investigated in a spatiotemporal resolved fashion in adult mice.

4.1.7.1 Deletion efficiency of CKO

For conditional inceptor deletion in pancreatic ß-cell of adult mice, we used *Iir*$^{flox/flox}$, which contains the floxed gene for *Iir*. In this mouse line the *Iir* gene can be removed by Cre/lox recombination. To overcome the leakiness of the CreERT, we generated *Iir*$^{+/FD}$ by crossing a Rosa-Cre line into the *Iir*$^{flox/flox}$. We next crossed *Iir*$^{+/FD}$ with MIP-CreERT mice to obtain MIP-CreERT+; *Iir*$^{+/FD}$. Finally, we crossed *Iir*$^{flox/flox}$ to obtain MIP-CreERT+; *Iir*$^{+/FD}$ mice hereafter named CKO line (Figure 4.24a).

For generating a stable conditional, specific knockout of inceptor in pancreatic β-cell adult (12-15 week old) mice were induced with tamoxifen (100 mg/kg body weight) for three times every 48h (Figure 4.24b). As controls we used the following genotypes; tamoxifen-treated MIP-CreERT+; *Iir*$^{flox/+}$ and the vehicle treated MIP-CreERT-; *Iir*$^{flox/+}$ (oil).

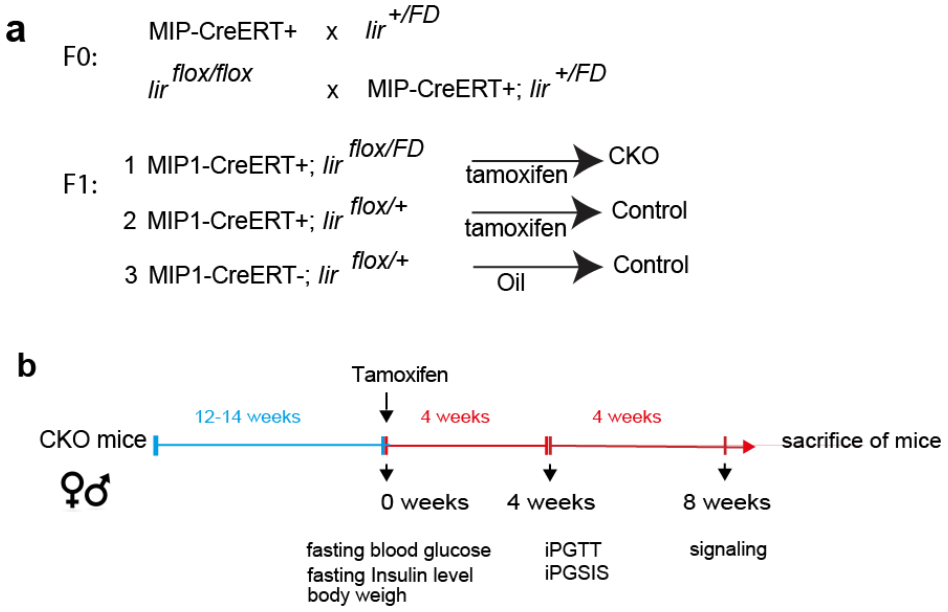

Figure 4.24: Deletion of *Iir* in CKO mice is induced by tamoxifen.

a. Mating scheme showed the strategy used to generate CKO and control mice. Genotypes used for the *in vivo* experiments.
b. Experimental design and timelines for metabolic analysis of CKO mice.

To determine whether tamoxifen injection influences fasting glucose level in these CKO mice. CKO and control mice at 14 weeks of age were injected for three times every 48 h with 100 mg/kg body weight. Fasting blood glucose levels did not change between control and CKO mice after 0-14- or 28-days post tamoxifen induction (Figure 4.25).

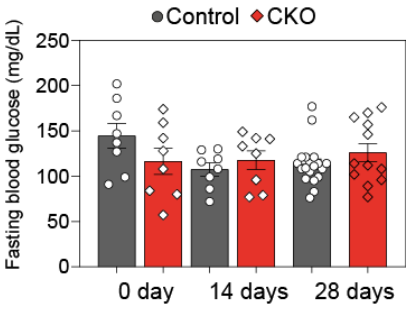

Figure 4.25: CKO animals exhibit normal fasting glucose level after tamoxifen induction.

Fasting blood glucose levels of CKO and control males before first tamoxifen injection (day 0), 14 and 28 days after the first tamoxifen induction.

After 4 weeks of tamoxifen administration, we assessed the KO efficiency on inceptor protein level by immunohistochemistry. Clearly, as shown in Figure 4.26a, there was approximately 90% absence of inceptor protein in the β-cells of CKO islets, whereas, it was not deleted in other endocrine cells (α, δ, Ɛ-cells) types.

Although staining data of the brain section from transgenic mice using Ins1 promotor do not exhibit Cre-recombinase-mediated gene excision (Cheng et al., 2015; Hasegawa et al., 2014) and the T/mG: MIP-CreERT mice given tamoxifen showed no GFP signal in hypothalamic cells (Oropeza et al., 2015). It has been reported that insulin 1 (Ins1)/ MIP promoter can drive transgene expression in cells isolated from the hypothalamus. To exclude the non-specific deletion of inceptor in other tissues than β-cells, we analyzed the expression levels of this protein in the brain. Immunofluorescence analysis of the hypothalamus of CKO mice showed no sign of Cre-recombination (Figure 4.26b). Based on these observations, we find that our model was β-cell specific and the induction through tamoxifen administration had high efficiency limited to β-cell.

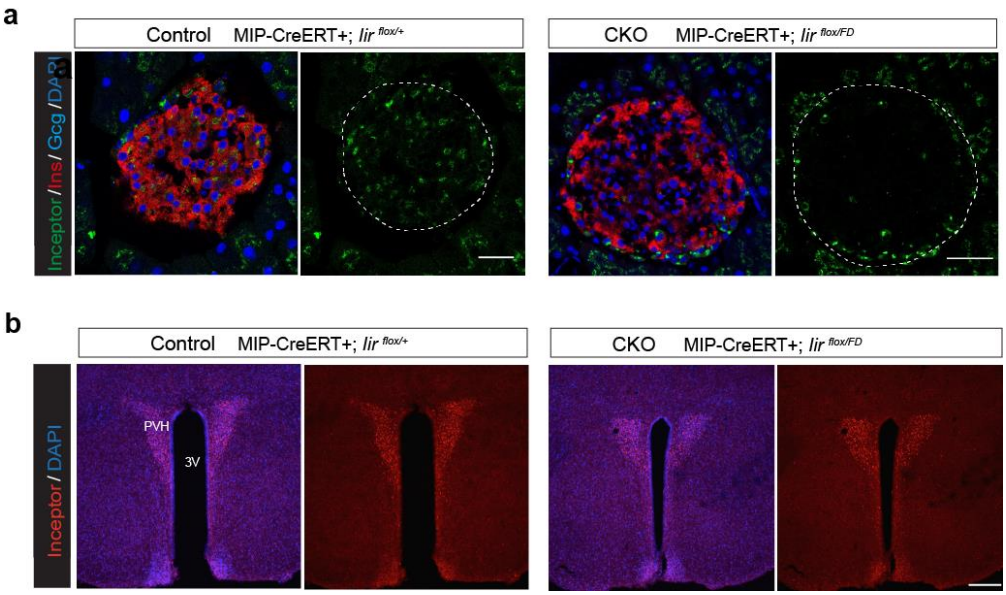

Figure 4.26: Deletion efficiency in vivo with tamoxifen in control and CKO mice.

a. Immunofluorescence analysis representing the β-cell specific deletion efficiency of inceptor from CKO (MIP-CreERT+; *lir*$^{fl/FD}$, Tamoxifen) and control (MIP-CreERT+; *lir*$^{fl/+}$, Tamoxifen). 18-weeks-old male mice 4-week post tamoxifen administration. Scale bar 120 µm.
b. Representative immunofluorescence analysis showed the inceptor immunoreactivity in the hypothalamus at the stage of the paraventricular nucleus in both control and CKO mice. PVH = Paraventricular nucleus, 3V = Third ventricle. Scale bar, 200 µm (Ansarullah et al., 2021).

Taken together, adult CKO mice analysis confirmed that CreERT under the control of the mouse Ins1 promoter is highly specific for pancreatic β-cells is inducible upon tamoxifen treatment and mediates recombination in the expected tissues. Furthermore, we also show that Cre-mediated recombination was highly efficient in the β-cell for inceptor.

4.1.7.2 Inceptor deletion does not alter body weight, fasting glucose or insulin levels

Tamoxifen induced control (MIP-CreERT+; *Iir*$^{flox/+}$) and CKO (MIP-CreERT+; *Iir*$^{flox/FD}$) mice were maintained on standard chow starting at 12-14 weeks old. Physiological parameters were analyzed at 16-18 weeks of age. First, we showed that body weight did not differ between control and CKO mice after 4 weeks of tamoxifen administration (Figure 4.27a).

Additionally, we evaluated glucose level of 16-weeks-old CKO animals. Fasted glucose was measured after 6 h fasting by tail vein using a glucometer. In all tested male animals, the indicated values were below 120 mg/dL of glucose in blood (Figure 4.27b), suggesting normal glucose homeostasis in these mice.

In addition, the serum insulin, which were, measured By ELISA after 6 h fasting, remain unaffected in CKO mice (Figure 4.27c).

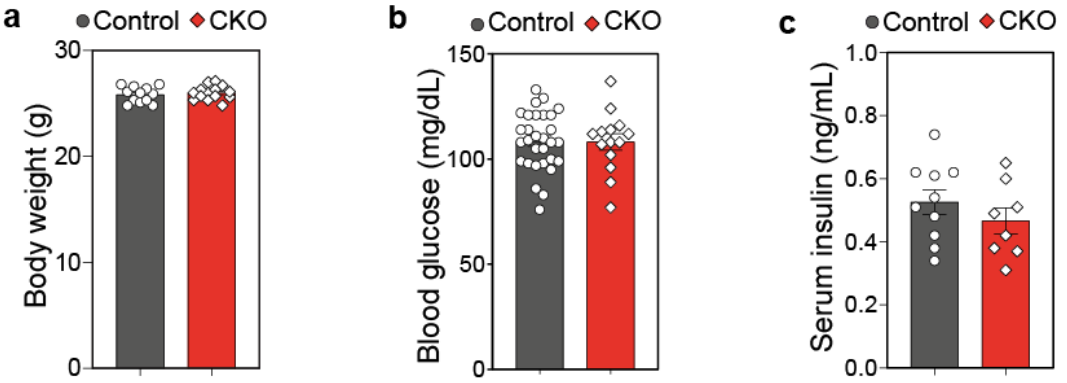

Figure 4.27: Body weight, fasting blood glucose and fasting serum insulin of CKO mice.

a. Body weight in control (n=12) and CKO mice (n=14).
b. Measurement of fasting blood glucose levels (n=30, control; n=14, CKO)
c. Analysis of fasting serum insulin levels (n=10, control; n=8, CKO).
16-weeks male control and CKO animals were analyzed 4 weeks after first tamoxifen injection. Data are mean ± s.e.m.

4.1.7.3 CKO mice demonstrated pronounced improvement in glucose tolerance

To assess the β-cell functionality of CKO mice, we subjected mice to intraperitoneal glucose tolerance test (ipGTT). The cohorts were followed over 14 weeks during which we measured different parameters to assess glucose homeostasis at 0, 2 and 4 weeks post induction (Figure 4.24b). Four weeks post tamoxifen induction, CKO mice were challenged with intraperitoneal injection of glucose (2g/kg of body weight). The CKO mice showed significant improvement in the ipGTT when compared to the control (MIP-CreERT+; *Iir*$^{flox/+}$) mice (

Figure 4.28a). This was further supported by the Area Under Curve (

Figure 4.28b); AUC(control)= 25989 ± 1129 (s.e.m.); AUC(CKO)=31988 ± 1295 (s.e.m.); P=0.002, tow way ANOVA, Bonferroni's multiple comparison).

To exclude any effects arising from tamoxifen treatment, we included a group of Cre negative animals treated with the oil. As shown in

Figure 4.28c, the two groups of control animals did not show any difference. However, we observed in CKO mice a significantly declined of two time points in the GTT curve compared to control (MIP-CreERT-; *Iir*$^{flox/+}$) mice (

Figure 4.28d); AUC(control)= 30535 ± 3073 (s.e.m.); AUC(CKO)=26429 ± 3040 (s.e.m.).

We saw an improved glucose tolerance in CKO mice, which might be due to increased insulin secretion. We next subjected the CKO and control mice to *in vivo* intraperitoneal glucose stimulated insulin secretion (ipGSIS) to evaluate if the insulin secretion is also increased. Interestingly, CKO mice showed a rise in first phase insulin secretion during 2 min time point (

Figure 4.28e); p=0.0362 (t-test)).

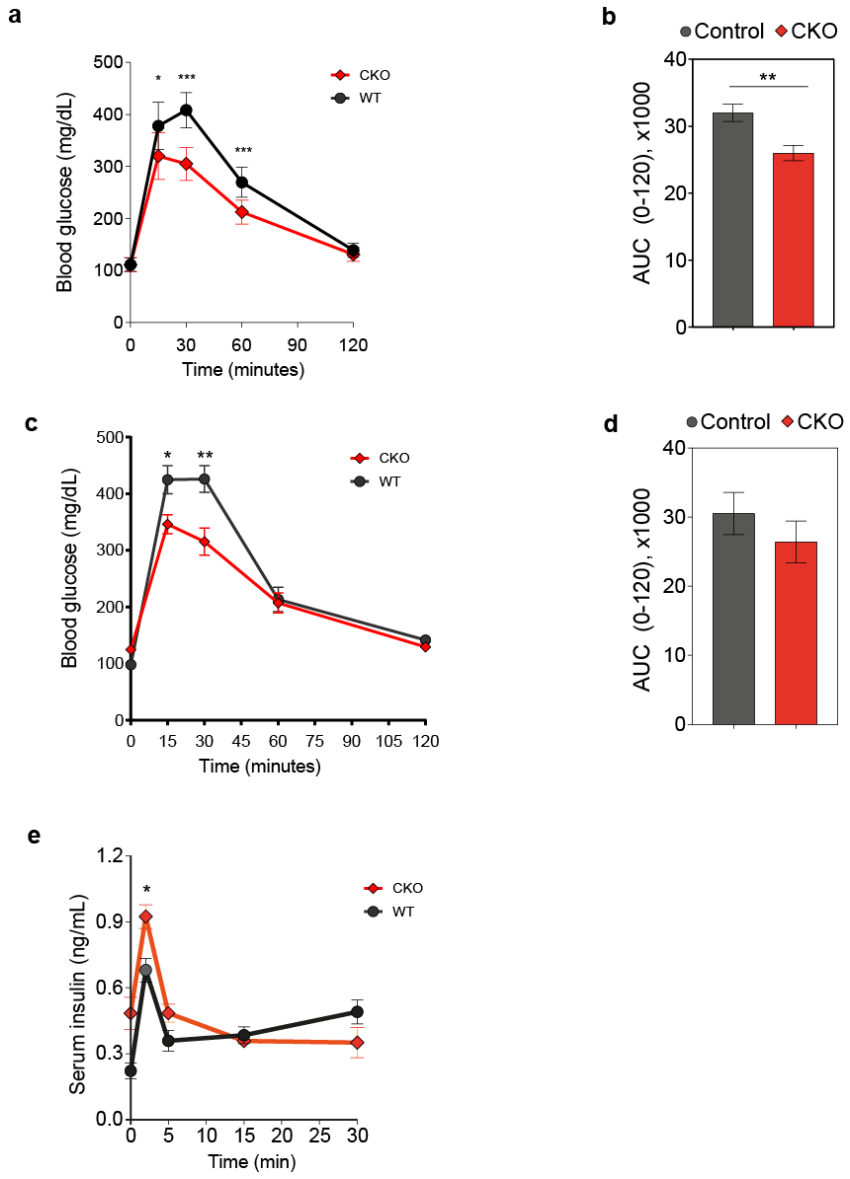

Figure 4.28: CKO male mice showed improve glucose tolerance.

a. Intraperitoneal glucose tolerance test (iP-GTT). Blood glucose levels were measured during an iP-GTT in control (MIP-CreERT+; *lir*$^{fl/+}$, tamoxifen) and CKO (MIP-CreERT+; *lir*$^{fl/FD}$, tamoxifen). n=12, control; n=15, CKO.

b. Area under curve (AUC) of ipGTT (a). Significance was calculated by unpaired t-test.

c. Intraperitoneal glucose tolerance test (IP-GTT). Blood glucose levels were measured during an IP-GTT in control (MIP-CreERT-; *lir*$^{fl/+}$, oil) and CKO (MIP-CreERT+; *lir*$^{fl/FD}$, tamoxifen). n=12, control; n=13, CKO.

d. Area under curve (AUC) of ipGTT (a). Significance was calculated by unpaired t-test.

e. In vivo intraperitoneal glucose stimulated insulin secretion (ip-GSIS). Serum insulin levels were measured during an ip-GSIS in control (MIP-CreERT+; *lir*$^{fl/+}$, tamoxifen) and CKO (MIP-CreERT+; *lir*$^{fl/FD}$, tamoxifen). n=7, control; n=8, CKO.

16-weeks male control and CKO animals were analyzed 4 weeks after first tamoxifen injection. Data are mean ± s.e.m; *P≤0.05, **P≤0.01, ***P≤0.001. Significance was calculated by two-way ANOVA followed by Bonferroni's multiple comparisons test (Ansarullah et al., 2021).

4.1.7.4 Increased β-cell mass in CKO pancreas

To understand whether improved glucose tolerance is correlated with increased β-cell mass, we next quantified β-cell mass in CKO and control mice. We systematically carried out morphometric quantification from four weeks post tamoxifen induction, a time when the CKO animals already showed an increase in insulin secretion during ipGTT and ipGSIS. β-cell mass was calculated by multiplying relative insulin-positive area (the percentage of insulin-positive area over total pancreas area) by pancreas weight. The quantification revealed an increase in β-cell mass in the CKO (p=0.07) compared to the control mice (Figure 4.29a), suggesting a proliferation dependent islet size increase in the β-cell number of CKO mice.

Additionally, we also analyzed α-cell mass in control and CKO mice and found no significant differences (Figure 4.29b).

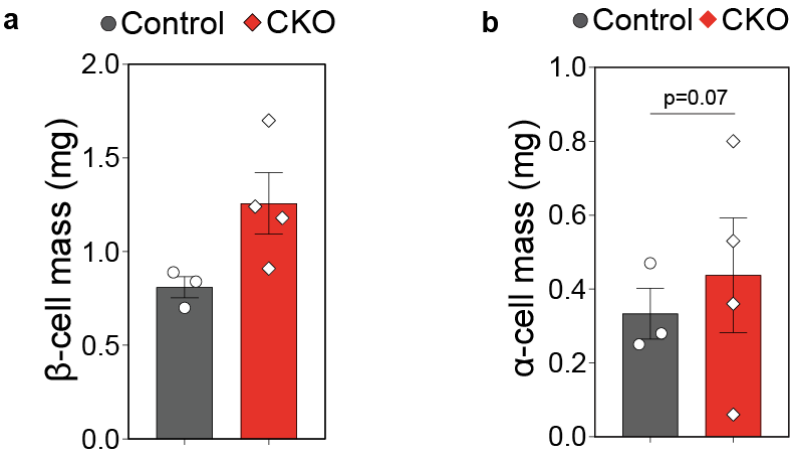

Figure 4.29: β-cell specific inceptor CKO mice display increase in β-cell mass

a. Quantification of β-cell area using immunofluorescence images of control (n=3) and CKO (n=4) mice pancreatic sections. Data are mean ± s.e.m; P=0.07.
b. Quantification of α-cell area using immunofluorescence images of control (n=3) and CKO (n=4) mice pancreatic sections. No significant changes were observed.
18-weeks male control (MIP-CreERT+; *Iir*$^{fl/+}$, tamoxifen) and CKO (MIP-CreERT+; *Iir*$^{fl/FD}$, tamoxifen) animals were sacrificed 4 weeks after first tamoxifen induction and the whole pancreas were cryo sectioned for immunostaining. Data are mean ± s.e.m (Ansarullah et al., 2021).

4.1.7.5 β-cell specific deletion of inceptor induces increased proliferation in β-cell of CKO mice

To understand the increase in β-cell mass in the CKO mice, we investigated β-cell proliferation in CKO and control mice.

For proliferation analysis, we added 5-ethynyl-2'-deoxyuridine (EdU) in drinking water (1 mg/mL) for at four-weeks post-tamoxifen injection and the analysis was performed one week prior to sacrifice. The quantification of EdU^+ β-cells confirmed 2-3 fold (P=0.08) elevated proliferation in the CKO compared to control mice (Figure 4.30b).

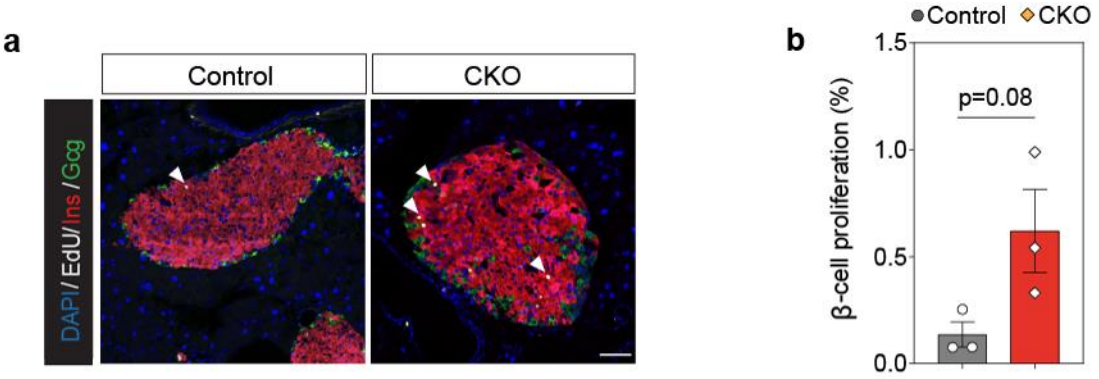

Figure 4.30: β-cell specific deletion of inceptor increases proliferation in β-cells.

(a. b) Representative LSM images (a) and quantification (b) of EdU incorporation after one week EdU pulse in the islets. Pancreatic sections derived from16 month male mice control (MIP-CreERT+; *Iir*$^{fl/+}$, tamoxifen) and CKO (MIP-CreERT+; *Iir*$^{fl/FD}$, tamoxifen), which were sacrificed 4 weeks after first tamoxifen administration. n=3, control; n=3, CKO. Grey indicate EdU labelled cells and blue indicate the nucleus. The endocrine cells marked by insulin (red) and glucagon (green). mean (100 islets counted per n) ± SD). Scale bar, 50 µm. (Ansarullah et al., 2021).

4.1.7.6 β-cell specific deletion of inceptor does not alter islet cyto-architecture or maturation markers.

To understand the impact of inceptor deletion on islet morphology and cyto-architecture, we next assessed the endocrine cell markers, and their distribution in control and CKO islets. Immunostaining with insulin, glucagon, somatostatin and pancreatic polypeptide revealed no significant differences in islet composition or ratio of α- to β-cells (Figure 4.31).

β-cell maturation is important due to its implications in β-cell regeneration and β-cell replacement. Therefore, identifying trigger of maturation might enable us to further discover novel modulators of this process. As we know that the embryonic development of *Iir*$^{-/-}$ mice appeared to be normal, we questioned if there are differences during β-cell differentiation and maturation in the postnatal stages. To this end, we examined the known maturity markers of the β-cell and found no differences in the expression levels of UCN3 and MafA in CKO mice as compared to controls (Figure 4.32).

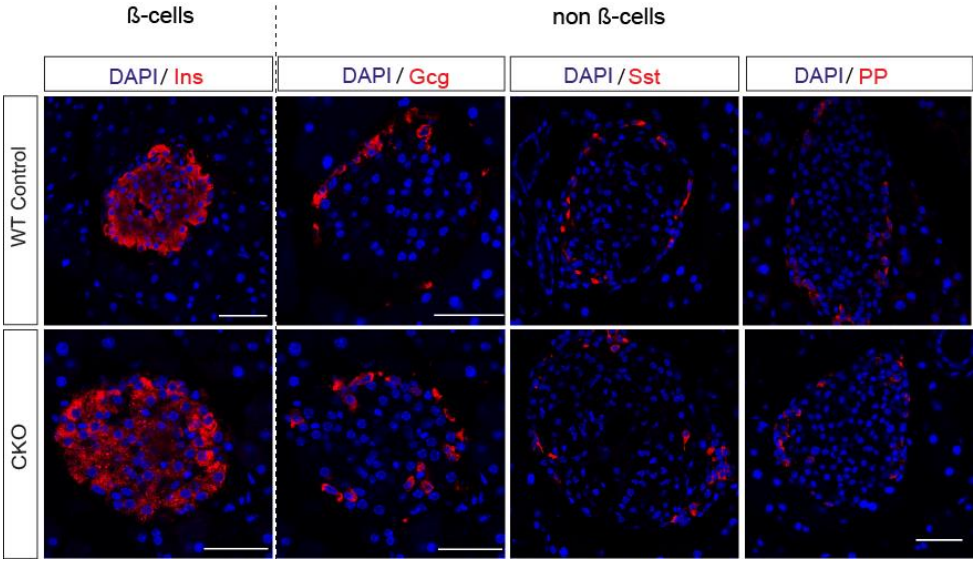

Figure 4.31: Islet cyto-architecture analysis in CKO mice.

Representative confocal images of endocrine markers for Ins (red, β-cells), Gcg (red, α-cells), Sst (red, δ-cells) and PP (red, PP-cells) in islets. 18-weeks- old male control and CKO animals were sacrificed 4 weeks after tamoxifen induction. Scale bar, 120 µm.

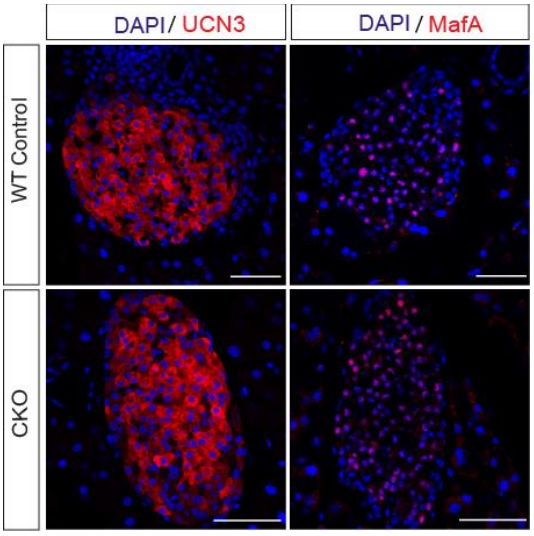

Figure 4.32: Expression of maturity markers in CKO mice.

Representative Immunostaining images of the expression of maturation markers Ucn3 and MafA in pancreas of control and CKO 18-weeks- old male mice. Scale bar = 50 µm (CKO), 20 µm (control). (Ansarullah et al., 2021).

4.1.7.7 Overactivation of IR/IGF-IR signalling in CKO islets

IR/IGF-IR signaling plays an important role in β-cell proliferation, survival and function. Moreover, impaired IR/IGF-IR signaling in β-cells contributes to a decrease in insulin secretion and β-cell mass. To see if the enhance in β-cell proliferation in CKO mice is a result of increased activity of IR/IGF-IR, we study IR/IGF-IR signaling.

To this end, we next cultured the isolated islets in nutrient depleted medium (starvation; HBSS) to minimize signal activity. Subsequently, we stimulated the islets in 100 nM insulin to activate the IR/IGF-IR pathway. As shown in Figure 4.33b and c an average KO efficiency of inceptor protein of nearly 90% resulted in increased upregulation of AKT phosphorylation in CKO islets relative to the control islets in both starvation and insulin induced conditions. The phosphorylation levels of AKT were quite low in starvation conditions but after 5 min of insulin stimulation, we observed a general increase in AKT phosphorylation after 5, 15 and 30 min of insulin stimulation (Figure 4.33b).

The phosphorylation of IR/IGF-IR was not changed in CKO islets upon starvation compared to control whereas there is a clear elevation of IR/IGF-IR phosphorylation during 5 min of insulin induction in CKO islets in comparison with control islets. The data collected on islets in different nutrient condition and time point are extremely valuable and informative. Unfortunately, the process to obtain them (deletion, isolation, induction etc.) is long and time consuming. To be more efficient we decided to repeat this experiment only upon insulin induction and starvation for 5 min.

In insulin induced CKO islets the levels of active pAKT were significantly ($p=0.001$) elevated in comparison with control islets. In line with the increased pAKT, IR/IGF-IR phosphorylation was significantly increased in both non-insulin and insulin treated CKO islets compare to control islets however is more pronounced in insulin induced islets (Figure 4.33d), resulting in an increased β-cell proliferation in CKO mice. The normalization of p-IR/IGF-IR to both IR and IGF-IR suggest that there are no differences in total protein of IR or IGF-IR in CKO islets. In conclusion, inceptor is involved in the desensitization of the Insulin/IGF-I signaling during both active and extenuate signaling states.

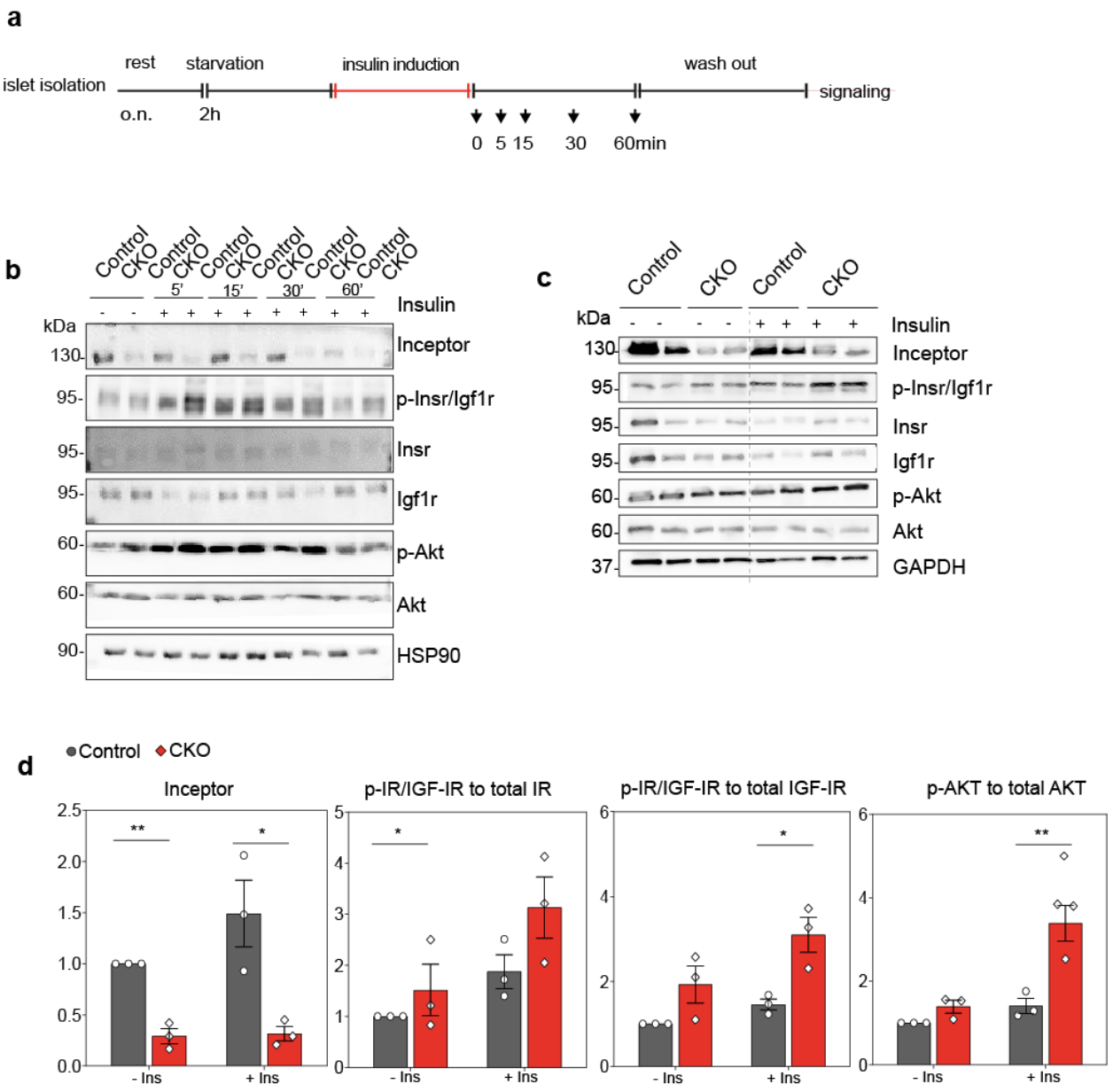

Figure 4.33: β-cell specific deletion of inceptor causes increased IR/IGF-IR signaling

a. Experimental design for the analysis of IR/IGF-IR signaling in 16-weeks-old male control (MIP-CreERT+; *Iir*$^{fl/+}$, tamoxifen) and CKO (MIP-CreERT+; *Iir*$^{fl/FD}$, tamoxifen) 4 weeks post tamoxifen administration.
b. Western blot of IR/IGF-IR signaling in control (n=5) and CKO (n=5) islets after islets isolation, islets were stimulated with 100nM insulin for 5, 15, 30 and 60min after 2 h starvation.
(c. d), Western blot (c) and quantification (d) of IR/IGF-IR signaling in control (n=3) and CKO (n=3) islets upon stimulation with 100 nM insulin for 5 min after 2 h starvation. Protein expression of relevant pathway components were analyzed in islets lysates from control and CKO animals. For quantification, signal intensities of all protein bands were normalized to GAPDH or HSP90; phosphorylated proteins were additionally normalized to the corresponding non-phosphorylated protein.
Data are mean ± s.e.m; *P≤0.05** P≤0.01*** P≤0.001. Significance was calculated by two-way ANOVA followed by Bonferroni's multiple comparisons test. (Ansarullah et al., 2021).

4.1.8 Analysis of inceptor in diabetes mellitus

Since *Iir*$^{-/-}$ mice die postnatal within the first hours after birth with signs of hypoglycemia and hyperinsulinemia and CKO mice showed improved glucose tolerance and increased first phase insulin secretion accompanied by increased IR/IGF-IR signaling in the β-cell, we assume that inceptor plays an important role in β-cell biology and entailed the question if inceptor might be a target in diabetes therapy. Therefore, we analyzed the expression and function of inceptor in diabetic animal models to identify whether expression of inceptor is beneficial for β-cell function and systemic glucose regulation as observed in *Iir*$^{-/-}$ and CKO mice.

From the age of 3 months on, WT mice were fed a 58% kcal high-fat diet (HFD) to metabolically challenge WT animals. We monitored metabolic parameters before starting the HFD feeding (“0 weeks of HFD”; 12 weeks of age), and after 28 weeks of HFD (9 months of age). Standard procedures for HFD mouse models recommend the analysis of male cohorts because estrogen, the major female gender determining hormone, is suggested to protect against the manifestation of insulin resistance (Pettersson et al., 2012). After 28 weeks of HFD we could confirm significantly increased expression of inceptor compared to control animals (Figure 4.34a). However, after 24 h starvation, inceptor was expressed in the endocrine pancreas of WT animals at comparable levels when no physiological difference in terms of food intake was applied (Figure 4.34c). These results support the idea of change of inceptor expression under different metabolic conditions. Furthermore, the Western blot data showed that mice fed for 6 months with high-fat diet exhibited significantly increased expression of inceptor in islets (Figure 4.34e).

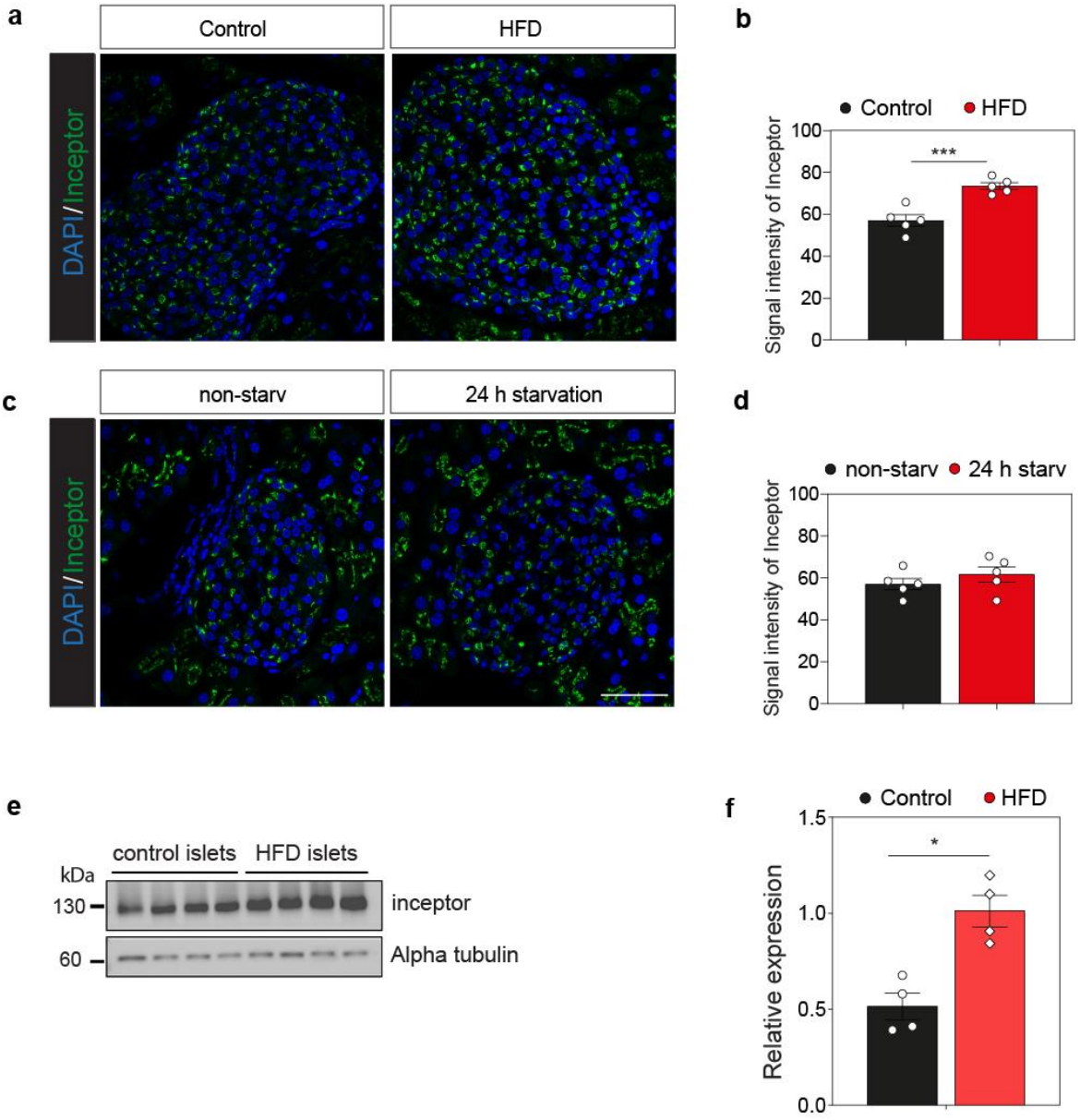

Figure 4.34: Increased protein expression of inceptor in islets of adult WT mice upon HFD.

a. Representative confocal images of inceptor (green) and DAPI (blue) and **b,** quantification of inceptor expression analysis in islets of 6 months old male WT BL6 mice in normal condition (left panel), after 6 months of HFD (right panel)
c. Representative confocal images of inceptor and **d,** quantification of 6 months old mice non-starved (left panel) and after 24h starvation (right panels). Blue indicate DAPI cells and green indicate inceptor.
e. Western blot analysis and **f,** quantification of WT Islets from 6 months old male WT BL6 mice after 6 months of HFD and in normal nutrition statue. (n=4, control islets; n=4, HFD islets).
Error bars represent SEM and *, P<0.05; **, P<0.01; ***, P<0.001. P-values were analyzed using a two-tailed, unpaired t-test.

5 Discussion

5.1 The biological function of inceptor

The aim of this thesis was to elucidate the function of inceptor in insulin signaling of pancreatic β-cells. To resolve the role of inceptor in insulin/IGF-I signaling, a clear understanding of the biological function of inceptor is crucial.
To investigate *Iir* expression, we performed a quantitive PCR and found that *Iir* mRNA was highly expressed in the pancreas. Additionally, bioinformatic analyses revealed that 5330417C22Rik has domain structure similarities to IR and IGF-IR in terms of the growth factor binding CRD, as well as to IGF-IIR in terms of the M6PR domain. Therefore, we hypothesized that 5330417C22Rik has a function in the Ins/IGF system and we renamed it insulin inhibitory receptor (inceptor).
Inceptor was highly expressed in embryonic and adult mouse islets at protein level, where it was localized in both endocrine cells where insulin-secreting β-cell are produced. These findings, together with the fact that the function, homeostasis and proliferation of pancreatic β-cells are regulated by IR/IGF-IR signaling, led us to hypothesize that inceptor is a novel regulator of the Ins/IGF system.

To understand the biological function of inceptor in the pancreas, full-body *Iir*$^{-/-}$ animals were generated. Neonates showed postnatal lethality and presented with hypoglycemia and hyperinsulinemia. In addition, we found that β-cell mass was increased in E19.5 *Iir*$^{-/-}$ pups due to elevated endocrine proliferation. Furthermore, we observed an overactivation of Ins/IGF signaling in pancreas of E19.5 *Iir*$^{-/-}$ pups.

To further study the function of inceptor in mature β-cells, we generated a tamoxifen-inducible β-cell-specific KO (CKO) line. Four weeks post tamoxifen induction we observed an improvement of glucose tolerance. In addition, CKO mice showed a rise in first phase insulin secretion during ipGSIS. Similarly, *Iir*$^{-/-}$, β-cell mass was increased in CKO. In this thesis, we achieved β-cell-specific deletion of inceptor after in vivo Cre induction by tamoxifen in isolated islets. After stimulation with insulin, the phosphorylation of Ir/Igf-IR as well as Akt was enhanced in these islets. After a 24 h EdU pulse, proliferation was elevated in CKO islets.

5.2 Analysis of inceptor function by whole body knock-out

In this study we utilized mouse genetics to show that removal of inceptor affects β-cell function. The *Iir*$^{-/-}$ mice were born at a normal mendelian ratio and without alteration of body weight. Additionally, P0 *Iir*$^{-/-}$ pups appeared to be morphologically normal without any developmental defect. However, P0 *Iir*$^{-/-}$ pups became lethargic within hours after birth and died after 5 hours postpartum, suggesting a potential metabolic imbalance. Hypoglycemia occurred after 2-5 h starvation in *Iir*$^{-/-}$ newborn mice, which was likely caused by excessive insulin secretion, as plasma insulin levels were higher in *Iir*$^{-/-}$ compared to WT newborn mice. Taking into consideration that P0 pups have immature β-cells and have a reduced threshold for glucose stimulated insulin secretion (Blum et al., 2012), we assume that the *Iir*$^{-/-}$ pups primarily died due to hypoglycemia as a consequence of hyperinsulinemia. We have verified this in two different sets of experiments in P0 pups. The first set of experiments was a glucose rescue experiment, which showed that 50%

of the *Iir*$^{-/-}$ newborn pups could be rescued with glucose injection. The second set of experiments included a glucose tolerance test, which showed a significant decrease in the rate of glucose elevation in the *Iir*$^{-/-}$ pups (exhibiting improved glucose tolerance). We hypothesize that this was due to increased insulin secretion or sensitivity. Moreover, there is increased β-cell mass in E19.5 *Iir*$^{-/-}$ pups, which could be explained by increased β-cell proliferation during developmental stages (E14.5-E18.5).

Additionally, plasma glucose did not differ between *Iir*$^{-/-}$ and *Iir*$^{+/+}$ mice immediately after birth, while the fasting blood glucose levels were 1,5 times lower in *Iir*$^{-/-}$ pups compared to *Iir*$^{+/+}$ pups. These observations could imply that inceptor is dispensable during embryonic development. In contrast, IR$^{-/-}$ mice were born in the expected mendelian ratio but with slight growth retardation, about 10% smaller compared to WT (Louvi et al., 1997a). Moreover, based on our microarray data, inceptor is not required for the baseline expression of metabolic target genes throughout life, but its function in metabolic control becomes evident under metabolic demand like starvation or feeding. Its first essential role is revealed directly after birth when neonatal mice switch from maternal to autonomous metabolic control. The immediate control of glycemia does not occur in *Iir*$^{-/-}$ pups, which leads to their postnatal death.

In accordance with this, the IR$^{-/-}$ mutants show an increase in glucose levels after birth, accompanied with an increase in insulin levels. In these mutants, β-cell failure was observed within few days, followed by death caused by ketoacidosis (Okamoto et al., 2004). These data suggest that similarly to the IR, inceptor is not essential for prenatal metabolic control but for postnatal glucose homeostasis. The fact that both Ins$^{-/-}$ and IR$^{-/-}$ mice develop diabetes in early postnatal stages indicates a fuel-sensing apparatus in perinatal stages.

The main reason for not observing any developmental impairment in *Iir*$^{-/-}$ pups could be due to the development of immature β-cells. The embryonic development of the endocrine pancreas is limited in prenatal stages. In mice, the insulin secretion begins at E15.5 (Herrera et al., 1991; McEvoy and Madson, 1980; Yoshinari and Daikoku, 1982). However, β-cells are first organized at E18.5 and birth stimulates increased insulin secretion (Girard et al., 1973; KERVRAN and GIRARD, 1974). In addition, a proper β-cell proliferation and appropriate β-cell mass is accomplished 3-4 weeks after birth (Finegood et al., 1995).

Furthermore, it was published that there is a correlation between the weight at birth and a tendency to developing diabetes, indicating a complex interaction between metabolism and growth (Dabelea et al., 1999). In this regard, there is evidence that the lack of significant growth retardation in IR$^{-/-}$ mice might be due to differences in developmental timing between humans and mice and is not because of the absence of growth-promoting function of insulin (Louvi et al., 1997b). Likewise, this could explain the absence of body weight alteration in *Iir*$^{-/-}$ newborn pups. Furthermore, we did not expect an opposite phenotype of *Iir*$^{-/-}$ mice, compared to IR$^{-/-}$ mice, because IR is ubiquitously expressed. In contrast, inceptor is restricted to certain tissues.

IGF-IR$^{-/-}$ mice, similar to *Iir*$^{-/-}$ newborn pups, die immediately at birth due to respiratory failure but display severe growth retardation, with about 55% reduced size compared to WT (Liu et al., 1993). However, there is evidence for a role of IR in embryonic growth from combined mutation studies, which show double mutation of IR and IGF-IR results in more severe growth retardation, with about 70% reduced size compared to WT (Abuzzahab et al., 2003). Similarly, the same effect of

growth retardation (~70%) has been observed in combined mutation of IGF-I and IGF-II (Ludwig et al., 1996), suggesting that IR acts as a substitute for the action of IGF-IR and IGF-IIR.

Interestingly, the phenotype of *Iir*$^{-/-}$ newborn pups seems to be a mixture of the phenotypes which were reported for the receptors of the Ins/IGF system. Additionally, the early postnatal lethality of *Iir*$^{-/-}$ resembles the phenotype of mice that are deficient in both Akt1 and Akt2 (Peng et al., 2003).

The fact that the *Iir*$^{-/-}$ newborn pups became lethargic prompted us to control the feeding behavior in these mice. As expected, we could not observe milk in the stomach, suggesting that because of the lack of energy they were not able to compete for nourishment. After birth, gluconeogenesis becomes a central source of glucose. gluconeogenesis is a metabolic pathway that results in production of glucose from lactate and pyruvate and is controlled by insulin, becomes a central source of glucose (Pilkis and Granner, 1992). We have shown that after birth, *Iir*$^{-/-}$ livers accumulated significantly higher levels of glycogen compared to *Iir*$^{+/+}$, implying that glycogen metabolism is not affected. This observation suggests that hepatic glycogen might not be converted to glucose and returned to the blood due to hyperinsulinemia.

In addition, since inceptor is strongly expressed in the endocrine compartment of the pancreas and the phenotype of *Iir* $^{-/-}$ newborn mice suggests a metabolic dysregulation, we analyzed the transcriptional program in endocrine cells of E18.5 pancreata, and immediately after birth, when maternal nutrition is interrupted. Indeed, a large set of key metabolic pancreatic genes are not changed in E18.5 when the embryonic metabolism is controlled by maternal factors. However, several genetic IGFR, PI3K-AKT and FOXO signaling target genes are differentially regulated in *Iir*$^{-/-}$ newborn pups.

In conclusion, we have observed overactivation of IR/IGF-IR in global mRNA expression and increased β-cell mass during development. This is associated with increased insulin secretion and therefore impaired glucose homeostasis after birth. These findings suggest a role of *Iir* in autoregulation of hormone secretion in pancreatic β-cells.

5.3 Analysis of inceptor function in insulin producing β-cells

The lethal phenotype of *Iir*$^{-/-}$ precludes a deep analysis of inceptor function in adult mice. It has been shown that lack of IR in one or more insulin target tissues, including muscle, adipocyte liver and β-cell causes diabetes. Further, insulin secretion is known to be regulated in the β-cell (Matschinsky, 1996), Thus, we generated a tamoxifen-inducible conditional β-cell specific KO (MIP-CreERT+; *Iir*$^{fl/FD}$) to address the role of inceptor in insulin signaling.

Generating this mouse line enabled us to circumvent postnatal lethality and to address the function of inceptor in adult β-cells in context of glucose regulation and insulin signaling activation. Four weeks after tamoxifen injection, specific deletion of inceptor was found only in β-cells. We did not find a different brain phenotype compared to non-transgenic controls. This observation is in line with studies showing that MIP-CreERT function in the brain of ROSA-*LacZ*: MIP-CreERT mice was not active (Tamarina et al., 2014b; Wicksteed et al., 2010). Moreover, the presence of inceptor expression in brain confirms the overall specify of the Cre recombination system.

In addition, we did not observe a significant difference in fasting blood glucose after tamoxifen administration between the WT and CKO groups. Moreover, there were no differences regarding

insulin and serum insulin levels in CKO mice, indicating, normal glucose homeostasis. In accordance with our results, Kulkarni et al., 1999 reported that βIRKO mice showed no significant differences at 2 months of age.

5.3.1 Inceptor controls glycemia

As mentioned above, we used a conditional knock-out strategy to delete *Iir* in pancreatic β-cells. Specifically, we aimed to investigate whether lack of inceptor could contribute to a modification of insulin signaling and further alteration in islet and β-cell function and glucose metabolism. In addition, we wanted to determine if the increase in β-cell mass, observed in $Iir^{-/-}$ pups, was due to an autonomous function of inceptor in β-cells.

The most important difference between full body $Iir^{-/-}$ KO and β-cell-specific CKO mice is that $Iir^{-/-}$ pups are born with fasting hypoglycemia, whereas CKO mice do not show any fasting hypoglycemia phenotype. Some physiological considerations may explain this difference. In $Iir^{-/-}$ pups, hypoglycemia develops during fasting, presumably as a result of limited glycogen reserves in liver (Backeljauw et al., 1994; BIER et al., 1980; Taylor et al., 1982).

To define the impact of the morphological changes in CKO mice on glucose homeostasis, we assessed glucose disposal by intraperitoneal glucose tolerance test (ipGTT). Additionally, we examined metabolic parameters by performing in vivo intraperitoneal glucose stimulated insulin secretion (ipGSIS). In the fasting state, blood glucose concentration was similar in CKO mice and control mice. However, after glucose injection, CKO mice demonstrated significant improvement in glucose tolerance at 5, 30 and 60 min as compared to control (MIP-CreERT+; $Iir^{flox/+}$) mice. The blood glucose levels returned to the same levels as in the fasting state in both groups at 120 min. This increased ability to dispose the injected glucose in CKO mice was further associated with alteration in insulin secretory function wherein CKO mice showed 2-fold increased first phase insulin secretion by ipGSIS. The insulin level remained higher than baseline value for up to 10 min. However, the levels were elevated after glucose challenge, suggesting some retention in insulin secretion. The observation that pancreatic β-cell IR knockouts (βIRKO) demonstrate a loss of the first phase of glucose stimulated insulin secretion (Kulkarni et al., 1999), a phenotype contrary of CKO mice suggested the inhibitory role of inceptor to control glycemia and an improvement of insulin secretion in response to glucose. These data indicate that inceptor plays an important role in glucose sensing in β-cells.

The effects of insulin action in the muscle and liver are well described. Several studies have demonstrated that insulin secreted from β-cells could regulate its own synthesis or secretion (Goldfine and Kulkarni, 2012; Leibiger et al., 2008b). For IR, it has been demonstrated that overexpression positively regulates insulin biosynthesis (Okada et al., 2007). IGF-IR, on the other hand, has been described to negatively regulate insulin secretion (VAN SCHRAVENDIJK et al., 1987; Thorens et al., 1990). There is also evidence which supports the necessity of IRS-1 and IRS-2 regulated signaling pathways in β-cells. IRS-$1^{-/-}$ mice have shown increased plasma insulin and β-cell hyperplasia (Araki et al., 1994; Brüning et al., 1997), indicating negative regulation of insulin secretion by IRS-1. IRS-$2^{-/-}$ mice have shown hypoplastic islets and β-cell failure. The islets of 2-months-old animals developed hyperglycemia and hyperinsulinemia (Withers et al., 1998a), which again suggests negative regulation of insulin secretion by IRS-2. Furthermore, it has been

shown that IRS-2 expression is increased by glucose, incretins such as GLP-1, and other factors, which elevate cytosolic Ca^{2+} and cAMP in β-cells (Demozay et al., 2011; Jhala et al., 2003). Altogether, these data indicate certain downstream elements in IRS-2 signaling pathways that play important roles in β-cell function and survival (Rhodes et al., 2013a).

Because of increased first-phase insulin secretion, inceptor CKO mice show improved glucose tolerance. This phenotype appears at 2 months of age, even though fasting blood glucose levels in these mice are not altered. To understand the exact mechanism behind this observation, further experiments are required. Two explanations are possible. First, glucose could regulate IR in β-cells by acting on the IR downstream effectors. Second, glucose could stimulate insulin release, which again acts on IR in an autocrine insulin pathway (Kulkarni et al., 1999; Rothenberg et al., 1995).

Insulin secretion in βIRKO mice could lead to age dependent glucose intolerance, suggesting that insulin-resistance in T2D might be in part a reason for the defect in insulin secretion (Kulkarni et al., 1999). However, it is unclear how IR controls insulin secretion. Moreover, paracrine contributions of glucagon and somatostatin-producing cells were shown to be important factors in insulin control (Huising, 2020). In conclusion, more work is required to assess the exact mechanism of IR regulation of insulin secretion. Nevertheless, the idea that inceptor is involved in IR signaling to regulate insulin, would provide a unifying mechanism for improved β-cell function and insulin sensitivity.

Similar to IR, specific deletion of IGF-IR in β-cells influences insulin secretion, leading to fasting hyperinsulinemia and impaired glucose tolerance (Kulkarni et al., 2002b). The reason for these combined phenotypes is that basal insulin is elevated. However, glucose-stimulated insulin secretion is impaired. In these βIGF-IR$^{-/-}$ mice, an increased amount of rough endoplasmic reticulum and Golgi stacks was observed, which is consistent with constitutively active insulin secretion. It was previously shown that IGF-I is an inhibitor of insulin secretion in β-cells (Zhao et al., 1997). Therefore, these observations suggest an overactivation of insulin in βIGF-IR$^{-/-}$ mice.

Due to the fact that inceptor is expressed at a higher level in β-cells, it appears to be involved in β-cells to counteract Ins/IGF signaling. Despite the essential role of peripheral insulin resistance in T2D, β-cell dysfunction is required for developing diabetes. In pre-T2D patients, β-cells have been noticed to secrete an increased amount of insulin to overcome impaired insulin action. However, when this balance between insulin secretion and insulin resistance is not maintained, the full phenotype of T2D will appear (DeFronzo, 1988). In addition, it has been published that loss of first-phase glucose stimulated insulin secretion is the earliest abnormality sign of secretory dysfunction in β-cells of T2D patients (Cerasi et al., 1972; Poitout and Robertson, 1996). This defect in early insulin secretion has been described to cause hyperglycemia in MODY patients (Fajans, 1989; Polonsky et al., 1995). However, the link between insulin level and blood glucose is more complex in T2D. Insulin resistance and impairment of glucose tolerance are correlated with increased insulin secretion. Nevertheless, after glucose desensitization appears, increased blood glucose is associated with declined insulin secretion (Bogardus et al., 1984; DeFronzo, 1988).

Altogether, we have demonstrated that deletion of inceptor in β-cells augments insulin sensitivity by engaging IR and IGF-IR. Our finding provided a functional role of inceptor in islet β-cells in the

maintenance of glucose homeostasis. Insulin resistance at the level of β-cells may correlate with impairment of glucose-stimulated insulin secretion as shown in βIRKO mice (Kulkarni et al., 1999). Therefore, our data support the hypothesis from βIRKO mice that insulin resistance in T2D at the level of β-cells is linked to insulin resistance in peripheral tissues. This results in classical pathophysiological symptoms of T2D, i.e. blunting of first-phase insulin secretion. In conclusion, we have shown that inceptor is expressed in the pancreas, that it can be shed from β-cells, and its deletion correlates with improved glucose tolerance and increased first-phase insulin secretion. Therefore, we propose inceptor as a novel regulator to control glycemia.

5.3.2 Inceptor regulates β-cell proliferation

To understand whether the improved glucose tolerance of inceptor CKO islets was associated with any changes in β-cell mass, we quantified α- and β-cell mass. We found an increased β-cell mass in CKO mice, while there was no difference in α-cell mass. In line with enhanced β-cell mass, we observed an increase in β-cell proliferation as well. This observation is similar to the data from transgenic mice in which a constitutively active form of Akt1 (myr-Akt1) was expressed in pancreatic β-cells (Kohn et al., 1996). This mouse line showed an increase in both islet number and size (Tuttle et al., 2001). However, in both inceptor CKO and myr-Akt1transgenic mice, despite increased β-cell size, the morphology of islets remained unaffected. Additionally, similar to deletion of inceptor, the transgene of Akt1 affected only the β-cell size, while both α and δ-cell appeared normal (Tuttle et al., 2001). Consistent with the improved glucose tolerance in CKO mice, the Akt1 transgenic mice showed a lower rise in blood glucose during an ipGTT, accompanied by increased glucose stimulated insulin secretion. According to β-cell function, the islets from CKO mice showed a slightly higher response upon high glucose induction. This is consistent with islets from overexpressing active Akt1 mice, which exhibited hypersecretion of insulin in response to 9.2 and 11.6 mM glucose.

It is known that receptor tyrosine kinase signaling is important for β-cell proliferation. The main evidence supporting that IR and IGF-IR promote β-cell proliferation is from β-cell specific Irs-2 knockout, which shows reduced β-cell mass (Withers et al., 1998a). Indeed, mice lacking Irs-2 develop diabetes duo to a combination of insulin deficiency and impaired insulin action. This metabolic phenotype has been explained by an impaired growth or increased apoptosis of β-cells (Kitamura et al., 2002; Kushner et al., 2002). Additionally, it has been shown in Irs-2 null background mice that haploinsufficiency for both IR (Kitamura et al., 2002) and IGF-IR (Withers et al., 1998a) expedite β-cell decline, thus resulting in rapid-onset diabetes. In line with this data, β-cell specific ablation of PDK1, a kinase activating Akt in insulin signaling, resulted in both reduced β-cell proliferation and reduced β-cell size. This leads to a T2D-like phenotype in mice(Hashimoto et al., 2006), which is the opposite phenotype than inceptor CKO mice.

It is known that regulation of glucose homeostasis by insulin is required for normal β-cell mass and function. IGF-IR has been linked to islet development and differentiation (Bonner-Weir, 1994; Swenne, 1992a) and both IGF-I and IGF-II elevate islet growth (Otonkoski et al., 1988; Rabinovitch et al., 1982). However, the specific deletion of IGF-IR in β-cell does not alter islet size in βIGF-I$^{-/-}$ mice (Kulkarni et al., 2002a). Accordingly, β-cell mass and proliferation remain unaffected in βIRKO mice.

Since Akt is a prominent mediator of the action of IR and IGF-IR, we demonstrated that inceptor plays a role in insulin-mediated processes regarding regulation of pancreatic β-cells. In addition, several studies from isolated islets and insulinoma cells have assessed the molecular mechanism involved in proliferation in islet β-cells. They showed that glucose induction increases proliferation, which is associated with a higher number of β-cells entering the cell cycle (Swenne, 1992b). Moreover, it has been shown that both glucose and IGF-I mediated proliferation are dependent on PI3K pathways (Hügl et al., 1998). According to this, a role of PI3K in mammalian cell growth has been described in constitutively-active PI3K mice, which exhibited larger cardiomyocytes (Shioi et al., 2000). Since Akt is the main target of PI3K (Kandel and Hay, 1999), once PI3K is activated, Akt phosphorylates a number of downstream effectors which predominantly modulate cell growth. Since the PI3K-Akt pathway seems to be involved in both glucose and islet β-cell proliferation, the current observations in our study strongly suggest that phenotypes observed in inceptor CKO mice are associated with increased Akt activity (Dickson et al., 2001) and inceptor may be an important component of this pathway. According to this, constitutive activation of Akt1 in β-cells leads to increased β-cell mass resulting in hyperinsulinemia in RIP-Akt mice (Bernal-Mizrachi et al., 2001b). Since both CKO and mice overexpressing myr-Akt1 in β-cell show the same phenotype in terms of increased β-cell mass and improved glucose tolerance, we assume that inceptor deletion seems to be similar to AKT1 activation.

It is already known that changes in cell size, replication, neogenesis and cell death regulate islet β-cell mass (Bonner-Weir, 2000). Ribosomal S6 kinase (p70S6K), the downstream target of activated Akt, is known to be involved in cell growth. Of more relevance to our finding, S6K1-deficient mice showed hypoinsulinemia, glucose intolerance and decreased islet cell mass (Pende et al., 2000). Moreover, S6K1-deficient *Drosophila* exhibited reduction in body size (Montagne et al., 1999). Additionally, it is known that modulation of protein translation is partially mediated by S6K (Montagne et al., 1999; Tuttle et al., 2001). These data suggest that S6K1 is a critical downstream target for activated Akt1. Moreover, it has been shown that disruption of S6k1 leads to a significant decrease in size of the organism (Shima, 1998). We propose that Akt1 may be regulated by inceptor to inhibit β-cell mass. Therefore, we plan to investigate the effect of inceptor on S6k1 as a downstream target in the future.

An additional transcription factor regulated by Akt is PDX1, which is known to control β-cell maturation and secretory function. In line with this, it has been reported that lowered PDX1 expression causes impairment of β-cell growth resulting in blunted glucose-stimulated insulin secretion (Kulkarni et al., 2002b; Otani et al., 2004b; Stewart et al., 2015; Withers et al., 1998b).

In addition, it is known that increased proliferation in β-cells in response to glucose stimulation is due to the number of cells, which enter the cell cycle (Swenne, 1982). Further, cyclin dependent kinases (Cdk') have been identified as a key regulator of cell cycle (Fatrai et al., 2006b; Jones and Kazlauskas, 2001). Interestingly, mice lacking Cdk-4 showed insulin-dependent diabetes. In contrast, activation of Cdk-4 leads to β-cell hyperplasia (Rane et al., 1999). In other related studies, it has been shown that Akt changes proliferation by regulating Cdk/cyclin through GSK3 (Fatrai et al., 2006a; Manning and Cantley, 2007). These data together with current study suggest that increased proliferation in inceptor CKO and *Iir*$^{-/-}$ mice could be due to the activation of Akt and cyclin/Cdk pathways through inceptor, thus high rates in EdU incorporation in both CKO and

Iir$^{-/-}$ mice could explain the increase in β-cell mass. Further research is needed to investigate this hypothesis.

In conclusion, this work has emphasized the role of the insulin-signaling pathway to regulate cell growth and proliferation, which has been mentioned in several publications (Bernal-Mizrachi et al., 2001c; Tuttle et al., 2001). In β-cells, the signaling cascade appears to include the IR/IGF-IR, Irs, PI3K and Akt. Therefore, we assume that inceptor acts as a counter regulator for β-cell mass by regulation of Akt-mediated-IR/IGF-IR signaling. To counteract uncontrolled β-cell proliferation and growth, we hypothesize that inceptor desensitizes IR/IGF-IR signaling in the pancreas.

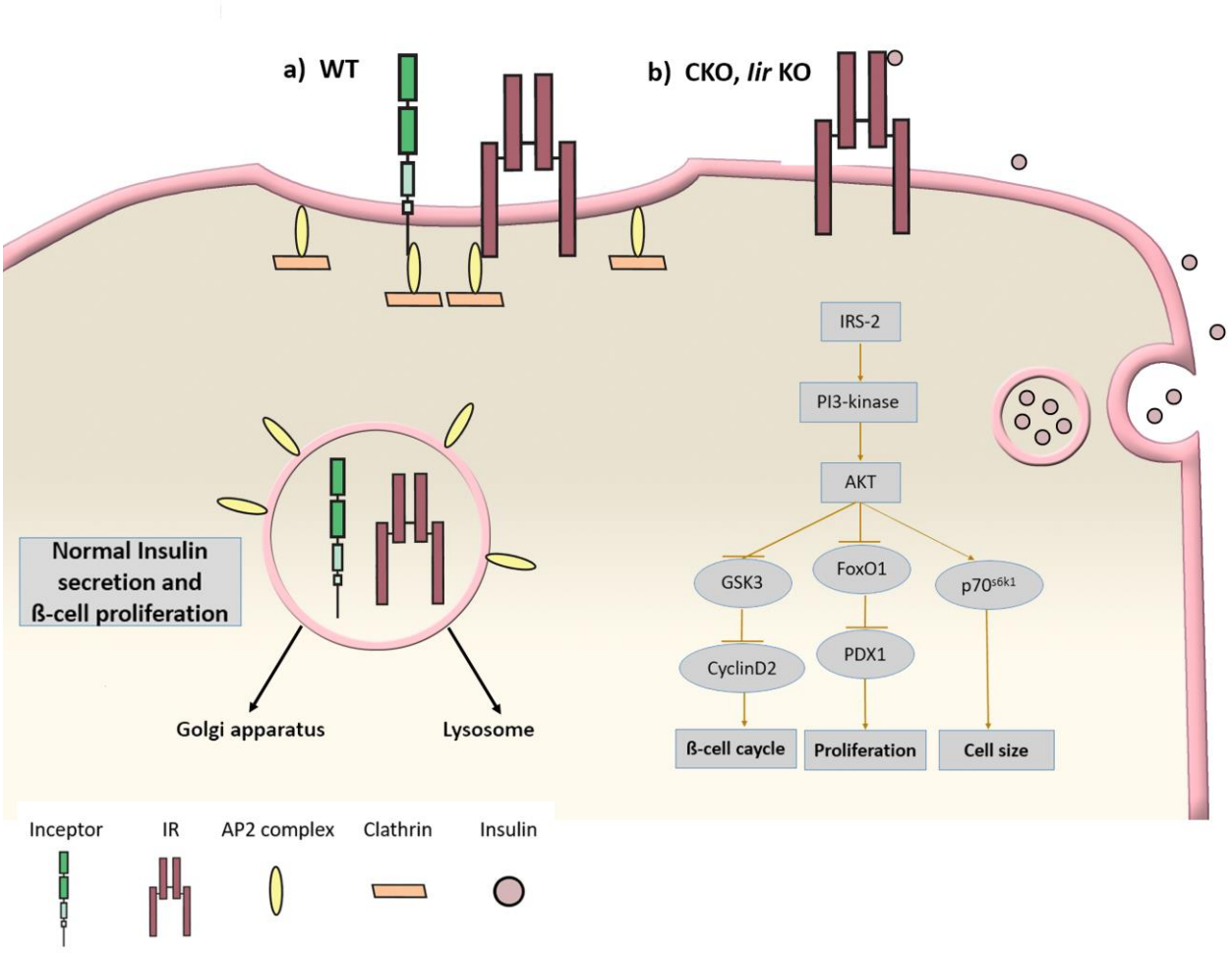

Figure 5.1: Schematic illustration of inceptor regulating IR/IGF-IR signaling in β-cell.

Inceptor contributes to decreased IR density on the cell surface through increasing clathrin-mediated endocytosis of IR. Therefore, insulin is not able to bind to its receptor, resulting in normal insulin secretion and proliferation (a). In absence of inceptor, the desensitization of IR is interrupted via this pathway, which causes enhanced activation of IR/IGF-IR downstream effectors (b).

5.3.3 Mechanism of action

The corresponding human gene of inceptor is called estrogen-induced gene 121 (*EIG121*), also known as endosome/lysosome-associated apoptosis and autophagy regulator 1 (*ELAPOR1*) or *KIAA1324*. EIG121 protein has so far been described in the context of cancer in various tissues and it has been published that it directly binds to estrogen receptor and fibroblast growth factor 3 receptor (Orchard et al., 2014). Additionally, it has been reported by Kang et al. that ELAPOR1 protein antagonizes the activation of PI3K-Akt kinase and caspase 7 by the general ER stress sensor GRP78/BiP (Kang et al., 2015). This observation suggests that ELAPOR1 plays a role as signaling repressor in specific tissues in which signaling must be inhibited, such as pancreatic β-cells that produce insulin and are exposed to high insulin concentrations.

The mechanisms which control insulin sensitivity and glucose metabolism are essential in the early phase of T2D development. The downstream signaling pathways of IR have been well described in β-cells. However, whether insulin sensitivity is regulated at the plasma membrane by interaction of IR with other co-receptors or other proteins is still unclear. The identification of a molecular sensor to adapt insulin sensitivity and secretion in β-cells would help our understanding on how autocrine insulin signaling controls excessive insulin secretion in β-cells. Additionally, whether β-cells are protected from constitutive activation of IR/IGF-IR signaling is currently unclear. As mentioned above (Section 4.1.2.3), inceptor was found to be highly expressed in pancreatic β-cells, the source of insulin production. In addition, many studies have ruled out an autocrine positive feedback of insulin to drive proinsulin biosynthesis (Leibowitz et al., 2003; Uchizono et al., 2007b; Wicksteed et al., 2003). If this is the case, higher insulin secretion leads to a more intense autocrine stimulus, thus causing deleterious consequences for β-cells. On the other hand, it is known that insulin causes β-cells to proliferate, which triggers more insulin production upon metabolic need. Due to these previous findings, we strongly believe that the insulin secretion is efficiently deactivated to avoid hyperinsulinemia. One of the mechanisms which could be considered is preventing the positive feedback loop in insulin signaling.

In addition to hyperinsulinemia, β-cell dysfunction is a sign of diabetes development. Both defects of insulin secretion and changes in β-cell mass have been seen in metabolic dysregulation. In addition, there is evidence of receptor tyrosine kinase involvement in insulin synthesis, release and β-cell proliferation. For instance, inactivation of IR (Kulkarni et al., 1999), IGF-IR (Kulkarni et al., 2002b; Xuan et al., 2002) and Irs1 (Kulkarni et al., 1999) in β-cell leads to an impairment of glucose-stimulated insulin secretion.

Since the inceptor protein has a cysteine-rich domain with similarities to IR/IGF-IR, it may be involved in binding a growth factor ligand. Therefore, we analyzed the phosphorylation of the downstream effectors of IR/IGF-IR such as PI3K-AKT, AMPK, and RAF-MAPK pathways both *in vivo* and *in vitro*. Western blot analysis showed that in the pancreas lysates of many KO mice Akt phosphorylation is upregulated. Since inceptor surface expression is regulated upon starvation in vitro, we have examined the impact of *Iir* knockout in *Iir*$^{-/-}$ on IR/IGF-IR signaling under starvation conditions. We have found that in both in vivo and in vitro phosphorylation of IR/IGF-IR and Akt is upregulated upon starvation when compared to the control. Thus, lack of inceptor leads to exacerbated insulin signaling upon starvation, suggesting that inceptor inhibits IR/IGF-IR signaling. However, we have demonstrated that inceptor directly mediates the IR/IGF-IR- ligand complex internalization via CME to an early endosome/lysosome compartment. In these

compartments the ligand is usually degraded and IR is recycled to the PM (Goh and Sorkin, 2013b). This process would be especially relevant for β-cells, the main source of insulin, where over-activation of IR due to high concentration of available ligand must be kept under control.

Multiple observations support the idea that insulin has a physiological role in β-cells (Otani et al., 2004b; Xu and Rothenberg, 1998). Moreover, pancreatic β-cell response to Ins/IGF-I, thus insulin itself is involved in regulation of insulin secretion, proliferation and survival of β-cells (Accili, 2004a; Goldfine and Kulkarni, 2012; LeRoith and Gavrilova, 2006). These data are in line with several *in vitro* and *in vivo* models which show that insulin signaling plays a direct role in β-cell biology (Aspinwall et al., 1999; Johnson and Misler, 2002; Leibiger et al., 1998; Ohsugi et al., 2005; da SILVA XAVIER et al., 2004). Despite the data from Alonzo and colleagues who have reported that IR is not required for glucose-stimulated β-cell proliferation (Stamateris et al., 2016), other groups have shown that glucose effects on β-cells through insulin acting upon its own receptor (Assmann et al., 2009b; Martinez et al., 2006). According to these, in βIRKO mice, a lack of phosphorylation of Akt and p70S6K after both glucose and insulin stimulation have been observed, suggesting the dependent effect of glucose and insulin on IR (Mezza et al., 2016). Consistent with this data, the phosphorylation of Akt remained unaffected in response to glucose stimulation in βIRKO cell lines (Assmann et al., 2009c). These data are consistent with current data showing that the effect of insulin and glucose on Akt activity both *in vitro* and *in vivo* are dependent on IR signaling. While these data indicate that Akt is the major target of insulin signaling, they also suggest the possibility that Akt can be activated by IGF-IR. Further investigations are required to dissect the mechanism of glucose and insulin on IR/IGF-IR in the regulation of target effectors involved in proliferation and/or secretory function in β-cells.

5.4 Function of inceptor in T2D

It is well known that the insulin/IGF1R signaling pathway in β-cells contributes to β-cell proliferation, differentiation, and protection against apoptosis (Cornu et al., 2010; Modi et al., 2015; Okada et al., 2007; Ueki et al., 2006a). Disruption of β-cell insulin signaling/resistance contributes to β-cell dysfunction leading to decline in β-cell mass or diabetes. Insulin acts as a growth factor during embryonic life and its primary role in adult animals is to maintain energy homeostasis in tissues (Accili, 2004b). Pathways downstream of insulin signaling control β-cell growth, function, and survival (Goldfine and Kulkarni, 2012)(Leibiger et al., 2008c). For diabetes therapy, insulin is the most common treatment, although it comes with potential unwanted effects such as weight gain or sudden hypoglycemia.

As mentioned in section (4.1.7.7), the lack of inceptor resulted in the sustained activation of IR and IGF-IR in β-cell. The expression of IR-mediated signaling molecules is known to be reduced in islets from T2D patients (Folli et al., 2011). Therefore, we were wondering whether treatments targeted at IR/IGF-IR signaling via inceptor might contribute to the development of therapy to recover β-cell function in T2D patients. However, further expression information is required to clearly verify the role of inceptor in T2D.

In addition, we have shown that blocking of inceptor with inceptor-specific monoclonal antibodies resulted in increased surface expression of IR and signal transduction (Ansarullah et al., 2021). We have shown that inceptor is able to directly calibrate IR expression, by interrupting the interaction between inceptor and IR/IGF-IR by using monoclonal antibodies against the

extracellular domain of inceptor, resulting in delayed internalization of IR. Targeting diseased β-cells with therapeutic mAb's of inceptor could pave the way to increased/sustained IR signaling which in turn could be beneficial for patients with low β-cell mass and congenital hyperinsulinemia. Overall, these data suggest promising opportunities for inceptor as an important target to regulate insulin signaling in diabetic β-cells.

Furthermore, to determine whether the lack of inceptor in pancreatic β-cells results in decreased susceptibility to experimental diabetes, for further investigation, CKO and control mice could be injected with streptozocin (STZ). We assume that CKO mice would be resistant to STZ-induced diabetes, which was shown in RIP-Akt mice (Bernal-Mizrachi et al., 2001b). The effect of activated Akt on cell survival together with increased β-cell proliferation and mass (Bernal-Mizrachi et al., 2001b) could explain the resistance of RIP-Akt mice to develop diabetes after multiple doses of STZ. Since CKO mice exhibit upregulation of Akt phosphorylation, we assume an augmented survival of CKO isletssubjected to STZ. However further investigation would be necessary to fully assess the contribution of inceptor in cell survival. The fact that RIP-Akt mice show resistance to develop STZ-induced experimental diabetes (Bernal-Mizrachi et al., 2001b), suggest that overactivation of Akt signal in CKO mice could rapidly replenish β-cell mass by replication. The resistance to developing diabetes in CKO mice can also be verified by crossbreeding with animals, which have intrinsic predisposition to β-cell failure.

In addition, it is known that insulin resistance and pancreatic β-cell failure are the most pathological effect involved in T2D. In the earlier phase of developing T2D, β-cell failure is involved in diminished glucose-responsive insulin secretion and decrease in cell volume. In T2D patients, β-cell failure causes impaired glucose tolerance over time. Hence, suppression of β-cell failure could be the best treatment of T2D.To develop drugs against β-cell failure, it is essential to understand the mechanism involved in both β-cell volume and glucose-responsive insulin secretion in β-cells. Inceptor plays an important role in regulation of β-cell mass and glucose-induced insulin secretion by inducing signals through IR and IGF-IR. Thus, we assume that the knowledge from the current study could eventually fulfill the establishment of a new treatment which could help the maintenance of normal β-cell function in T2D. Importantly, insulin secreted in β-cells binds IR in an autocrine or paracrine manner to increase β-cell function. Desensitization of IR/IGF-IR could modulate their downstream molecules involved in signal transduction.

In conclusion, dissecting molecular pathways involved in regulation of β-cells through inceptor might help to prevent or manage diabetes. Since β-cells are secreting a high amount of insulin, a process is needed to weaken a continuous autocrine stimulation in these cells. As we know, insulin signaling is required for normal β-cell function, but too much activation of IR could be detrimental. Therefore, the role of inceptor is essential in pancreatic β-cells to blunt the response to insulin. Despite the not fully clear physiological role of inceptor, the discovery of inceptor could aid in obtaining a full understanding of IR signaling in pancreatic β-cells. Further investigation will be required to clearly verify the role of inceptor in IR/IGF-IR signaling in β-cells during development, adulthood and acute versus chronic stimulation.

6 Material and methods

6.1 Material

6.1.1 Equipment

Following equipment were used in this study (Table 6.1).

Table 6.1: List of equipment

Equipment	Model	Manufacturer
Agarose gel chamber	Midi 450	Neolab, Heidelberg
Automatic pipettes	0.5- 10 µl 10- 100 µl 100- 1000 µl	Eppendorf, Hamburg
Balances	ScoutTM Pro	OHAUS
Biorep perfusion system	Biorep Technologies	Miami USA
Centrifuges	5417R, 5430C, 5804 R Microcentrifuge Micro 220 Universal 320R	Eppendorf, Hamburg Roth, Karlsruhe Hettich, Tuttlingen Hettich, Tuttlingen
CO_2-Incubator	BBD6220 Incubator C16 KBF Shake'n'Stack	Thermo Scientific, Waltham Labortect, Rosdorf Binder, Tuttlingen Möhringen Thermo Fisher, Waltham
Cryostat	Ag Protect	Leica, Wetzlar
Developing machine	AGFA Curix 60	AGFA HealthCare GmbH, Bonn
ELISA reader	PHERAastar FS	BMG Labtech, Ottenberg
Film cassettes	hypercassette	Amersham, München
Freezer	-20°C Medline, premium nofrost -80°C	Liebherr, Ochsenhausen Thermo Scientific, Waltham
Fridge	4°C comfort	Liebherr, Ochsenhausen
Glass ware	Schott-Duran	Schott, Mainz
Glucometer	Freestyle freedom lite ContourXT	Ascenia Diabetes Care Deutschland, Leverkusen
Heating block	Thermo mixer comfort	Eppendorf, Hamburg, DE
Incubation systems/ovens	Thermomixer comfort Thermomixer 5436	Eppendorf, Hamburg Eppendorf, Hamburg
Microtome	HM355s	Thermo Fisher, Waltham
Microwave	700 W	Severin Elektrogeräte, Sundern
Microscopes	MS5, MZ75	Leica Microsystems, Wetzlar

Equipment	Model	Manufacturer
	TCS SP5 and Cube M80 and Dissection light	Leica Microsystems, Wetzlar Leica Microsystems, Wetzlar
N2 tank	Biostore systems	Cryo Anlagenbau, Wilnsdorf
Paraffin embedding machine	EG1150H	Leica, Wetzlar
PCR machines	Personal Thermocycler Professional Trio Thermocycler PXE0.2 Thermo Cycler	Biometra, Goettingen Biometra, Goettingen Thermo Fisher Scientific , Waltham
pH meter	Mettler Toledo	HANNA Instrumentes, Kehl am Rhein
Photometer	NanoDrop 2000c	Thermo Fisher Scientific , Waltham
Pipetboy	Accu-jet® pro	Brand GmbH, Wertheim
Pipettes	0.2- 10 µl 100 µL, 200 µL, 1000 µL	Eppendorf, Hamburg, DE Gilson, Limburg-Offenheim
Plastic ware	Vitlab GmbH	Großostheim
Polyacrylamide gel chamber	Mini Trans-Blot® Cell	Bio-Rad, Heidelberg
Power supply (gel chamber)	Power Source 300V	VWR International, Darmstadt
Roller/Mixer	VSR 23 Shaker DOS-10L RMS (I), Rocker 247	VWR International, Darmstadt Neolab, Heidelberg Everlast
Sonicator	Sonoplus HD2070 Elmasonic, UW 2070	Bandelin electronic, Berlin Bandelin electronics, Berlin
Sterile hoods	MSC Advantage	Thermo Scientific, Waltham
Stirrer	D-6011	Neolab, Heidelberg
Thermo cage	Advanced animal warming system	Data Sand technologies, Mondivi USA
Timer	Roth	Karlsruhe
Tissue homogenizer	Ultra Turrax T25	IKA
Ultrasonic bath	ultrasonic cleaner	VWR International, Darmstadt
Vortex	vortexer	VWR International, Darmstadt
Water bath	SWB25	Thermo Fisher Scientific, Langenselbold
Water purification system	Millipore Q-POD (0.22 µl filter)	Merck Chemicals, Schwalbach
Western blot semi-dry	Trans-Blot® SD, Semi-Dry Transfer Cell	Bio-Rad, Heidelberg

Equipment	Model	Manufacturer
WB imager	ChemStudio AS	Analytik, Jena

6.1.2 Consumables

Following consumables were used in this study (Table 6.2).

Table 6.2: List of consumables

Consumables	Model	Manufacturer
15/50 mL tubes	Becton and Dickinson Company	Franklin Lakes
6/10/15 cm dishes	Nunc	Thermo Scientific Fisher, Waltham
96/48/24/12/6 well plates	Nunc	Thermo Scientific Fisher, Waltham
10 cm bacterial plates	BD FalconTM	Becton and Dickinson and Company, Franklin Lakes
8/16 well chambers	uncoated and coated 8-well imaging plate	Ibidi, Planegg
EDTA-treated tubes	Microvette Di-pottasium-EDTA	Sarstedt, Kleinstadt
Embedding moulds	Peel-A-Way®	Roth, Karlsruhe
1/2/5/10/25/50 mL plastic pipettes	Greiner Bio-One GmbH	Frickenhausen
Adhesive covers	Optical adhesive covers	Life Technologies, Frankfurt
Blotting paper	Whatman paper	GE Healthcare Buchler GmbH & Co. KG, München
Cell strainer	Nylon cell stainer 70 µm	Falcon, Fisher Scientific, Waltham
Clamp (pancreas)	Bulldog SerrefinE-Straight 35 mm	Fine Science Tools GmbH, Heidelberg
Cryotubes	Sarstedt	Kleinstadt
Cover slips	VWR International	Darmstadt
Embedding molds	Peel-A-WayR	Roth, Karlsruhe
Films	Hyperfilm ECL CEA, Rö.Blaufilm, RP new	Healthcare Buchler, München Christianse&Linhardt, München
Glass slides	Menzel Gläser superfrost plus	Thermo Scientific, Waltham
microvettes	with clotting activator	Sarstedt, München
Forceps	Dumount Inox	11251-, 11252-20, Fine Science Tools GmbH, Heidelberg
Freezing boxes	Freezing container, Nalgene®	Sigma-Aldrich, München BioCision LLC, USA, CA

Consumables	Model	Manufacturer
	CoolCell® Alcohol-Free	
Glass slides	Menzel Gläser superfrost plus	Thermo Scientific, Waltham
Needles	Sterican 27G ½ , Sterican 30G ½	B.Braun, Puchheim
Nitrocellulose membrane	GE Healthcare Buchler GmbH & Co. KG	München
Parafilm	Pechiney Plastic Packaging	
PVDF membrane	Biorad	München
Scalpels	Sterile	B.Braun, Tuttlingen
Scissors	14088-10	Fine Science Tools GmbH, Heidelberg
Spacer	Secure-Sela, 9mm 0.12 mm deep	Life Technologies, Frankfurt
Syringes	Omnifix 3/30 mL Omnican 50 mL	Braun Melsungen, Melsungen Braun Melsungen, Melsungen
Syringe filter	Filter unit fast flow and low binding 0.22 µm	Millex-GP
qPCR 96-well plates	MicroAmp Fast optcal 96-well reaction plate	Life Technologies, Frankfurt
Pasteur pipettes, plastic	3 mL	Roth, Karlsruhe
Pasteur pipettes, glass	12/23 cm	LABOR-BRAND, Gießen; Hirschmann Laborgeräte GmbH & Co. KG, Eberstadt
PCR Tubes		Eppendorf, Hamburg
0.2/1.5/2 ml tubes	safe-lock reaction tubes	Eppendorf, Hamburg

6.1.3 Kits and Mastermix

5x VILO™ reaction mix and 10x SuperScript (Life Technologies)

Agilent RNA 6000 Nano kit (Agilent Technologies # 5067-1521)

Click-IT EDU Alexa Fluor 647 (#C10340, Life Technologies)

Dynamo Color Flash SYBR Green qPCR kit (Life Technologiest)

ECL Clarity Western ECL substrate kit (Biorad)

Insulin Ultra Sensitive Assay Kit, HTRF assay (Cisbio # 62IN2PEH)

Mouse Glucagon ELISA kit (Crystal chem)

Pierce BCA Protein Assay Kit (Thermo Fisher Scientific# SA244527)

QIAquick PCR Purification Kit (Qiagen Holding)

RNeasy Lipid tissue mini kit (Qiagen#74804)

SuperScript Vilo cDNA synthesis kit (Life Technologies)

SuperSignal West femto maximum sensitivity substrate (Life Technologies)

TaqMan Fast Advanced Master Mix (Life Technologies)

Ultrasensitive mouse insulin ELISA kit (Crystal Chem INC., #90080)

C-peptide ELISA kit (Crystal Chem INC., #90080)

LabAssayTM Glucose (Mutarotase-GOD method) (WAKO. #298-6570)

Periodic acid-schiff (PAS) staining system (Sigma-Aldrich., #395)

ABC peroxidase standard staining kit (Thermo Fisher Scientific., #32020)

6.1.4 Chemicals

If not indicated, chemicals were purchased from Roth, Karlsruhe; Merck, Darmstadt; Sigma Aldrich, Hamburg.

Table 6.3: List of chemicals

A	Acetic acid
	Acrylamide/bisacrylamide (Rotiphorese)
	Agarose (Biozym Scientific)
	Ammoniumpersulfat (APS)
	L-Arginine
B	BCA
	Big Dye/ Big Dye Buffer (Life Technologies 4337457 or Lager 5000986)
	Bovine Serum Albumine (BSA)
	Bradford reagent
	Bromophenol blue
C	Calcium chloride
	Chloroform, 99+%
D	4', 6-diamidino-2-phenylindole (DAPI)
	Developer G135 A/B (AGFA, Bonn)
	Dimethylsulfoxide (DMSO)
	DNAZap (Thermo Fisher Scientific, Waltham)
	dNTPs (Fermentas, Leon-Rot)
	Dithiothreitol (DTT)
E	Ethylene glycol-bis(β-aminoethyl ether)-N,N,N',N',-tetraacetic acid (EGTA)
	Ethylendiaminetetracetat (EDTA)
	5-Ethynyl-2'-deoxyuridine (EdU, Life Technologies, Frankfurt)
	Ethanol, 96%

	Ethidium bromide
F	Formaldehyde
	Formamide
G	Glucose (D-)
	Glutaraldehyde
	Glycerol
	Glycine
H	HEPES
	Hydrochloric acid
	Hydrogen chloride (HCl)
I	Isopropanol, 100%
M	Magnesium chloride
	Magnesium sulphate
	Methanol, 100%
	Milk powder (Becton Dickinson GmbH, Heidelberg)
	Mounting medium (Leica, Wetzlar)
N	Natrium citrate
	Nitrogen(l) (Linde AG, München)
	NP-40 nonylphenoxypolyethoxyethanol (Nonidet NP-40) (Life Technologies, Frankfurt)
O	Orange G
P	Paraformaldehyde (PFA)
	Polyacrylamide
	Polyvinyl-alcohol
	Potassium chloride (KCl)
	Potassium hydrogenphosphate (KH2PO4)
R	Rapid fixer G356 (AGFA, Bonn)
	RNaseZAP
	RNase (Promega GmbH, Mannheim)
	RNase inhibitors (Fermentas GmbH, St. Leon-Rot)
S	Sodium chloride (NaCl)
	Sodium deoxycholate (C24H39O4Na)
	Sodium dodecyl sulphate (SDS)
	Sodium hydrogenic phosphate (Na2HPO4)
	Sodium hydroxide
	Sodium tetraborate (Na2B2O7)
	Superscript II (Fermentas GmbH, St. Leon-Rot)
T	TEMED

	Tris(hydroxymethyl) aminomethane
	Triton X-100
	Tween-20
	Tamoxifen
X	5-bromo-4-chloro-3-indolyl-β-D-galactopyranoside (X-Gal)
	Xylene

6.1.5 Buffers and solutions

Western blot

10x TBST:	100 mM Tris/HCl, 1.5 M NaCl, 2.0% Tween20 (adjust to pH7.4)
10x Tris-Glycine (running buffer):	1.0% SDS, 0.25 M Tris, 1.92 M Glycine
4x SDS-loading buffer:	200 mM Tris/HCl, pH 6.8, 8% SDS, 40% Glycerol, 0.4% bromine phenol blue (add freshly 400 mM DTT)
4x Tris-HCl/SDS buffer:	1.5 M Tris, 0.4% SDS (adjust to pH 8.8)
4x Tris-HCl/SDS buffer:	0.5 M Tris, 0.4% SDS (adjust to pH 6.8)
APS:	10% APS (in dH_2O)
Blocking solution:	5% milk powder in 1x TBST
Buffer cathode (KP):	25 mM Tris/HCl, 40 mM Glycine, 10% Methanol (adjust to pH9.4)
Buffer anode I (API):	300 mM Tris/HCl, 10% Methanol (adjust to pH10.4)
Buffer anode II (APII):	25 mM Tris/HCl, 10% Methanol (adjust to pH10.4)
RIPA buffer:	75 mM NaCl, 6.37 mM Natriumdesoxycholat 0.005% NP40, 0.05% SDS, 25 mM Tris pH8
Ponceau-solution:	0.2% PonceauS, 3% TCA
Protein ladder:	PageRuler Plus Pre-Stained (Life Technologies, Frankfurt)
(Femto-) ECL-solution:	Solution A and B mix: 1:1 (mix shortly before usage)
β-mercaptoethanol (50mM):	Gibco / Life Technologies
Bio-Gel P-4 polyacrylamide:	Biorep Technologies, Miami USA

Immunostainings

10x PBS:	1.37 M NaCl, 26.8 mM KCl, 0,101 M Na_2HPO_4, 13.8 mM KH_2PO_4
PBST:	1x PBS + 0.1% Tween20 (adjust to pH7.4)
4% PFA:	1.3 M PFA in 1x PBS (adjust to pH7.2-7.4)
Permeabilization (sections):	0.2% TritonX-100, 100 mM Glycin in dH_2O

Permeabilization (islets):	0.5% TritonX-100, 100 mM Glycin in dH_2O
Blocking solution:	5% FCS, 1% serum (goat or donkey) in PBST
DAPI:	5 mg DAPI in 25 ml PBS
Elvanol (embedding):	0.015 mM Polyvinyl-alcohol, 24 mM Tris pH 6.0, 2 g DABCO in 90 ml H_2O and 37.8 ml Glycerol
Antigen retrieval:	Rodent Decloaker 10x (Biocare medical #RD913M)
10x Tris-Borat-Buffer:	10 mM $Na_2B_2O_7$ in dH_2O
Xylene mounting medium:	Roti® Histokitt (Carl-Roth GmbH, Karlsruhe)
Hematoxylin solution:	Mayer´s MHS1 (Sigma # MHS16-500ML)
OCT medium:	optimal cutting temperature (Leica Microsystems GmbH, Wetzlar)
Eosin	(Sigma #HT110216-500ML)
Xylen	(Pan reac application #UN1307)

Dynamic glucose induced insulin secretion

Krebs-Ringer buffer (KRB):	140 mM NaCl, 3.6 mM KCl, 0.5 mM KH2PO4, 0.5 mM MgSO4 x 7 H2O, 1.5 mM CaCl2, 10 mM HEPES, 2 mM NaHCO3, 0.1 % BSA, pH 7.4.

Islet isolation

G-Solution:	HBSS (Lonza Verviers, Belgium) 1x Penicillin/Streptomycin (100x) (Gibco) 1% BSA (Sigma, Hamburg) (5 g BSA sterile filtered)
Gradient medium:	30 µl 1M HEPES (Life Technologies, Frankfurt) 970 µl DPBS (Lonza Verviers, Belgium) 2 ml Optiprep density gradient medium (Sigma, Hamburg) 5 ml G-solution
Islet culture medium:	RPMI1640 (Lonza) supplemented with 1x P/S (Gibco) and 10% FCS (PAA)
Islet culture medium:	RPMI1640 (Lonza) supplemented with 1x P/S (Gibco) and 3% FCS (PAA)
DPBS:	Lonza

Isolation of genomic DNA

Tail Lysis buffer	(100 mM Tris pH 8.5, 200 mM NaCl, 5 mM EDTA, 0.2 % SDS)

The pancreatic insulin content

Acid-ethanol buffer (5mL 1.5% HCl in 70% EtOH)

6.1.6 Enzymes, inhibitors and growth factors

Collagenase: 1 mg/ml Collagenase P (Roche) in G-solution

DNA-Polymerase: Thermo Fisher Scientific (Taq DNA Polymerase, recombinant)

RNase-free DNase I: Qiagen

Phosphatase and Proteinase inhibitors: Sigma-Aldrich

Insulin (islet): Sigma Aldrich, Hamburg

Insulin (mice): Actrapid penfill (Bagsværd, Denmark)

6.1.7 Antibodies

A list of used antibodies together with their optimal concentrations and using technics in vivo are listed in Table 6.4.

Table 6.4: List of inceptor antibodies for validation.

Name	Species	Clonality	inceptor	Signal
14F1-1141	rat	monoclonal	peptide of cytoplasmic domain	WB, 1:1000
16F6-311	rat	monoclonal	peptide of cytoplasmic domain	IHC, 1:10
Animal 3	rabbit	polyclonal	peptide of cytoplasmic domain	WB, 1:1000
1692	rabbit	polyclonal	recombinant protein of extracellular domain	IHC
1374	rabbit	polyclonal	recombinant protein of extracellular domain	IHC

A list of all primary antibodies used in this thesis. Abbreviations: WB: Western Blot, IF: Immunofluorescence.

Table 6.5: List of primary antibodies

ID	Protein Name	Generated in	Dilution	Company
29	α-Tubulin	mouse	WB 1:5000	Sigma
111	E-cadherin	rabbit	IF 1:500	CST
173	gamma-tubulin	mouse	WB 1:10000	Abcam
193	Insulin	guinea pig	IF 1:1000	Thermo Fisher
206	Gapdh	mouse	WB 1:5000	Merck Biosciences

ID	Protein Name	Generated in	Dilution	Company
213	Nkx6.1	goat	IF 1:200	R&D systems
214	Somatostatin	goat	IF 1:300	SCBT
218	CD49f	rat	IF:1:300	BD
221	MafA	rabbit	IF 1:300	Novusbio
238	Chromogranin A	goat	IF 1:100	SCBT
257	Pancreatic polypeptide	goat	IF 1:300	Abcam
277	Urocortin 3	rabbit	IF 1:300	Phoenix Pharmaceuticals
270	Akt-Phospho	rabbit	WB 1:1000	Cell signaling
302	Insulin	rabbit	IF 1:500	Thermo Fisher Scientific
315	Glucagon	guinea pig	IF 1:2500	Takara Bio
251	Sox9	rabbit	IF 1:300	Millipore
262	Insulin Receptor beta	rabbit	WB 1:1000	NEB
616	Insulin Receptor beta	mouse	WB 1:1000	Cell signaling
383	Pdx1	goat	IF:250	Abcam
428	Foxa2	rabbit	IF 1:300	CST
432	HSP90	rabbit	WB 1:5000	Cell signaling
440	Insulin	rabbit	IF 1:300	CST
274	mTOR-Phospho	rabbit	WB 1:1000	Cell signaling
433	IGF-I Receptor β	rabbit	WB 1:1000	Cell signaling
434	Insulin Receptor/IGF1R phospho	rabbit	WB 1:500	Cell Signaling
511	Akt(pan)	mouse	WB 1:1000	Cell Signaling/NEB
512	mTOR	mouse	WB 1:1000	Cell Signaling
642	α amylase	rabbit	IF 1:400	Abcam

Secondary antibodies used in this thesis. Abbreviations: WB: Western Blot, IF: Immunofluorescence

Table 6.6: Secondary antibodies

ID	Name	Conjugated	Dilution	Company
15	Goat anti-mouse IgG	HRP	WB 1:20000	Dianova
18	Donkey anti-goat IgG	633	IC 1:800	Invitrogen
19	Goat anti-rabbit lgG	HRP	WB 1:20000	Dianova
23	Donkey anti-mouse IgG	488	IC 1:800	Invitrogen
24	Donkey anti-rabbit IgG	555	IC 1:800	Invitrogen
26	Donkey anti- rabbit lgG	488	IC 1:800	Invitrogen
35	Donkey anti-goat IgG	555	IC 1:800	Invitrogen
45	donkey anti-rat IgG	649	IC 1:800	Dianova

ID	Name	Conjugated	Dilution	Company
46	donkey anti-guinea pig	649	IC 1:800	Dianova
56	Donkey anti-mouse IgG	594	IC 1:800	Invitrogen
62	Donkey anti-rat IgG	647	IC 1:800	Dianova
63	Donkey anti-goat IgG	594	IC 1:800	Invitrogen
64	Donkey anti- rabbit lgG	594	IC 1:800	Invitrogen
75	Donkey anti-rat IgG	488	IC 1:800	Invitrogen
76	Donkey anti- guinea pig IgG	488	IC 1:500	Invitrogen

6.1.8 Mouse lines

C57BL/6NCrl	BL6 mice were obtained from Charles River
CD1	Outbred strain (Helmholtz Zentrum München)
Rosa-Cre	(Grippo, Nowlin, Cassaday, & Sandgren, 2002)
FLPe	(Farley, Soriano, Steffen, & Dymecki, 2000)
Iir ko (ΔEx3)	5330417C22Rik $^{tm1a(EUCOMM)Hmgu}$ stem cells (H03) were aggregated with CD1 morula (Artus & Hadjantonakis, 2011). ESC clone bought from the European Conditional Mouse Mutagenesis Program. (Ansarullah et al., 2021)
Iir gene trap	Background: CD1
Iir flox	Background: mixed CD1, C57BL/6J
Iir FD	Background: mixed CD1, C57BL/6J
MIP1-CreERT	(Tamarina et al., 2014)
MIP-CreERT2; *Iir* $^{flox/FD}$	(Ansarullah et al., 2021)

6.1.9 Primers

All primers were purchased from Eurofins MWG Operon, Munich.

Table 6.7: List of primers for sequencing

ID	T_m (°C)	sequence 5' → 3'
EP: 0485	65	ATGCCCAAGAAGAAGAGGAAGGT
EP: 0486	67	GAAATCAGTGCGTTCGAACGCTAGA
EP 0176	57	CTAATGTTGTGGGAAATTGGAGC
EP 0177	54	CTCGAGGATAACTTGTTTATTGC
EP 1486	70	CCTGGCGATCCCTGAACATGTCCT
EP 1487	65	TGGACTATAAAGCTGGTGGGCAT
EP 1583	60	GTGCACTCTGGGTAGTGTTC
EP 1584	60	GATGCCTGTCAGCCTTCATC

ID	T_m (°C)	sequence 5' → 3'
EP 1585	64	CACCTCCCCCTGAACCTGAAAC
EP 1586	62	GAGTGGGATGAGCTACCTCAC
EP 1270	63	CCAAGGCCAGCGATACAACC
EP 1425	59	GGAACTTCGTCGAGATAACTTCGTATAG

6.2 Methods

6.2.1 General mouse handling

Animal studies improvements. The animal experiments were carried out in compliance with the German Animal Protection Act, the guidelines of the Society of Laboratory Animals (GV-SOLAS) and Federation of Laboratory Animal Science Associations (FELASA). Mice were housed at an ambient temperature of 23ºC with a constant humidity and a 12 hours' light - dark cycle.

6.2.2 Genotyping

Isolation of genomic DNA. DNA was extract from ear punches collected during weaning (P>21 days). They were then lysed in 500 µl of Tail Lysis Buffer with 100 µg/ml of Proteinase K. After overnight incubation at 55°C the tubes were vortexed and 500 µl of Isopropanol was added to the tubes. To pellet the DNA, the tubes were centrifuged at 14000 rmp for 15 min at RT. Additionally; the DNA was washed in ice-cold 70% ethanol and after another centrifugation at 14000 rpm for 10 min at 4°C, was dried for 10 min at room temperature and dissolved in 100 µl of nuclease-free water at RT for overnight. The genotyping part of the samples was processed through Polymerase Chain Reaction (PCR).

Polymerase Chain Reaction (PCR). DNA segments were amplified in a PCR: The PCR mix contained genomic DNA (1µL), 10x Taq buffer without (NH4)2SO4 and MgCl2 (2 µL), 25 mM MgCl2 (2 µL), 10 mM dNTPS (1µL), 10 µM primer (1 µL each) and 5U/µL Taq DNA polymerase (0.3 µL) in a final volume of 20 µL.

Electrophoresis. The PCR reaction was added with 5 µl of Orange G (1:5) and loaded on 2% Agarose gel. Therefore, 2 g agarose powder were dissolved in 100 mL Tris acetate-EDTA buffer (40 mM Tris, 1 mM glacial acetic acid, 1 mM EDTA) using a microwave. After cooling, the solution Midori Green Advance gel stain (NIPPON Genetics EUROPE GmbH, MG04) was added to the solution. The solid gel was transferred into a TAE buffer filled gel chamber. The gel was run for 30 to 45 min at 100 V and detected in UVsolo TS Imaging System (Biometra).

Table 6.8: Genotyping PCRs

Gene	Primers	PCR program	Size
Rosa-Cre	EP: 0485 EP: 0486	94ºC 5 min [94°C 30s / 58°C 40s / 72°C 90s] x 35 72°C 2min 4°C ∞	Rosa-Cre+: 450 bp
FLPe	EP 0176 EP 0177	94°C 5min [94°C 60s / 50°C 60s / 72°C 60s] x 36	FLPe+: 550 bp

Gene	Primers	PCR program	Size
		72°C 10min 4°C ∞	
MIP-CreERT	EP 1486 EP 1487	95°C 5min [95°C 30s / 70°C 45s / 72°C 45s] x 11 [95°C 30s / 60°C 45s / 72°C 45s] x 30 72°C 5min 4°C ∞	MIP-CreERT+: 513 bp
Iir gene trap	EP 1583 EP 1584	95°C 5min [95°C 30s / 55°C 45s / 72°C 45s] x 34 72°C 5min 4°C ∞	Gene trap: 239 bp WT: 203 bp
Iir ΔEx3/flox	EP 1584 EP 1585 EP 1586	95°C 3min [95°C 30s / 64°C 45s / 72°C 45s] x 1 [95°C 30s / 55°C 30s / 72°C 30s] x 35 72°C 5min 4°C ∞	ΔEx3: 341 bp WT: 239 bp flox: 431 bp
Iir FD/flox	EP 1270 EP 1425 EP 1583	95°C 3min [94°C 30s / 64°C 45s / 72°C 45s] x 9 [95°C 30s / 55°C 30s / 72°C 30s] x 35 72°C 5min 4°C ∞	FD: 285 bp WT: 395 bp flox: 431 bp

6.2.3 Analysis of new born mice

6.2.3.1 Mouse husbandry and mating

The mice were kept in a day-night cycle (6.30 am-6.30 pm). *Iir* $^{+/-}$ (ΔEx3) animals were mated during the night (from 7 pm to 6 am). For determination of the embryonic stages, bred female mice where check in the morning for the presence of a vaginal plug. Noon of the day of the plug was considered as embryonic day 0.5 (E0.5). At E19.5, embryos were obtained by Cesarean section. Additionally, they were weighed and sacrificed for dissection of the pancreas or measurement of metabolic parameters.

6.2.3.2 Isolation of embryos and organs

Dissection of embryos and organs were performed according to Nagy and Behringer („Manipulating the mouse embryo: a laboratory manual “).

6.2.3.3 Administration of EdU

To assess endocrine proliferation, the modified Uracil analogs 5´ethynyl-2´-desoxyuridine (EdU) was used to label proliferating cells. This analog enters the cells and is incorporated into the DNA strain during the S-phase and can be visualized by specific antibodies. To analyze endocrine

proliferation in embryonic stages, Edu was injected to pregnant *Iir* $^{+/+}$ and *Iir* $^{-/-}$ mice at a dose of 10 mg/g body weight intraperitoneal 2 h prior to sacrifice. Pancreata were dissected from E14.4, E16.5 and E18.5 embryos and stained for chromogranin-A and EdU as per manufacturer's protocol (Click-IT EdU Alexa Fluor 647 Imaging Kit, Thermo Fisher Scientific).

6.2.3.4 Metabolic parameters

Pregnant mice were starved for 2 h bevor C-section at E19.5. After C-section, blood glucose in the non-starved pups were measured using a glucometer (FreeStyleTM). To measure the fasting blood glucose, blood was collected from E19.5 pups after 2-5 hrs. starvation in microvettes coated with clotting activator. Serum was separated at 3500 rpm at 4°C for 15 min kept on dry ice. According the enzymatic kits as per the manufacturer's protocol (Wako #298-65701) fasting glucose was measured. Among same blood collection method and fasting protocol, measurement of circulating serum insulin, C-peptide and glucagon were examined using mouse-specific ELISA kits (CrystalChem, 273 #90080, #90050, Mercodia #10-1281-01). For rescue experiments, *Iir* $^{-/-}$ E19.5 pups were injected D-glucose (10%, 50 µl per injection; s.c) immediately after birth and injection were repeated every 6 h up to 24 h. To evaluate glucose tolerance, *Iir* $^{-/-}$ E19.5 pups were administered a single injection of D-glucose (10%, 50 µl per injection; s.c). After the single injection, an individual E19.5 pup was sacrificed at a predefined time point (0, 30, 60, 90 or 120 min) and blood glucose were measured using a glucometer (FreeStyleTM). For each time point, 4-12 pups were used for analysis.

6.2.3.5 The pancreatic insulin content

Pancreatic insulin content determined using acid ethanol extraction method. Therefore, whole pancreases at E19.5 stage were dissected, washed in 1x PBS, homogenized and incubated overnight in acid-ethanol buffer at 20°C. After that, the homogenize tissue was centrifuged (2000 rpm, 15 min, 4°C) and the supernatant transferred into a new tube and neutralized with 100 µl of 1M Tris pH 7.5. Subsequently, insulin was quantified using mouse-specific ELISA kit and normalized over the protein concentration that was determined by BCA protein assay.

6.2.3.6 Liver glycogen measurement

To assess the accumulation of glycogen in liver, whole liver at E19.5 stage were dissected, washed in cold PBS, suspended in 200 µl of ddH_2O on ice and homogenized with a Dounce homogenizator on ice. After that the homogenize tissue was boiled for 10 min to inactive enzymes in the samples. Subsequently tissue was centrifuged (18000 g, 10 min, 4°C) and the supernatant transferred into a new tube. Glycogen levels were quantified using a colorimetric assay kit according to the manufacturer's protocol (Abcam, #ab65620).

6.2.3.7 Dynamic glucose induced insulin secretion

Pancreata of *Iir* $^{+/+}$ and *Iir* $^{-/-}$ E19.5 pups were dissected in PBS, washed and kept in KRB buffer in the incubator until perfusion. Columns were loaded with Bio-Gel P-4 polyacrylamide beads and pancreata embedded inside. The following protocol was set up: 26 repetition of low glucose (0.5 mM) for 52 min, 10 repetition of low glucose (1.8 mM), 10 repetition of low glucose (2.8 mM),10

repetition of high glucose (16.7 mM), 10 repetition of low glucose (0.5 mM) and 5 repetitions of 20 mM KCl. Each repetition was 120 seconds long with a flow rate of 100µl/minute. After the experiment, the islets were collected from the column in clean 1.5ml tubes, centrifuged at 1600rpm for 3 minutes to discard to supernatant. The flow through was collected in 96 well plates every minute and stored at -20 °C until performance of the insulin using insulin ultra-sensitive kit (cisbio #62IN2PEH).

6.2.4 *in vivo* analysis of adult mice

6.2.4.1 Tamoxifen induction

Between P84 (post-natal day 84) and P98, MIP-CreERT+; *Iir* $^{fl/FD}$ (CKO) and MIP-CreERT+; *Iir* $^{fl/+}$ (control) were induced by intraperitoneal injection (100 mg/kg body weight of tamoxifen dissolved in corn oil) for three times every 48 hours.

6.2.4.2 Administration of EdU

For labeling the proliferating cells in CKO mice, EdU was added in drinking water (1 mg/mL) for one week prior to sacrifice (stock: 10 mg/ ml in PBS; 10 µl/ g body injected). EdU detection on cryosections of pancreata was carried out using the Click-IT EDU Alexa Fluor 647 kit.

6.2.4.3 Metabolic parameters

For the analysis of metabolic parameters of CKO (MIP-CreERT+; *Iir* $^{fl/FD}$), body weight and blood glucose were monitored at the age of 12-14 weeks (before tamoxifen injection). After tamoxifen injection, mice were maintained in standard conditions, fed and watered ab libitum or fasted 6 h before the measurements. Blood glucose values were determined from venous blood using glucometer (FreeStyleTM/ Bayer Contour next).

6.2.4.4 Intraperitoneal glucose tolerance test (ipGTT)

The glucose clearance and glucose tolerance was measured by an intraperitoneal GTT (ipGTT) in control and CKO mice. Therefore, a cohort of 12 mice (six control and CKO mice) per group was set up. The mice were fasted for 12 h, injected with 2 g glucose per kg body weight and the blood glucose was measured at 0, 15, 30, 60 and 120 min using glucometer (Bayer Contour next).

6.2.4.5 Intraperitoneal glucose stimulated insulin secretion test (ipGSIS)

The secreted insulin was measured by an intraperitoneal GSIS. Therefore, a cohort of 12 mice (six control and CKO mice) per group was set up. Mice were injected with 3 g glucose 3 per kg body weight after 12 h starvation. Additionally, blood samples were collected at 0, 2, 5, 15 and 30 min post-glucose administration from the tail vain using EDTA-treated tubes. To separate the plasma, blood samples were centrifuged at 3500 rpm at 4°C for 15 min. Insulin concentration was quantified using ultrasensitive mouse-specific ELISA kits as per manufacturer's guidelines (CrystalChem).

6.2.4.6 Dynamic GSIS of islets

After overnight culture of islets in RPMI medium, 50 islets per mouse (size matched) were starved in 100 µl KRB buffer for one h. Subsequently, islets were transferred to a perfusion chamber containing a Bio-Gel P-4 polyacrylamide beads suspension. The following protocol was set up: 26 repetition of low glucose (2.8 mM), 10 repetition of high glucose (16.7 mM), 10 repetition of low glucose (2.8 mM), 10 repetition of high glucose (16.7 mM+ 10 nM Ex-4), 10 repetition of low glucose (2.8 mM) and 5 repetitions of 25 mM KCl. Each repetition was 120 seconds long with a flow rate of 100µl/minute. After the experiment, the islets were collected from the column in clean 1.5ml tubes, centrifuged at 1600rpm for 3 minutes to discard to supernatant. The DNA was then isolated as described for mice genotyping and measure with Nanodrop 2000c (Thermo Scientific) to assess the quantity and normalized the insulin content.

6.2.4.7 Islet isolation

The collagenase P (Roche) solution (1 mg/mL in G-solution) was injected in the common bile duct after sealing the connection of the central pancreatic duct with the duodenum using a clamp. After inflating the pancreas with the collagenase, pancreas was transferred into 3 mL of collagenase P solution. The pancreas was digested at 37°C for 15 min (mixing after 7.5 min). The digestion was stopped by adding of 15 mL of cold G-solution on ice. The tube was centrifuged (1620 rpm, 3 min, 4°C), the pellet was washed 2x with10 mL of G-solution. Subsequently, the pellet was resuspended in 5.5 ml of gradient medium. The suspension (2^{nd} phase) was added slowly on the 2.5 mL remaining gradient medium (1^{st} phase) and finally 6 mL of G-solution were added slowly on top to form the 3^{rd} phase. After 10 min of incubation at RT the gradient was centrifuged (1700 rpm, 10 min, RT, acceleration 3, brake 0). This enable the enrichment of islet in the interphase between the middle and the upper phase. This interphase was filtered through a pre-wet cell strainer (70 µm). To harvest the islets, the cell strainer was turned and washed 2x with 10 mL G-solution to transfer the islets into a petri dish. To purify the islets, the islets were handpicked under the stereomicroscope and were cultured overnight in RPMI medium.

6.2.5 immunohistochemistry and histology

6.2.5.1 Immunohistochemistry (IHC)

Cryosections. After dissection in PBS, tissues were fixed in 4% PFA overnight at 4°C. Afterwards, tissues were incubated at 4°C in a sucrose gradient (7,5%, 15%, 30% sucrose in PBS), each step at least for 2 h. Saturation of the tissues with sucrose was indicated by the tissue at the bottom of the vial. In the last step 1:1 solution of 30% sucrose and OCT was used as embedding media. After overnight incubation at 4°C, tissues were transferred to an embedding mold and orientated. Freezing was accomplished by dry ice and stored at -80°C. Prior sectioning, tissue samples were deposit at -20 for 30 min. Sectioning was carried out at the cryostat with section thickness between 10 µm – 20 µm.

Immunostainings of cryosections. The cryosections were rehydrated by 3x washing with 1X PBS for 15 min, permeabilized with 0.5% Triton X-100 in PBS for 20 min. After sections were washed 3x with 1X PBS for 15 min they were blocked in blocking solution (0.1% BSA, 0.1% Tween-20, 3% donkey serum, 10% FCS) for 1 hrs. Afterwards, the sections were incubated with

the primary antibody in blocking solution O/N at 4 °C. Prior to the incubation in secondary antibody in blocking solution, the sections were washed 5x with 1X PBS-T for 5 min. Finally, after being incubated during 2 hrs. with the 2nd antibody in dark, the sections were stained for DAPI (1:1000 in 1X PBS) for 20 min, washed 5x with 1X PBS-T for 5 min and mounted using Vectashield (Vector laboratories, #H-1000-10) or Elvanol.

β- and α-cell mass. Whole pancreata of E19.5 or adult mice were cryosectioned and immunostained for insulin and glucagon. Epifluorescence images were taken with a xyz microscope (Annette Feuchtinger) and insulin- or glucagon-positive area was quantified and normalized to the whole tissue area.

Microscopy & analysis. Slides were imaged using confocal microscopy (Leica SP5, Zeiss LSM880). The acquired images were analyzed using Leica LAS AF software or Imaris (Bitplane) software. Imaris was used to quantify signal intensity in which the, mean intensity of the analyzed channel was determined. Additionally, counting of Edu and other nucleus markers were done by counting function of Imaris and hormone positive cells were counted by hand.

6.2.5.2 Histology

Paraffin sections. Zinc formalin fixed samples were washed in PBS over night at 4°C. The next day dehydration is done in an increasing EtOH series: 70%EtOH 2 hrs, 96%EtOH 2 hrs., 100% EtOH 2hrs, Xylene 5-10 min. After the last step, the organs were transferred to molten paraffin and incubated overnight at 65°C. The tissues were embedded in plastic molds and after solidification mounted onto embedding cassettes. Paraffin sections were cut at a thickness of 5-7µm using microtome, transferred to a 37°C water bath and mounted onto charged glass slides. Sections are dried over night at 37°C before further processing.

6.2.5.2.1. Haematoxylin and eosin (H&E) staining

The sections were dewaxed for 5 min in xylene I and II. Afterwards, the slides were rehydrated using 100 %, 96 %, 90%, 80 % and 70 % ethanol, each for 3 min. After rehydration, paraffin sections were washed in tab water for 5 min and stained with freshly prepared Mayer´s solution (Sigma) for up to eight minutes, depending on the strength of the staining. Subsequently, slides were stained with eosin for several minutes and again washed in tab water for 5 min. After washing step, the slides were dehydrated using the same alcohol series for 2 min each dilution. Then the slides were incubated for 5 min in xylene before embedding in mounting medium. The slides were dried and evaporated at room temperature overnight.

6.2.5.2.2. *LacZ* staining

Organs were dissected in PBS. Dissected organs were fixed in PBS containing 0.02 % NP-40, 5 mM EGTA, 2mM MgCl2, 1 % formaldehyde and 0.2 % glutaraldehyde at room temperature for 20-40 min. After 3 times washing step in PBS containing 0.02 % NP-40, organs were stained in in *LacZ* staining solution (PBS containing 0.02 % NP-40, 2 mM MgCl2, 5 mM K3[Fe(CN)6], 5 mM K4[Fe(CN)6]x6H2O, 0,01 % sodium deoxycholate, 1 mg/ml X-gal). Dissected organs (E14.5) were kept in staining solution for overnight at room temperature (RT) under rotation. Samples were washed 3x 10 min in PBS containing 0.02 % NP-40 and fixed in 4 % para-formaldehyde

(PFA) for 1 hrs. at RT. Then the organs were washed with PBS and incubated in 15 % saccharose at 4 °C overnight. The next day, the organs were transferred to 30 % saccharose for 3 h at room temperature and then to 30 % saccharose/OCT (1:1) for another hour at room temperature. The organs were incubated in OCT and transferred to an embedding mould and covered with OCT. The embedded organs were frozen on dry ice and stored at -80 °C. Embedded organs were put at -20 °C 1 hrs. before sectioning. The block was fixed to the cryostat using OCT and sectioned at a thickness of 10 µm. The sections were melted on cover slips and dried for 30 min at room temperature. Sections were stored at -20 °C.

6.2.5.2.3. DAB staining

The sections were deparafinized for 5 min in xylene I and II. Afterwards, the slides were dehydrated using 100 %, 96 %, 90%, 80 % and 70 % ethanol, each for 3 min. After dehydration, paraffin sections were washed 2x in ddH_2O for 5 min and 1x in PBS. After permeabilization with 0.2% Triton X-100+ 0.1 % saponin in PBS for 20 min, sections were blocked in blocking solution (1% BSA, 0.1% saponin, 10% goat serum) for 1 hrs. at RT. Afterwards, the sections were incubated with the primary antibody in blocking solution O/N at 4 °C. Prior to the incubation in secondary antibody in blocking solution, the sections were washed 3x with 1X TBS for 5 min. Finally, after being incubated during 30 min with the 2nd antibody (biotinylated Secondary Antibody from ABC Kit #32020), the sections were washed 3x with 1X TBS. the sections were incubate for 30 min in ABC reagent which were freshly prepared. After washing 2x with PBS. Subsequently, the sections were incubated in DAB solution (20µl DAB Chromogen+1 ml DAB substrate) for maximal 10 min. after the DAB staining appeared, reaction was stopped by rinsing the sections with tap water. After sections were counter stained with freshly prepared Mayer´s solution for up to eight minutes, they were rinsed with tap water. The slides were washed again for 5 min in water and dehydrated using alcohol series (70%, 80%, 90%, 96%, 100%) for 3 min each dilution. Then the slides were incubated for 5 min in xylene I and II before embedding in xylene mounting medium.

6.2.5.2.4. PAS staining

Sections are dewaxed for 5 min in 100% Xylene I and II, thereafter rehydrated in a series of 100%, 96%, 90%, 80%, 70% EtOH for 3 min each. The slides were immersed for 5 min in Periodic Acid Solutions (Sigma Aldrich #395) and afterwards were rinsed for several times in distilled water. After immersing the slides for 15 min in Schiffs Reagent, they were washed in running tap water for 5 min. finally the slides were counter stained with freshly prepared Mayer´s solution for 90 sec. The slides were rinsed in running tap water and dehydrated using alcohol series (70%, 80%, 90%, 96%, 00%) for 2 min each dilution. Then they were incubated for 5 min in xylene I and II before embedding in xylene based mounting medium.

6.2.6 Protein biochemistry

Starvation and stimulation of islets. After overnight culture of islets in RPMI medium, 50 islets per mouse were washed 5x with PBS. Subsequently, islets were starved for 2 hrs. in HBSS 114 mM NaCl, 4.7 mM KCl, 1.2 mM KH2PO4, 1.16 mM MgSO4, 20 mM HEPES, 2.5 mM CaCl2, 25.5 mM

NaHCO3 (pH 7.2). Subsequently, Stimulation was performed with 100 nM insulin in HBSS for predefined time point (5, 15, 30, 60 min).

Protein extraction of Islets. Islets were washed with PBS and lysed on ice in RIPA supplemented with protease inhibitor cocktail (Sigma, P8340, 1:100), phosphatase inhibitor cocktail II (Sigma, P5726, 1:100) and III (Sigma, P0044, 1:100). Islets were sonicating in water bath sonicator. After centrifugation at 14,000 rpm for 30 min at 4 °C, the supernatant was collected into a new epi.

Pancreata whole-cell lysates. C-sectioned pubs at E19.5 were starved for 5 h and pancreata were dissected in PBS. Tissues were rinsed with 1x PBS and incubated with RIPA lysis buffer including protease inhibitor cocktail 1:100, phosphatase inhibitor cocktail II and III 1:100 on ice for 10 min (100 µl RIPA per 1mg tissue). Tissues were homogenized by sonication with lowest power for 20 secs to enhance the lysis process. After cells were centrifuged at full speed (14000 rpm), at 4º C for 10 min, the supernatant was collected and diluted with RIPA buffer.

Determination of protein concentrations. To determine the protein concentration, the Pierce BCA Protein Assay Kit (Thermos Fisher Scientific) was used. The assay was carried out according to the user manual. Based on the absorption at 562 nm and on a BSA concentration curve, the protein concentrations of the samples were calculated. Finally, all samples were adjusted to the same concentration and boiled for 5 min at 95°C mixed after addition of 4x Laemmli buffer mixed 1:1 with 2 M dithiothreitol (DTT) and immediately cooled on ice.

SDS-PAGE. To separate the proteins of islets or tissue lysates according to their size the mixtures were loaded in different pockets of a SDS poly acrylamide gel. The 7,5 % separating gel solution (3.26 mL acrylamide, 3.75 mL 4x Tris/SDS buffer, pH8.8, 8 mL H_2O, 20 µL TEMED, 150 µL 10% APS) was poured between two sealed glass plates and overlaid with isopropanol to ensure horizontal margins at the top. After removing the isopropanol, the stacking gel solution (650 µl acrylamid, 1.25 mL 4x Tris/SDS buffer, pH6.8, 3.10 mL H_2O, 10 µL TEMED, 50 µL 10% APS) was added above the solid separating gel. Additionally, protein lysates were loaded in the pockets of a SDS poly acrylamide gel and the protein ladder (PageRuler, Life Technologies) was added in one pocket to identify the molecular weight of proteins after separation. Proteins were separated at 120 v about 1.5 h.

Western blot. The Western blot is used and specifically detect and quantify the abundance of proteins by antibody and horse radish peroxidase (HRP)-based labeling. The separated proteins from SDS-PAGE were transferred onto a PVDF in a semi-dry immunoblot. Therefore, the PVDF membrane was activated in 100% methanol for 15 secs due to their hydrophobic surface quickly washed in H_2O for 2 min and incubated in APII buffer for 10 min. To blot the gel on the membrane, first of all the gels were equilibrated in KP buffer for 10 min and immunoblot sandwich was built in a specific order: Top/ 2x Whatman paper in KP, SDS-gel, PVDF membrane, 1 x Whatman paper in APII buffer and 2 x Whatman paper in API buffer / bottom. Using a semi-dry blot chamber the blotting was started at 25 v for 30 min. After blotting the membrane was blocked with the blocking solution (TBS-T and 5% milk powder) for 2 hrs. at RT to saturate unspecific binding sites for the antibodies.

The primary antibody was added in blocking solution and incubated at 4^0C O/N. Prior the 2nd antibody in blocking solution, the membrane was washed 3x with 1x TBST-T for 15 min. After 1h incubation of the membrane with 2nd antibody (in blocking solution), membrane was washed 3x

with 1x TBS-T for 15 min. Finally, membrane was developed in enhanced chemoluminescence solution (ECL, Bio-Rad) for 3 min and covered with foil and transfer to a developer machine. It is possible to strip the antibodies for the membrane to blot them again. In this case, the membrane was incubated for 30 min at 55^0 C in stripping solution (Thermo scientific), then washed 2x with TBS-T for 15 min. After the washing steps, the protocol was repeated from the blocking step.

Quantification of protein abundancies were performed using the ImageJ software. Intensity values of proteins were normalized to reference proteins such as Hsp90 detected on the same membrane. Phospho-proteins were additionally normalized to intensity values of their total form.

6.2.7 RNA biochemistry

RNA work. In order to prevent RNA degradation all steps of RNA isolation have to be done at a RNase free working place. Purified RNA has to be stored at -80°C.

RNA isolation. C-sectioned E18.5 embryos and P0 pups which were delivered by natural birth were starved for 5 hrs. Pancreases from embryos or pups were dissected in RNAlaterTM (Ambion #AM7020) and was immediately frozen on dry ice. After pancreata were homogenized, RNA was extracted from pancreata using TRIzol reagent (Thermo Fisher) and RNeasy Lipid tissue mini kit (Qiagen) according to the kit manual. The RNA was eluted in 14-32 µl of nuclease-free water for immediate use or stored at -80°C.

RNA concentration and determination of the RNA integrity. The RNA concentration was measured by a NanoDrop using the extinction at 260 nm. To assess the integrity number (RIN) of the RNA by the Agilent 2100 Bioanalyzer. The RNA was prepared using Aglient RNA 6000 kit according to the manufacturer's protocol.

Reverse transcription. To transcribes RNA into cDNA. For cDNA the 5x SuperScript Vilo cDNA synthesis kit (Life Technologies) was used. Thereby, the solution of RNA (100 – 500 ng RNA), 5x VILO™ reaction mix and 10x SuperScript™ enzyme mix was incubated at 25°C for 10 min, 60 min at 42°C, followed by 5 min at 85°C. Afterwards the cDNA was stored at -20°C.

Gene profiling. For gene profiling, only high quality RNA (RIN>7) was used. 30 ng of RNA was amplified using the Ovation PicoSL WTA System V2 together with the Encore Biotin Module (Nugen). The amplified cDNA was hybridized on Affymetrix Mouse Gene 1.0 ST arrays (Affymetrix/Thermo Fisher Scientific). Staining and scanning (Scanner 3000 7G) was done according to the Affymetrix expression protocol. This protocol was supplemented with minor modifications as suggested in the Encore Biotion protocol (NuGENTechnologies, Inc). For quality control and achievement of the normalized SST-RMA gene-level data (standard settings including median polish and sketchquantile normalization) the expression console (v.1.4.1.46, Affymetrix) was used. Thereby, for the analysis settings a normalized log $[_2]$ expression data were employed. For the statistical analysis of the microarray, the programming environment R implemented in Bioconducter packages was used. Mta10 transcript cluster.db (v.8.7.0) and filtered (mean log [2] expression value >= 5) were used to annotate the probe sets. The limma (v.3.40.2) *t*-test and Benjamini-Hochberg multiple testing correction (FDR < 10%) were used for differential expression analysis. Functional enrichment analysis was performed using Homer (v.4.10).

Heatmaps were generated with Genesis [2] and cluster dendrograms with the R script hclust. The pathway analyses were generated through the use of QIAGEN's Ingenuity Pathway Analysis (IPA®, QIAGEN Redwood City, www.qiagen.com/ingenuity). The GO-term enrichments and ingenuity pathway analysis were generated using 1.5 fold changed genes which exhibit *P*-values < 0.01 and < 0.05, respectively. GO-term enrichments were created with the Genomatix Software v3.1 (Genomatix).

quantitative RT-PCR. To further validate the microarray results, we carried out quantitative RT-PCR of selected metabolic genes using custom designed Taqman based probe-primer sets (Taqman low density array).

6.2.8 Statistics

Statistical analysis was performed using GraphPad Prism 8 (GraphPad Software Inc., La Jolla, CA). a paired or unpaired Student's t-test was used * P-values < 0.05, ** P-Values<0.01, *** P-Values<0.001. For GTT and ipGSIS two-way ANOVA analysis and area under the curve (AUC) was performed. The statistical analysis was carried out using three independent biological experiments.

7 List of figures and tables

7.1 Figures

Figure 3.1: Pathways of islet-subtype specification. 9
Figure 3.2: Schematic illustration of Glucose-regulated insulin secretion 12
Figure 3.3: Effect of IR/IGF-IR signaling in various tissues and cell types. 13
Figure 3.4: Schematic representation of the insulin-like growth factor system 14
Figure 3.5: The IR/IGF-IR signaling system 16
Figure 3.6: Schematic representation of the IR/IGF-IR signaling in β-cell 19
Figure 3.7: Schematic representation of gene *5330417C22Rik/Iir* and its predicted alternative protein coding splice variants 20
Figure 3.8: Predicted domain structures of the inceptor protein 22
Figure 4.1: mRNA expression profile of *Iir* in various mouse tissues. 24
Figure 4.2: Inceptor antibody specificity in immunocytochemistry in WT pancreas. 25
Figure 4.3: Inceptor is widely expressed in mouse tissues 27
Figure 4.4: Inceptor is highly expressed in brain. 28
Figure 4.5: Inceptor expression during pancreas development 30
Figure 4.6: Inceptor expression in different endocrine cell types. 31
Figure 4.7: Gene trap allele with the *LacZ* reporter and NeoR cassette as well as LoxP and FRTsites. 32
Figure 4.8: Targeting strategy of *5330417C22Rik/Iir* allele to generate full body *Iir*$^{-/-}$ mice. 33
Figure 4.9: Schematic reperesentation of *lacZ*-reporter analysis 34
Figure 4.10: Confirmation of KO efficiency in *vivo*. 35
Figure 4.11: No morphological differences in *Iir*$^{-/-}$ organs in E19.5 animals. 37
Figure 4.12: Morphology, body weight and mendelian ratio of *Iir*$^{-/-}$ mice 38
Figure 4.13: *Iir*$^{-/-}$ new born mice show hypoglycemia and hyperinsulinemia phenotype. 39
Figure 4.14: Elevated β-cell area in *Iir*$^{-/-}$ pups. 40
Figure 4.15: Increased in endocrine cell proliferation in *Iir*$^{-/-}$ mice. 41
Figure 4.16: Effect of Inceptor deletion on proliferation of β-, α-, δ- and PP-cells. 43
Figure 4.17: *Iir*$^{-/-}$ activates IR/IGF-IR signaling during nutritional starvation 44
Figure 4.18: *Iir*$^{-/-}$ activates phosphorylation of AKT upon glucose induction. 45
Figure 4.19: *Iir*$^{-/-}$ newborn mice could be rescued from death by glucose injection 46
Figure 4.20: Dynamic glucose induced insulin secretion in E19.5 pancreata 47
Figure 4.21: Increased glycogen accumulation in liver of *Iir*$^{-/-}$ mice. 48
Figure 4.22: Differential gene expression changes in control vs *Iir*$^{-/-}$ P0 pups. 50
Figure 4.23: Targeting strategy of *Iir* gene trap allele to generate MIP-CreERT; *Iir*$^{flox/FD}$ 52
Figure 4.24: Deletion of *Iir* in CKO mice is induced by tamoxifen. 53

Figure 4.25: CKO animals exhibit normal fasting glucose level after tamoxifen induction. 54
Figure 4.26: Deletion efficiency in vivo with tamoxifen in control and CKO mice. 54
Figure 4.27: Body weight, fasting blood glucose and fasting serum insulin of CKO mice. 55
Figure 4.28: CKO male mice showed improve glucose tolerance. 57
Figure 4.29: β-cell specific inceptor CKO mice display increase in β-cell mass 58
Figure 4.30: β-cell specific deletion of inceptor increases proliferation in β-cells. 59
Figure 4.31: Islet cyto-architecture analysis in CKO mice. 60
Figure 4.32: Expression of maturity markers in CKO mice. 60
Figure 4.33: β-cell specific deletion of inceptor causes increased IR/IGF-IR signaling 62
Figure 4.34: Increased protein expression of inceptor in islets of adult WT mice upon HFD. 64
Figure 5.1: Schematic illustration of inceptor regulating IR/IGF-IR signaling in β-cell. 72

7.2 Tables

Table 6.1: List of equipment 76
Table 6.2: List of consumables 78
Table 6.3: List of chemicals 80
Table 6.4: List of inceptor antibodies for validation. 84
Table 6.5: List of primary antibodies 84
Table 6.6: Secondary antibodies 85
Table 6.7: List of primers for sequencing 86
Table 6.8: Genotyping PCRs 87

8 References

Abuzzahab, M.J., Schneider, A., Goddard, A., Grigorescu, F., Lautier, C., Keller, E., Kiess, W., Klammt, J., Kratzsch, J., Osgood, D., et al. (2003). IGF-I Receptor Mutations Resulting in Intrauterine and Postnatal Growth Retardation. N. Engl. J. Med. *349*, 2211–2222. https://doi.org/10.1056/NEJMoa010107.

Accili, D. (2004a). Lilly Lecture 2003. Diabetes *53*, 1633–1642. https://doi.org/10.2337/diabetes.53.7.1633.

Accili, D. (2004b). Lilly lecture 2003: The struggle for mastery in insulin action: From triumvirate to republic. In Diabetes, pp. 1633–1642.

Accili, D., Drago, J., Lee, E.J., Johnson, M.D., Cool, M.H., Salvatore, P., Asico, L.D., José, P.A., Taylor, S.I., and Westphal, H. (1996). Early neonatal death in mice homozygous for a null allele of the insulin receptor gene. Nat. Genet. *12*, 106–109. https://doi.org/10.1038/ng0196-106.

Adams, T.E., Epa, V.C., Garrett, T.P.J., and Ward, C.W. (2000). Structure and function of the type 1 insulin-like growth factor receptor. Cell. Mol. Life Sci. *57*, 1050–1093. https://doi.org/10.1007/PL00000744.

Aguayo-Mazzucato, C., Koh, A., El Khattabi, I., Li, W.-C., Toschi, E., Jermendy, A., Juhl, K., Mao, K., Weir, G.C., Sharma, A., et al. (2011). Mafa expression enhances glucose-responsive insulin secretion in neonatal rat beta cells. Diabetologia *54*. https://doi.org/10.1007/s00125-010-2026-z.

Ahlgren, U., Jonsson, J., and Edlund, H. (1996). The morphogenesis of the pancreatic mesenchyme is uncoupled from that of the pancreatic epithelium in IPF1/PDX1-deficient mice. Development *122*, 1409–1416. https://doi.org/10.1242/dev.122.5.1409.

Alberti, K.G.M.M., and Zimmet, P.Z. (1998). Definition, diagnosis and classification of diabetes mellitus and its complications. Part 1: diagnosis and classification of diabetes mellitus. Provisional report of a WHO Consultation. Diabet. Med. *15*. https://doi.org/10.1002/(SICI)1096-9136(199807)15:7<539::AID-DIA668>3.0.CO;2-S.

Anik, A., Çatli, G., Abaci, A., and Böber, E. (2015). Maturity-onset diabetes of the young (MODY): An update. J. Pediatr. Endocrinol. Metab. https://doi.org/10.1515/jpem-2014-0384.

Ansarullah, Jain, C., Far, F.F., Homberg, S., Wißmiller, K., von Hahn, F.G., Raducanu, A., Schirge, S., Sterr, M., Bilekova, S., et al. (2021). Inceptor counteracts insulin signalling in β-cells to control glycaemia. Nature *590*, 326–331. https://doi.org/10.1038/s41586-021-03225-8.

Araki, E., Lipes, M.A., Patti, M.-E., Brüning, J.C., Haag III, B., Johnson, R.S., and Kahn, C.R. (1994). Alternative pathway of insulin signalling in mice with targeted disruption of the IRS-1 gene. Nature *372*, 186–190. https://doi.org/10.1038/372186a0.

Aspinwall, C.A., Lakey, J.R.T., and Kennedy, R.T. (1999). Insulin-stimulated Insulin Secretion in Single Pancreatic Beta Cells. J. Biol. Chem. *274*, 6360–6365. https://doi.org/10.1074/jbc.274.10.6360.

Asplund, K. (1973). Effects of Glucose on Insulin Biosynthesis in Foetal and Newborn Rats. Horm. Metab. Res. *5*. https://doi.org/10.1055/s-0028-1093914.

Assmann, A., Hinault, C., and Kulkarni, R.N. (2009a). Growth factor control of pancreatic islet regeneration and function. Pediatr. Diabetes *10*, 14–32. https://doi.org/10.1111/j.1399-5448.2008.00468.x.

Assmann, A., Ueki, K., Winnay, J.N., Kadowaki, T., and Kulkarni, R.N. (2009c). Glucose Effects on Beta-Cell Growth and Survival Require Activation of Insulin Receptors and Insulin Receptor Substrate 2. Mol. Cell. Biol. *29*, 3219–3228. https://doi.org/10.1128/mcb.01489-08.

Avruch, J. (1998). Insulin signal transduction through protein kinase cascades. In Insulin Action, (Boston, MA: Springer US), pp. 31–48.

Backeljauw, P.F., Alves, C., Eidson, M., Cleveland, W., Underwood, L.E., and Davenport, M.L. (1994). Effect of Intravenous Insulin-like Growth Factor I in Two Patients with Leprechaunism. Pediatr. Res. *36*, 749–754. https://doi.org/10.1203/00006450-199412000-00012.

Bastidas-Ponce, A., Scheibner, K., Lickert, H., and Bakhti, M. (2017). Cellular and molecular mechanisms coordinating pancreas development. Dev. *144*, 2873–2888. https://doi.org/10.1242/dev.140756.

Belfiore, A., Frasca, F., Pandini, G., Sciacca, L., and Vigneri, R. (2009). Insulin receptor isoforms and insulin receptor/insulin-like growth factor receptor hybrids in physiology and disease. Endocr. Rev. *30*, 586–623. https://doi.org/10.1210/er.2008-0047.

Bernal-Mizrachi, E., Wen, W., Stahlhut, S., Welling, C.M., and Permutt, M.A. (2001c). Islet β cell expression of constitutively active Akt1/PKBα induces striking hypertrophy, hyperplasia, and hyperinsulinemia. J. Clin. Invest. *108*, 1631–1638. https://doi.org/10.1172/JCI13785.

Beucher, A., Martín, M., Spenle, C., Poulet, M., Collin, C., and Gradwohl, G. (2012). Competence of failed endocrine progenitors to give rise to acinar but not ductal cells is restricted to early pancreas development. Dev. Biol. *361*. https://doi.org/10.1016/j.ydbio.2011.10.025.

BIER, D.M., SCHEDEWIE, H., LARNER, J., JERROLD, O., RUBENSTEIN, A., FISER, R.H., CRAIG, J.W., and ELDERS, J.M. (1980). Glucose Kinetics in Leprechaunism: Accelerated Fasting due to Insulin Resistance*. J. Clin. Endocrinol. Metab. *51*, 988–994. https://doi.org/10.1210/jcem-51-5-988.

Black, C., Donnelly, P., McIntyre, L., Royle, P., Shepherd, J.J., and Thomas, S. (2007). Meglitinide analogues for type 2 diabetes mellitus. Cochrane Database Syst. Rev. *2010*. https://doi.org/10.1002/14651858.CD004654.pub2.

Blum, B., Hrvatin, S., Schuetz, C., Bonal, C., Rezania, A., and Melton, D.A. (2012). Functional beta-cell maturation is marked by an increased glucose threshold and by expression of urocortin 3. Nat. Biotechnol. *30*, 261–264. https://doi.org/10.1038/nbt.2141.

Blundell, T.L., Bedarkar, S., Rinderknecht, E., and Humbel, R.E. (1978). Insulin-like growth factor: A model for tertiary structure accounting for immunoreactivity and receptor binding. Proc. Natl. Acad. Sci. U. S. A. *75*, 180–184. https://doi.org/10.1073/pnas.75.1.180.

Bogardus, C., Lillioja, S., Howard, B. V, Reaven, G., and Mott, D. (1984). Relationships between insulin secretion, insulin action, and fasting plasma glucose concentration in nondiabetic and noninsulin-dependent diabetic subjects. J. Clin. Invest. *74*, 1238–1246. https://doi.org/10.1172/JCI111533.

Bonner-Weir, S. (1994). Regulation of pancreatic β-cell mass in vivo. Recent Prog. Horm. Res. *49*, 91–104. https://doi.org/10.1016/b978-0-12-571149-4.50008-8.

Bonner-Weir, S. (2000). Life and death of the pancreatic β cells. Trends Endocrinol. Metab. *11*, 375–378. https://doi.org/10.1016/S1043-2760(00)00305-2.

Bonner-Weir, S., and Orci, L. (1982). New perspectives on the microvasculature of the islets of Langerhans in the rat. Diabetes *31*, 883–889. https://doi.org/10.2337/diab.31.10.883.

Boothe, T., Lim, G.E., Cen, H., Skovsø, S., Piske, M., Li, S.N., Nabi, I.R., Gilon, P., and Johnson,

J.D. (2016). Inter-domain tagging implicates caveolin-1 in insulin receptor trafficking and Erk signaling bias in pancreatic beta-cells. Mol. Metab. *5*, 366–378. https://doi.org/10.1016/j.molmet.2016.01.009.

Boschero, A.C., Bordin, S., Herchuelz, A., and Lebrun, P. (1990). Effects of glucose on 45Ca2+ outflow, cytosolic Ca2+ concentration and insulin release from freshly isolated and cultured adult rat islets. Cell Calcium *11*. https://doi.org/10.1016/0143-4160(90)90015-M.

Brüning, J.C., Winnay, J., Bonner-Weir, S., Taylor, S.I., Accili, D., and Kahn, C.R. (1997). Development of a novel polygenic model of NIDDM in mice heterozygous for IR and IRS-1 null alleles. Cell *88*, 561–572. https://doi.org/10.1016/S0092-8674(00)81896-6.

Burcelin, R., Knauf, C., and Cani, P.D. (2008). Pancreatic α-cell dysfunction in diabetes. Diabetes Metab. *34*. https://doi.org/10.1016/S1262-3636(08)73395-0.

Burlison, J.S., Long, Q., Fujitani, Y., Wright, C.V.E., and Magnuson, M.A. (2008). Pdx-1 and Ptf1a concurrently determine fate specification of pancreatic multipotent progenitor cells. Dev. Biol. *316*. https://doi.org/10.1016/j.ydbio.2008.01.011.

Carpentier, J.L., Fehlmann, M., Van Obberghen, E., Gorden, P., and Orci, L. (1985). Insulin receptor internalization and recycling: mechanism and significance. Biochimie *67*, 1143–1145. https://doi.org/10.1016/S0300-9084(85)80112-7.

Carty, M.D., Lillquist, J.S., Peshavaria, M., Stein, R., and Soeller, W.C. (1997). Identification of cis- and trans-Active Factors Regulating Human Islet Amyloid Polypeptide Gene Expression in Pancreatic β-Cells. J. Biol. Chem. *272*. https://doi.org/10.1074/jbc.272.18.11986.

Cerasi, E., Luft, R., and Efendic, S. (1972). Decreased Sensitivity of the Pancreatic Beta Cells to Glucose in Prediabetic and Diabetic Subjects: A Glucose Dose-Response Study. Diabetes *21*, 224–234. https://doi.org/10.2337/diab.21.4.224.

Chakrabarti, S.K., James, J.C., and Mirmira, R.G. (2002). Quantitative Assessment of Gene Targeting in Vitroand in Vivo by the Pancreatic Transcription Factor, Pdx1. J. Biol. Chem. *277*. https://doi.org/10.1074/jbc.M111857200.

Cheng, Y., Su, Y., Shan, A., Jiang, X., Ma, Q., Wang, W., Ning, G., and Cao, Y. (2015). Generation and characterization of transgenic mice expressing mouse Ins1 promoter for pancreatic β-cell-specific gene overexpression and knockout. Endocrinology *156*, 2724–2731. https://doi.org/10.1210/en.2015-1104.

Chiang, M.-K., and Melton, D.A. (2003). Single-Cell Transcript Analysis of Pancreas Development. Dev. Cell *4*. https://doi.org/10.1016/S1534-5807(03)00035-2.

Choudhury, A.I., Heffron, H., Smith, M.A., Al-Qassab, H., Xu, A.W., Selman, C., Simmgen, M., Clements, M., Claret, M., MacColl, G., et al. (2005). The role of insulin receptor substrate 2 in hypothalamic and β cell function. J. Clin. Invest. *115*, 940–950. https://doi.org/10.1172/JCI24445.

Clemmons, D.R. (1997). Insulin-like growth factor binding proteins and their role in controlling IGF actions. Cytokine Growth Factor Rev. *8*, 45–62. https://doi.org/10.1016/S1359-6101(96)00053-6.

Cooper, M.S., and Stewart, P.M. (2009). 11β-hydroxysteroid dehydrogenase type 1 and its role in the hypothalamus-pituitary-adrenal axis, metabolic syndrome, and inflammation. J. Clin. Endocrinol. Metab. *94*, 4645–4654. https://doi.org/10.1210/jc.2009-1412.

Cornu, M., Modi, H., Kawamori, D., Kulkarni, R.N., Joffraud, M., and Thorens, B. (2010). Glucagon-like Peptide-1 Increases β-Cell Glucose Competence and Proliferation by Translational Induction of Insulin-like Growth Factor-1 Receptor Expression. J. Biol. Chem. *285*, 10538–10545. https://doi.org/10.1074/jbc.M109.091116.

Dabelea, D. (2007). The predisposition to obesity and diabetes in offspring of diabetic mothers. Diabetes Care https://doi.org/10.2337/dc07-s211.

Dabelea, D., Pettitt, D.J., Hanson, R.L., Imperatore, G., Bennett, P.H., and Knowler, W.C. (1999). Birth weight, type 2 diabetes, and insulin resistance in Pima Indian children and young adults. Diabetes Care *22*, 944–950. https://doi.org/10.2337/diacare.22.6.944.

Dahms, N.M., Seetharam, B., and Wick, D.A. (1996). Expression of insulin-like growth factor (IGF)-I receptors, IGF-II/cation-independent mannose 6-phosphate receptors (CI-MPRs), and cation-dependent MPRs in polarized human intestinal Caco-2 cells. Biochim. Biophys. Acta - Biomembr. *1279*, 84–92. https://doi.org/10.1016/0005-2736(95)00234-0.

Damm, P. (2009). Future risk of diabetes in mother and child after gestational diabetes mellitus. Int. J. Gynecol. Obstet. https://doi.org/10.1016/j.ijgo.2008.11.025.

Daughaday, W.H., Rotwein, P., and Rotwein, P. (1989). Insulin-like growth factors I and II. Peptide, messenger ribonucleic acid and gene structures, serum, and tissue concentrations. Endocr. Rev. *10*, 68–91. https://doi.org/10.1210/edrv-10-1-68.

DeFronzo, R.A. (1988). The Triumvirate: β-Cell, Muscle, Liver: A Collusion Responsible for NIDDM. Diabetes *37*, 667–687. https://doi.org/10.2337/diab.37.6.667.

Delous, M., Yin, C., Shin, D., Ninov, N., Debrito Carten, J., Pan, L., Ma, T.P., Farber, S.A., Moens, C.B., and Stainier, D.Y.R. (2012). sox9b Is a Key Regulator of Pancreaticobiliary Ductal System Development. PLoS Genet. *8*. https://doi.org/10.1371/journal.pgen.1002754.

Demozay, D., Tsunekawa, S., Briaud, I., Shah, R., and Rhodes, C.J. (2011). Specific glucose-induced control of insulin receptor substrate-2 expression is mediated via Ca 2+-dependent calcineurin/NFAT signaling in primary pancreatic islet β-cells. Diabetes *60*, 2892–2902. https://doi.org/10.2337/db11-0341.

Deng, L., Broaddus, R.R., McCampbell, A., Shipley, G.L., Loose, D.S., Stancel, G.M., Pickar, J.H., and Davies, P.J.A. (2005). Identification of a novel estrogen-regulated gene, EIG121, induced by hormone replacement therapy and differentially expressed in type I and type II endometrial cancer. Clin. Cancer Res. *11*, 8258–8264. https://doi.org/10.1158/1078-0432.CCR-05-1189.

Desgraz, R., and Herrera, P.L. (2009). Pancreatic neurogenin 3-expressing cells are unipotent islet precursors. Development *136*. https://doi.org/10.1242/dev.039214.

Dickson, L.M., Lingohr, M.K., McCuaig, J., Hügl, S.R., Snow, L., Kahn, B.B., Myers, M.G., and Rhodes, C.J. (2001). Differential Activation of Protein Kinase B and p70S6K by Glucose and Insulin-like Growth Factor 1 in Pancreatic β-Cells (INS-1). J. Biol. Chem. *276*, 21110–21120. https://doi.org/10.1074/jbc.M101257200.

Diehl, J.A., Cheng, M., Roussel, M.F., and Sherr, C.J. (1998). Glycogen synthase kinase-3β regulates cyclin D1 proteolysis and subcellular localization. Genes Dev. *12*, 3499–3511. https://doi.org/10.1101/gad.12.22.3499.

Dor, Y., Brown, J., Martinez, O.I., and Melton, D.A. (2004). Adult pancreatic β-cells are formed by self-duplication rather than stem-cell differentiation. Nature *429*. https://doi.org/10.1038/nature02520.

Drucker, D.J., and Nauck, M.A. (2006). The incretin system: glucagon-like peptide-1 receptor agonists and dipeptidyl peptidase-4 inhibitors in type 2 diabetes. Lancet *368*, 1696–1705. https://doi.org/10.1016/S0140-6736(06)69705-5.

Estrella, J.S., Ma, L.T., Milton, D.R., Yao, J.C., Wang, H., Rashid, A., and Broaddus, R.R. (2014).

Expression of Estrogen-Induced Genes and Estrogen Receptor β in Pancreatic Neuroendocrine Tumors. Pancreas *43*, 996–1002. https://doi.org/10.1097/MPA.0000000000000203.

Fajans, S.S. (1989). Maturity-onset diabetes of the young (MODY). Diabetes / Metab. Rev. *5*, 579–606. https://doi.org/10.1002/dmr.5610050705.

Fatrai, S., Elghazi, L., Balcazar, N., Cras-Méneur, C., Krits, I., Kiyokawa, H., and Bernal-Mizrachi, E. (2006b). Akt Induces β-Cell Proliferation by Regulating Cyclin D1, Cyclin D2, and p21 Levels and Cyclin-Dependent Kinase-4 Activity. Diabetes *55*, 318–325. https://doi.org/10.2337/diabetes.55.02.06.db05-0757.

Federici, M., Porzio, O., Zucaro, L., Fusco, A., Borboni, P., Lauro, D., and Sesti, G. (1997). Distribution of insulin/insulin-like growth factor-I hybrid receptors in human tissues. Mol. Cell. Endocrinol. *129*, 121–126. https://doi.org/10.1016/S0303-7207(97)04050-1.

Finegood, D.T., Scaglia, L., and Bonner-Weir, S. (1995). Dynamics of β-cell Mass in the Growing Rat Pancreas: Estimation With a Simple Mathematical Model. Diabetes *44*, 249–256. https://doi.org/10.2337/diab.44.3.249.

Firth, S.M., and Baxter, R.C. (2002). Cellular actions of the insulin-like growth factor binding proteins. Endocr. Rev. *23*, 824–854. https://doi.org/10.1210/er.2001-0033.

Folli, F., Okada, T., Perego, C., Gunton, J., Liew, C.W., Akiyama, M., D'Amico, A., Rosa, S., Placidi, C., Lupi, R., et al. (2011). Altered insulin receptor signalling and β-cell cycle dynamics in type 2 diabetes mellitus. PLoS One *6*. https://doi.org/10.1371/journal.pone.0028050.

Frasca, F., Pandini, G., Scalia, P., Sciacca, L., Mineo, R., Costantino, A., Goldfine, I.D., Belfiore, A., and Vigneri, R. (1999). Insulin Receptor Isoform A, a Newly Recognized, High-Affinity Insulin-Like Growth Factor II Receptor in Fetal and Cancer Cells. Mol. Cell. Biol. *19*, 3278–3288. https://doi.org/10.1128/mcb.19.5.3278.

Freinkel, N., Lewis, N.J., Johnson, R., Swenne, I., Bone, A., and Hellerström, C. (1984). Differential Effects of Age Versus Glycemic Stimulation on the Maturation of Insulin Stimulus-Secretion Coupling During Culture of Fetal Rat Islets. Diabetes *33*. https://doi.org/10.2337/diab.33.11.1028.

Freychet, P., Roth, J., and Neville, D.M. (1971). Insulin receptors in the liver: specific binding of (125 I)insulin to the plasma membrane and its relation to insulin bioactivity. Proc. Natl. Acad. Sci. U. S. A. *68*, 1833–1837. https://doi.org/10.1073/pnas.68.8.1833.

Garber, A.J. (2010). Incretin-based therapies in the management of type 2 diabetes: rationale and reality in a managed care setting. Am. J. Manag. Care *16*. .

Georgia, S., and Bhushan, A. (2004). β cell replication is the primary mechanism for maintaining postnatal β cell mass. J. Clin. Invest. *114*. https://doi.org/10.1172/JCI22098.

Giddings, S.J., and Carnaghi, L.R. (1992). Insulin receptor gene expression during development: Developmental regulation of insulin receptor mRNA abundance in embryonic rat liver and yolk sac, developmental regulation of insulin receptor gene splicing, and comparison to abundance of insulin-like g. Mol. Endocrinol. *6*, 1665–1672. https://doi.org/10.1210/mend.6.10.1448116.

Giddings, S.J., Chirgwin, J., and Permutt, M.A. (1982). Effects of glucose on proinsulin messenger RNA in rats in vivo. Diabetes *31*, 624–629. https://doi.org/10.2337/diab.31.7.624.

Girard, J.R., Cuendet, G.S., Marliss, E.B., Kervran, A., Rieutort, M., and Assan, R. (1973). Fuels, Hormones, and Liver Metabolism at Term and during the Early Postnatal Period in the Rat. J. Clin. Invest. *52*, 3190–3200. https://doi.org/10.1172/JCI107519.

Goh, L.K., and Sorkin, A. (2013b). Endocytosis of receptor tyrosine kinases. Cold Spring Harb.

Perspect. Biol. *5*. https://doi.org/10.1101/cshperspect.a017459.

Goldfine, A.B., and Kulkarni, R.N. (2012). Modulation of β-cell function: A translational journey from the bench to the bedside. Diabetes, Obes. Metab. *14*, 152–160. https://doi.org/10.1111/j.1463-1326.2012.01647.x.

Gouzi, M., Kim, Y.H., Katsumoto, K., Johansson, K., and Grapin-Botton, A. (2011). Neurogenin3 initiates stepwise delamination of differentiating endocrine cells during pancreas development. Dev. Dyn. *240*. https://doi.org/10.1002/dvdy.22544.

Gradwohl, G., Dierich, A., LeMeur, M., and Guillemot, F. (2000). neurogenin3 is required for the development of the four endocrine cell lineages of the pancreas. Proc. Natl. Acad. Sci. *97*. https://doi.org/10.1073/pnas.97.4.1607.

Groskopf, J.C., Syu, L.J., Saltiel, A.R., and Linzer, D.I.H. (1997). Proliferin induces endothelial cell chemotaxis through a G protein- coupled, mitogen-activated protein kinase-dependent pathway. Endocrinology *138*, 2835–2840. https://doi.org/10.1210/endo.138.7.5276.

Gu, G., Dubauskaite, J., and Melton, D.A. (2002). Direct evidence for the pancreatic lineage: NGN3+ cells are islet progenitors and are distinct from duct progenitors. Development *129*. .

Guz, Y., Montminy, M.R., Stein, R., Leonard, J., Gamer, L.W., Wright, C. V, and Teitelman, G. (1995). Expression of murine STF-1, a putative insulin gene transcription factor, in beta cells of pancreas, duodenal epithelium and pancreatic exocrine and endocrine progenitors during ontogeny. Development *121*. .

Haeusler, R.A., McGraw, T.E., and Accili, D. (2018). Metabolic Signalling: Biochemical and cellular properties of insulin receptor signalling. Nat. Rev. Mol. Cell Biol. *19*, 31–44. https://doi.org/10.1038/nrm.2017.89.

Haft, C.R., Klausner, R.D., and Taylor, S.I. (1994). Involvement of dileucine motifs in the internalization and degradation of the insulin receptor. J. Biol. Chem. *269*, 26286–26294. https://doi.org/10.1016/s0021-9258(18)47192-x.

Hancock, M.K., Haskins, D.J., Sun, G., and Dahms, N.M. (2002). Identification of residues essential for carbohydrate recognition by the insulin-like growth factor II/mannose 6-phosphate receptor. J. Biol. Chem. *277*, 11255–11264. https://doi.org/10.1074/jbc.M109855200.

Hasegawa, Y., Daitoku, Y., Mizuno, S., Tanimoto, Y., Mizuno-Iijima, S., Matsuo, M., Kajiwara, N., Ema, M., Oishi, H., Miwa, Y., et al. (2014). Generation and characterization of Ins1-cre-driver C57BL/6N for exclusive pancreatic beta cell-specific Cre-loxP recombination. Exp. Anim. *63*, 183–191. https://doi.org/10.1538/expanim.63.183.

Hashimoto, N., Kido, Y., Uchida, T., Asahara, S., Shigeyama, Y., Matsuda, T., Takeda, A., Tsuchihashi, D., Nishizawa, A., Ogawa, W., et al. (2006). Ablation of PDK1 in pancreatic β cells induces diabetes as a result of loss of β cell mass. Nat. Genet. *38*, 589–593. https://doi.org/10.1038/ng1774.

Heaton, J.H., and Gelehrter, T.D. (1981). Desensitization of hepatoma cells to insulin action. Evidence for a post-receptor mechanism. J. Biol. Chem. *256*, 12257–12262. https://doi.org/10.1016/s0021-9258(18)43263-2.

Herrera, P.L., Huarte, J., Sanvito, F., Meda, P., Orci, L., and Vassalli, J.D. (1991). Embryogenesis of the murine endocrine pancreas; early expression of pancreatic polypeptide gene. Development *113*, 1257–1265. https://doi.org/10.1242/dev.113.4.1257.

Hick, A.-C., van Eyll, J.M., Cordi, S., Forez, C., Passante, L., Kohara, H., Nagasawa, T., Vanderhaeghen, P., Courtoy, P.J., Rousseau, G.G., et al. (2009). Mechanism of primitive duct

formation in the pancreas and submandibular glands: a role for SDF-1. BMC Dev. Biol. *9*. https://doi.org/10.1186/1471-213X-9-66.

Hole, R.L., Pian-Smith, M.C., and Sharp, G.W. (1988). Development of the biphasic response to glucose in fetal and neonatal rat pancreas. Am. J. Physiol. Metab. *254*. https://doi.org/10.1152/ajpendo.1988.254.2.E167.

Hong Jung Chen, Remmler, J., Delaney, J.C., Messner, D.J., and Lobel, P. (1993). Mutational analysis of the cation-independent mannose 6- phosphate/insulin-like growth factor II receptor. A consensus casein kinase II site followed by 2 leucines near the carboxyl terminus is important for intracellular targeting of lysosomal enzymes. J. Biol. Chem. *268*, 22338–22346. https://doi.org/10.1016/s0021-9258(18)41533-5.

Howell, S.L., and Tyhurst, M. (1984). Insulin secretion: The effector system. Experientia *40*. https://doi.org/10.1007/BF01971457.

Huang, X.F., and Arvan, P. (1995). Intracellular transport of proinsulin in pancreatic β-cells: Structural maturation probed by bisulfide accessibility. J. Biol. Chem. *270*. https://doi.org/10.1074/jbc.270.35.20417.

Hügl, S.R., White, M.F., and Rhodes, C.J. (1998). Insulin-like Growth Factor I (IGF-I)-stimulated Pancreatic β-Cell Growth Is Glucose-dependent. J. Biol. Chem. *273*, 17771–17779. https://doi.org/10.1074/jbc.273.28.17771.

Huising, M.O. (2020). Paracrine regulation of insulin secretion. Diabetologia *63*, 2057–2063. https://doi.org/10.1007/s00125-020-05213-5.

Jamiolkowski, R.M., Guo, L.Y., Li, Y.R., Shaffer, S.M., and Naji, A. (2012). Islet transplantation in type I diabetes mellitus. Yale J. Biol. Med. *85*. .

Jensen, J., Heller, R.S., Funder-Nielsen, T., Pedersen, E.E., Lindsell, C., Weinmaster, G., Madsen, O.D., and Serup, P. (2000). Independent development of pancreatic alpha- and beta-cells from neurogenin3-expressing precursors: a role for the notch pathway in repression of premature differentiation. Diabetes *49*. https://doi.org/10.2337/diabetes.49.2.163.

Jhala, U.S., Canettieri, G., Screaton, R.A., Kulkarni, R.N., Krajewski, S., Reed, J., Walker, J., Lin, X., White, M., and Montminy, M. (2003). cAMP promotes pancreatic β-cell survival via CREB-mediated induction of IRS2. Genes Dev. *17*, 1575–1580. https://doi.org/10.1101/gad.1097103.

Johansson, K.A., Dursun, U., Jordan, N., Gu, G., Beermann, F., Gradwohl, G., and Grapin-Botton, A. (2007). Temporal Control of Neurogenin3 Activity in Pancreas Progenitors Reveals Competence Windows for the Generation of Different Endocrine Cell Types. Dev. Cell *12*. https://doi.org/10.1016/j.devcel.2007.02.010.

Johnson, J.D., and Misler, S. (2002). Nicotinic acid-adenine dinucleotide phosphate-sensitive calcium stores initiate insulin signaling in human beta cells. Proc. Natl. Acad. Sci. *99*, 14566–14571. https://doi.org/10.1073/pnas.222099799.

Johnson, K.F., and Kornfeld, S. (1992). The cytoplasmic tail of the mannose 6-phosphate/insulin-like growth factor-II receptor has two signals for lysosomal enzyme sorting in the Golgi. J. Cell Biol. *119*, 249–257. https://doi.org/10.1083/jcb.119.2.249.

Jones, S.M., and Kazlauskas, A. (2001). Growth factor-dependent signaling and cell cycle progression. FEBS Lett. *490*, 110–116. https://doi.org/10.1016/S0014-5793(01)02113-5.

Kahn, S.E., Hull, R.L., and Utzschneider, K.M. (2006). Mechanisms linking obesity to insulin resistance and type 2 diabetes. Nature *444*. https://doi.org/10.1038/nature05482.

Kahn, S.E., Carr, D.B., Faulenbach, M. V., and Utzschneider, K.M. (2008). An examination of β-

cell function measures and their potential use for estimating β-cell mass. In Diabetes, Obesity and Metabolism, (Blackwell Publishing Ltd), pp. 63–76.

Kandel, E.S., and Hay, N. (1999). The Regulation and Activities of the Multifunctional Serine/Threonine Kinase Akt/PKB. Exp. Cell Res. *253*, 210–229. https://doi.org/10.1006/excr.1999.4690.

Kang, C.M., Kim, D.H., Choi, G.H., Kim, K.S., Choi, J.S., and Lee, W.J. (2009). Detrimental Effect of Postoperative Complications on Oncologic Efficacy of R0 Pancreatectomy in Ductal Adenocarcinoma of the Pancreas. J. Gastrointest. Surg. *13*. https://doi.org/10.1007/s11605-009-0823-9.

Kang, J.M., Park, S., Kim, S.J., Kim, H., Lee, B., Kim, J., Park, J., Kim, S.T., Yang, H.K., Kim, W.H., et al. (2015). KIAA1324 suppresses gastric cancer progression by inhibiting the oncoprotein GRP78. Cancer Res. *75*, 3087–3097. https://doi.org/10.1158/0008-5472.CAN-14-3751.

Kataoka, K., Han, S., Shioda, S., Hirai, M., Nishizawa, M., and Handa, H. (2002). MafA Is a Glucose-regulated and Pancreatic β-Cell-specific Transcriptional Activator for the Insulin Gene. J. Biol. Chem. *277*. https://doi.org/10.1074/jbc.M206796200.

Katz, M., Amit, I., and Yarden, Y. (2007). Regulation of MAPKs by growth factors and receptor tyrosine kinases. Biochim. Biophys. Acta - Mol. Cell Res. *1773*, 1161–1176. https://doi.org/10.1016/j.bbamcr.2007.01.002.

Kawaguchi, Y., Cooper, B., Gannon, M., Ray, M., MacDonald, R.J., and Wright, C.V.E. (2002). The role of the transcriptional regulator Ptf1a in converting intestinal to pancreatic progenitors. Nat. Genet. *32*. https://doi.org/10.1038/ng959.

KERVRAN, A., and GIRARD, J.R. (1974). GLUCOSE-INDUCED INCREASE OF PLASMA INSULIN IN THE RAT FOETUS IN UTERO. J. Endocrinol. *62*, 545–551. https://doi.org/10.1677/joe.0.0620545.

Kitamura, T., Nakae, J., Kitamura, Y., Kido, Y., Biggs, W.H., Wright, C.V.E., White, M.F., Arden, K.C., and Accili, D. (2002). The forkhead transcription factor Foxo1 links insulin signaling to Pdx1 regulation of pancreatic β cell growth. J. Clin. Invest. *110*, 1839–1847. https://doi.org/10.1172/jci16857.

Kitamura, T., Kahn, C.R., and Accili, D. (2003). Insulin Receptor Knockout Mice. Annu. Rev. Physiol. *65*, 313–332. https://doi.org/10.1146/annurev.physiol.65.092101.142540.

Klara Feldman, R., Tieu, R.S., and Yasumura, L. (2016). Gestational diabetes screening the international association of the diabetes and pregnancy study groups compared with carpenter-coustan screening. Obstet. Gynecol. *127*, 10–17. https://doi.org/10.1097/AOG.0000000000001132.

Kohn, A.D., Summers, S.A., Birnbaum, M.J., and Roth, R.A. (1996). Expression of a Constitutively Active Akt Ser/Thr Kinase in 3T3-L1 Adipocytes Stimulates Glucose Uptake and Glucose Transporter 4 Translocation. J. Biol. Chem. *271*, 31372–31378. https://doi.org/10.1074/jbc.271.49.31372.

Kopp, J.L., Dubois, C.L., Schaffer, A.E., Hao, E., Shih, H.P., Seymour, P.A., Ma, J., and Sander, M. (2011). Sox9+ ductal cells are multipotent progenitors throughout development but do not produce new endocrine cells in the normal or injured adult pancreas. Development *138*. https://doi.org/10.1242/dev.056499.

Krapp, A., Knofler, M., Ledermann, B., Burki, K., Berney, C., Zoerkler, N., Hagenbuchle, O., and Wellauer, P.K. (1998). The bHLH protein PTF1-p48 is essential for the formation of the exocrine and the correct spatial organization of the endocrine pancreas. Genes Dev. *12*.

https://doi.org/10.1101/gad.12.23.3752.

Kubota, N., Terauchi, Y., Tobe, K., Yano, W., Suzuki, R., Ueki, K., Takamoto, I., Satoh, H., Maki, T., Kubota, T., et al. (2004). Insulin receptor substrate 2 plays a crucial role in β cells and the hypothalamus. J. Clin. Invest. *114*, 917–927. https://doi.org/10.1172/JCI21484.

Kulkarni, R.N., Brü, J.C., Winnay, J.N., Postic, C., Magnuson, M.A., and Kahn, R. (1999). Tissue-Specific Knockout of the Insulin Receptor in Pancreatic Cells Creates an Insulin Secretory Defect Similar to that in Type 2 Diabetes.

Kulkarni, R.N., Holzenberger, M., Shih, D.Q., Ozcan, U., Stoffel, M., Magnuson, M.A., and Kahn, C.R. (2002b). β-cell-specific deletion of the Igf1 receptor leads to hyperinsulinemia and glucose intolerance but does not alter β-cell mass. Nat. Genet. *31*, 111–115. https://doi.org/10.1038/ng872.

Kushner, J.A. (2006). β-Cell Growth: An Unusual Paradigm of Organogenesis That is Cyclin D2/cdk4 Dependent. Cell Cycle *5*. https://doi.org/10.4161/cc.5.3.2399.

Kushner, J.A., Ye, J., Schubert, M., Burks, D.J., Dow, M.A., Flint, C.L., Dutta, S., Wright, C.V.E., Montminy, M.R., and White, M.F. (2002). Pdx1 restores β cell function in Irs2 knockout mice. J. Clin. Invest. *109*, 1193–1201. https://doi.org/10.1172/JCI14439.

Lau, M.M.H., Stewart, C.E.H., Liu, Z., Bhatt, H., Rotwein, P., and Stewart, C.L. (1994). Loss of the imprinted IGF2/cation-independent mannose 6-phosphate receptor results in fetal overgrowth and perinatal lethality. Genes Dev. *8*, 2953–2963. https://doi.org/10.1101/gad.8.24.2953.

Leibiger, B., Wåhlander, K., Berggren, P.O., and Leibiger, I.B. (2000). Glucose-stimulated insulin biosynthesis depends on insulin-stimulated insulin gene transcription. J. Biol. Chem. *275*, 30153–30156. https://doi.org/10.1074/jbc.M005216200.

Leibiger, I.B., Leibiger, B., Moede, T., and Berggren, P.O. (1998). Exocytosis of insulin promotes insulin gene transcription via the insulin receptor/PI-3 kinase/p70 s6 kinase and CaM kinase pathways. Mol. Cell *1*, 933–938. https://doi.org/10.1016/S1097-2765(00)80093-3.

Leibiger, I.B., Leibiger, B., and Berggren, P.O. (2008a). Insulin signaling in the pancreatic β-cell. Annu. Rev. Nutr. *28*, 233–251. https://doi.org/10.1146/annurev.nutr.28.061807.155530.

Leibowitz, G., Oprescu, A.I., Üçkaya, G., Gross, D.J., Cerasi, E., and Kaiser, N. (2003). Insulin Does Not Mediate Glucose Stimulation of Proinsulin Biosynthesis. Diabetes *52*, 998–1003. https://doi.org/10.2337/diabetes.52.4.998.

LeRoith, D., and Gavrilova, O. (2006). Mouse models created to study the pathophysiology of Type 2 diabetes. Int. J. Biochem. Cell Biol. *38*, 904–912. https://doi.org/10.1016/j.biocel.2005.01.019.

Lin, X., Taguchi, A., Park, S., Kushner, J.A., Li, F., Li, Y., and White, M.F. (2004). Dysregulation of insulin receptor substrate 2 in β cells and brain causes obesity and diabetes. J. Clin. Invest. *114*, 908–916. https://doi.org/10.1172/jci200422217.

Liu, J.-P., Baker, J., Perkins, A.S., Robertson, E.J., and Efstratiadis, A. (1993). Mice carrying null mutations of the genes encoding insulin-like growth factor I (Igf-1) and type 1 IGF receptor (Igf1r). Cell *75*, 59–72. https://doi.org/10.1016/S0092-8674(05)80084-4.

Louvi, A., Accili, D., and Efstratiadis, A. (1997a). Growth-promoting interaction of IGF-II with the insulin receptor during mouse embryonic development. Dev. Biol. *189*, 33–48. https://doi.org/10.1006/dbio.1997.8666.

Ludwig, T., Eggenschwiler, J., Fisher, P., D'Ercole, A.J., Davenport, M.L., and Efstratiadis, A. (1996). Mouse mutants lacking the type 2 IGF receptor (IGF2R) are rescued from perinatal

lethality in Igf2 and Igf1r null backgrounds. Dev. Biol. *177*, 517–535. https://doi.org/10.1006/dbio.1996.0182.

Magenheim, J., Ilovich, O., Lazarus, A., Klochendler, A., Ziv, O., Werman, R., Hija, A., Cleaver, O., Mishani, E., Keshet, E., et al. (2011). Blood vessels restrain pancreas branching, differentiation and growth. Development *138*. https://doi.org/10.1242/dev.066548.

Manchem, V.P., Goldfine, I.D., Kohanski, R.A., Cristobal, C.P., Lum, R.T., Schow, S.R., Shi, S., Spevak, W.R., Laborde, E., Toavs, D.K., et al. (2001). A Novel Small Molecule That Directly Sensitizes the Insulin Receptor In Vitro and In Vivo. Diabetes *50*. https://doi.org/10.2337/diabetes.50.4.824.

Manning, B.D., and Cantley, L.C. (2007). AKT/PKB Signaling: Navigating Downstream. Cell *129*, 1261–1274. https://doi.org/10.1016/j.cell.2007.06.009.

Marron-Terada, P.G., Hancock, M.K., Haskins, D.J., and Dahms, N.M. (2000). Recognition of Dictyostelium discoideum lysosomal enzymes is conferred by the amino-terminal carbohydrate binding site of the insulin-like growth factor II/mannose 6-phosphate receptor. Biochemistry *39*, 2243–2253. https://doi.org/10.1021/bi992226o.

Marshak, S., Totary, H., Cerasi, E., and Melloul, D. (1996). Purification of the -cell glucose-sensitive factor that transactivates the insulin gene differentially in normal and transformed islet cells. Proc. Natl. Acad. Sci. *93*. https://doi.org/10.1073/pnas.93.26.15057.

Martinez, S.C., Cras-Méneur, C., Bernal-Mizrachi, E., and Permutt, M.A. (2006). Glucose regulates Foxo1 through insulin receptor signaling in the pancreatic islet β-cell. Diabetes *55*, 1581–1591. https://doi.org/10.2337/db05-0678.

Mastracci, T.L., and Sussel, L. (2012). The endocrine pancreas: insights into development, differentiation, and diabetes. Wiley Interdiscip. Rev. Dev. Biol. *1*. https://doi.org/10.1002/wdev.44.

Matschinsky, F.M. (1996). A Lesson in Metabolic Regulation Inspired by the Glucokinase Glucose Sensor Paradigm. Diabetes *45*, 223–241. https://doi.org/10.2337/diab.45.2.223.

Matsuoka, T., Zhao, L., Artner, I., Jarrett, H.W., Friedman, D., Means, A., and Stein, R. (2003). Members of the Large Maf Transcription Family Regulate Insulin Gene Transcription in Islet β Cells. Mol. Cell. Biol. *23*. https://doi.org/10.1128/MCB.23.17.6049-6062.2003.

McEvoy, R.C., and Madson, K.L. (1980). Pancreatic Insulin-, Glucagon-, and Somatostatin-Positive Islet Cell Populations during the Perinatal Development of the Rat. Neonatology *38*, 248–254. https://doi.org/10.1159/000241372.

McKinnon, T., Chakraborty, C., Gleeson, L.M., Chidiac, P., and Lala, P.K. (2001). Stimulation of human extravillous trophoblast migration by IGF-II is mediated by IGF type 2 receptor involving inhibitory G protein(s) and phosphorylation of MAPK. J. Clin. Endocrinol. Metab. *86*, 3665–3674. https://doi.org/10.1210/jcem.86.8.7711.

De Meyts, P., and Whittaker, J. (2002). Structural biology of insulin and IGF1 receptors: Implications for drug design. Nat. Rev. Drug Discov. *1*, 769–783. https://doi.org/10.1038/nrd917.

Mezza, T., Shirakawa, J., Martinez, R., Hu, J., Giaccari, A., and Kulkarni, R.N. (2016). Nuclear export of FoxO1 is associated with ERK signaling in β-cells lacking insulin receptors. J. Biol. Chem. *291*, 21485–21495. https://doi.org/10.1074/jbc.M116.735738.

Modi, H., Jacovetti, C., Tarussio, D., Metref, S., Madsen, O.D., Zhang, F.-P., Rantakari, P., Poutanen, M., Nef, S., Gorman, T., et al. (2015). Autocrine Action of IGF2 Regulates Adult β-Cell Mass and Function. Diabetes *64*, 4148–4157. https://doi.org/10.2337/db14-1735.

Montagne, J., Stewart, M.J., Stocker, H., Hafen, E., Kozma, S.C., and Thomas, G. (1999).

Drosophila S6 kinase: A regulator of cell size. Science (80-.). *285*, 2126–2129. https://doi.org/10.1126/science.285.5436.2126.

Mulder, H., and Ling, C. (2009). Mitochondrial dysfunction in pancreatic β-cells in Type 2 Diabetes. Mol. Cell. Endocrinol. *297*, 34–40. https://doi.org/10.1016/j.mce.2008.05.015.

Muller, D., Jones, P.M., and Persaud, S.J. (2006). Autocrine anti-apoptotic and proliferative effects of insulin in pancreatic β-cells. FEBS Lett. *580*, 6977–6980. https://doi.org/10.1016/j.febslet.2006.11.066.

Murtaugh, L.C. (2007). Pancreas and beta-cell development: From the actual to the possible. Development *134*, 427–438. https://doi.org/10.1242/dev.02770.

Nakae, J., Kitamura, T., Kitamura, Y., Biggs, W.H., Arden, K.C., and Accili, D. (2003). The forkhead transcription factor Fox01 regulates adipocyte differentiation. Dev. Cell *4*, 119–129. https://doi.org/10.1016/S1534-5807(02)00401-X.

Ohsugi, M., Cras-Méneur, C., Zhou, Y., Bernal-Mizrachi, E., Johnson, J.D., Luciani, D.S., Polonsky, K.S., and Permutt, M.A. (2005). Reduced Expression of the Insulin Receptor in Mouse Insulinoma (MIN6) Cells Reveals Multiple Roles of Insulin Signaling in Gene Expression, Proliferation, Insulin Content, and Secretion. J. Biol. Chem. *280*, 4992–5003. https://doi.org/10.1074/jbc.M411727200.

Okada, T., Liew, C.W., Hu, J., Hinault, C., Michael, M.D., Kŕtzfeldt, J., Yin, C., Holzenberger, M., Stoffel, M., and Kulkarni, R.N. (2007). Insulin receptors in β-cells are critical for islet compensatory growth response to insulin resistance. Proc. Natl. Acad. Sci. *104*, 8977–8982. https://doi.org/10.1073/pnas.0608703104.

Okamoto, H., Nakae, J., Kitamura, T., Park, B.-C., Dragatsis, I., and Accili, D. (2004). Transgenic rescue of insulin receptor–deficient mice. J. Clin. Invest. *114*, 214–223. https://doi.org/10.1172/JCI21645.

Olbrot, M., Rud, J., Moss, L.G., and Sharma, A. (2002). Identification of β-cell-specific insulin gene transcription factor RIPE3b1 as mammalian MafA. Proc. Natl. Acad. Sci. *99*. https://doi.org/10.1073/pnas.102168499.

Olofsson, C.S., Göpel, S.O., Barg, S., Galvanovskis, J., Ma, X., Salehi, A., Rorsman, P., and Eliasson, L. (2002). Fast insulin secretion reflects exocytosis of docked granules in mouse pancreatic B-cells. Pflügers Arch. *444*. https://doi.org/10.1007/s00424-002-0781-5.

Orchard, S., Ammari, M., Aranda, B., Breuza, L., Briganti, L., Broackes-Carter, F., Campbell, N.H., Chavali, G., Chen, C., del-Toro, N., et al. (2014). The MIntAct project—IntAct as a common curation platform for 11 molecular interaction databases. Nucleic Acids Res. *42*, D358–D363. https://doi.org/10.1093/nar/gkt1115.

Oropeza, D., Jouvet, N., Budry, L., Campbell, J.E., Bouyakdan, K., Lacombe, J., Perron, G., Bergeron, V., Neuman, J.C., Brar, H.K., et al. (2015). Phenotypic characterization of MIP-CreERT1Lphi mice with transgene-driven islet expression of human growth hormone. Diabetes *64*, 3798–3807. https://doi.org/10.2337/db15-0272.

Otani, K., Kulkarni, R.N., Baldwin, A.C., Krutzfeldt, J., Ueki, K., Stoffel, M., Kahn, C.R., and Polonsky, K.S. (2004a). Reduced β-cell mass and altered glucose sensing impair insulin-secretory function in βIRKO mice. Am. J. Physiol. - Endocrinol. Metab. *286*. https://doi.org/10.1152/ajpendo.00533.2001.

Otonkoski, T., Knip, M., Wong, I., and Simell, O. (1988). Effects of Growth Hormone and Insulin-Like Growth Factor I on Endocrine Function of Human Fetal Islet-Like Cell Clusters During Long-Term Tissue Culture. Diabetes *37*, 1678–1683. https://doi.org/10.2337/diab.37.12.1678.

Pan, F.C., and Wright, C. (2011). Pancreas organogenesis: From bud to plexus to gland. Dev. Dyn. *240*, 530–565. https://doi.org/10.1002/dvdy.22584.

Pan, F.C., Bankaitis, E.D., Boyer, D., Xu, X., Van de Casteele, M., Magnuson, M.A., Heimberg, H., and Wright, C.V.E. (2013). Spatiotemporal patterns of multipotentiality in *Ptf1a* -expressing cells during pancreas organogenesis and injury-induced facultative restoration. Development *140*. https://doi.org/10.1242/dev.090159.

Pandini, G., Frasca, F., Mineo, R., Sciacca, L., Vigneri, R., and Belfiore, A. (2002). Insulin/insulin-like growth factor I hybrid receptors have different biological characteristics depending on the insulin receptor isoform involved. J. Biol. Chem. *277*, 39684–39695. https://doi.org/10.1074/jbc.M202766200.

Pende, M., Kozma, S.C., Jaquet, M., Oorschot, V., Burcelin, R., Le Marchand-Brustel, Y., Klumperman, J., Thorens, B., and Thomas, G. (2000). Hypoinsulinaemia, glucose intolerance and diminished β-cell size in S6K1-deficient mice. Nature *408*, 994–997. https://doi.org/10.1038/35050135.

Peng, X. ding, Xu, P.Z., Chen, M.L., Hahn-Windgassen, A., Skeen, J., Jacobs, J., Sundararajan, D., Chen, W.S., Crawford, S.E., Coleman, K.G., et al. (2003). Dwarfism, impaired skin development, skeletal muscle atrophy, delayed bone development, and impeded adipogenesis in mice lacking Akt1 and Akt2. Genes Dev. *17*, 1352–1365. https://doi.org/10.1101/gad.1089403.

Peterson, J.D., Nehrlich, S., Oyer, P.E., and Steiner, D.F. (1972). Determination of the Amino Acid Sequence of the Monkey, Sheep, and Dog Proinsulin C-Peptides by a Semi-micro Edman Degradation Procedure. J. Biol. Chem. *247*. https://doi.org/10.1016/S0021-9258(19)44991-0.

Petitt, D.J., Bennett, P.H., Knowler, W.C., Baird, H.R., and Aleck, K.A. (1985). Gestational diabetes mellitus and impaired glucose tolerance during pregnancy. Long-term effects on obesity and glucose tolerance in the offspring. Diabetes https://doi.org/10.2337/diab.34.2.S119.

Pettersson, U.S., Waldén, T.B., Carlsson, P.O., Jansson, L., and Phillipson, M. (2012). Female Mice are Protected against High-Fat Diet Induced Metabolic Syndrome and Increase the Regulatory T Cell Population in Adipose Tissue. PLoS One *7*. https://doi.org/10.1371/journal.pone.0046057.

Petyuk, V.A., Qian, W.J., Hinault, C., Gritsenko, M.A., Singhal, M., Monroe, M.E., Camp, D.G., Kulkarni, R.N., and Smith, R.D. (2008). Characterization of the mouse pancreatic islet proteome and comparative analysis with other mouse tissues. J. Proteome Res. *7*, 3114–3126. https://doi.org/10.1021/pr800205b.

Pilkis, S.J., and Granner, D.K. (1992). Molecular Physiology of the Regulation of Hepatic Gluconeogenesis and Glycolysis. Annu. Rev. Physiol. *54*, 885–909. https://doi.org/10.1146/annurev.ph.54.030192.004321.

Poitout, D.V., and Robertson, M.D.R.P. (1996). AN INTEGRATED VIEW OF β-CELL DYSFUNCTION IN TYPE-II DIABETES. Annu. Rev. Med. *47*, 69–83. https://doi.org/10.1146/annurev.med.47.1.69.

Poitout, V., Hagman, D., Stein, R., Artner, I., Robertson, R.P., and Harmon, J.S. (2006). Regulation of the insulin gene by glucose and fatty acids. J. Nutr. *136*, 873–876. https://doi.org/10.1093/jn/136.4.873.

Polonsky, W.H., Anderson, B.J., Lohrer, P.A., Welch, G., Jacobson, A.M., Aponte, J.E., and Schwartz, C.E. (1995). Assessment of Diabetes-Related Distress. Diabetes Care *18*, 754–760. https://doi.org/10.2337/diacare.18.6.754.

Puigserver, P., Rhee, J., Donovan, J., Walkey, C.J., Yoon, J.C., Oriente, F., Kitamura, Y.,

Altomonte, J., Dong, H., Accili, D., et al. (2003). Insulin-regulated hepatic gluconeogenesis through FOXO1-PGC-1α interaction. Nature *423*, 550–555. https://doi.org/10.1038/nature01667.

Rabinovitch, A., Quigley, C., Russell, T., Patel, Y., and Mintz, D.H. (1982). Insulin and Multiplication Stimulating Activity (an Insulin-like Growth Factor) Stimulate Islet β-Cell Replication in Neonatal Rat Pancreatic Monolayer Cultures. Diabetes *31*, 160–164. https://doi.org/10.2337/diab.31.2.160.

Ramos, J.W. (2008). The regulation of extracellular signal-regulated kinase (ERK) in mammalian cells. Int. J. Biochem. Cell Biol. *40*, 2707–2719. https://doi.org/10.1016/j.biocel.2008.04.009.

Ramsey, M.R., Krishnamurthy, J., Pei, X.-H., Torrice, C., Lin, W., Carrasco, D.R., Ligon, K.L., Xiong, Y., and Sharpless, N.E. (2007). Expression of p16 ^{Ink4a} Compensates for *p18* ^{Ink4c} Loss in Cyclin-Dependent Kinase 4/6–Dependent Tumors and Tissues. Cancer Res. *67*. https://doi.org/10.1158/0008-5472.CAN-06-3437.

Rane, S.G., Dubus, P., Mettus, R. V., Galbreath, E.J., Boden, G., Reddy, E.P., and Barbacid, M. (1999). Loss of Cdk4 expression causes insulin-deficient diabetes and Cdk4 activation results in β-islet cell hyperplasia. Nat. Genet. *22*, 44–52. https://doi.org/10.1038/8751.

Reaven, G.M. (1988). Role of insulin resistance in human disease. Diabetes *37*, 1595–1607. https://doi.org/10.2337/diab.37.12.1595.

Reis, A.F., Ye, W.Z., Dubois-Laforgue, D., Bellanne-Chantelot, C., Timsit, J., and Velho, G. (2000). Mutations in the insulin promoter factor-1 gene in late-onset type 2 diabetes mellitus. Eur. J. Endocrinol. *143*, 511–513. https://doi.org/10.1530/eje.0.1430511.

Rena, G., Shaodong, G., Cichy, S.C., Unterman, T.G., and Cohen, P. (1999). Phosphorylation of the transcription factor forkhead family member FKHR by protein kinase B. J. Biol. Chem. *274*, 17179–17183. https://doi.org/10.1074/jbc.274.24.17179.

Rhodes, C.J., White, M.F., Leahy, J.L., and Kahn, S.E. (2013a). Direct autocrine action of insulin on β-cells: Does it make physiological sense? Diabetes *62*, 2157–2163. https://doi.org/10.2337/db13-0246.

Rinderknecht, E., and Humbel, R.E. (1978). The amino acid sequence of human insulin-like growth factor I and its structural homology with proinsulin. J. Biol. Chem. *253*, 2769–2776. https://doi.org/10.1016/s0021-9258(17)40889-1.

Le Roith, D. (2003). The insulin-like growth factor system. Exp. Diabesity Res. *4*, 205–212. https://doi.org/10.1155/edr.2003.205.

Rose, S.D., Swift, G.H., Peyton, M.J., Hammer, R.E., and MacDonald, R.J. (2001). The Role of PTF1-P48 in Pancreatic Acinar Gene Expression. J. Biol. Chem. *276*. https://doi.org/10.1074/jbc.M106264200.

Roskoski, R. (2012). ERK1/2 MAP kinases: Structure, function, and regulation. Pharmacol. Res. *66*, 105–143. https://doi.org/10.1016/j.phrs.2012.04.005.

Rothenberg, P.L., Willison, L.D., and Wolf, B.A. (1995). Glucose-Induced Insulin Receptor Tyrosine Phosphorylation in Insulin-Secreting β-Cells. Diabetes *44*, 802–809. https://doi.org/10.2337/diab.44.7.802.

Rotwein, P. (1986). Two insulin-like growth factor I messenger RNAs are expressed in human liver. Proc. Natl. Acad. Sci. U. S. A. *83*, 77–81. https://doi.org/10.1073/pnas.83.1.77.

Rozzo, A., Meneghel-Rozzo, T., Delakorda, S.L., Yang, S.-B., and Rupnik, M. (2009). Exocytosis of Insulin. Ann. N. Y. Acad. Sci. *1152*. https://doi.org/10.1111/j.1749-6632.2008.04003.x.

Schaffer, A.E., Freude, K.K., Nelson, S.B., and Sander, M. (2010). Nkx6 Transcription Factors and Ptf1a Function as Antagonistic Lineage Determinants in Multipotent Pancreatic Progenitors. Dev. Cell *18*. https://doi.org/10.1016/j.devcel.2010.05.015.

Schlumbrecht, M.P., Xie, S.-S., Shipley, G.L., Urbauer, D.L., and Broaddus, R.R. (2011a). Molecular clustering based on ERα and EIG121 predicts survival in high-grade serous carcinoma of the ovary/peritoneum. Mod. Pathol. *24*, 453–462. https://doi.org/10.1038/modpathol.2010.211.

VAN SCHRAVENDIJK, C.F.H., FORIERS, A., VAN DEN BRANDE, J.L., and PIPELEERS, D.G. (1987). Evidence for the Presence of Type I Insulin-Like Growth Factor Receptors on Rat Pancreatic A and B Cells*. Endocrinology *121*, 1784–1788. https://doi.org/10.1210/endo-121-5-1784.

Seino, S., and Bell, G.I. (1989). Alternative splicing of human insulin receptor messenger RNA. Biochem. Biophys. Res. Commun. *159*, 312–316. https://doi.org/10.1016/0006-291X(89)92439-X.

Seino, S., Seino, M., Nishi, S., and Bell, G.I. (1989). Structure of the human insulin receptor gene and characterization of its promoter. Proc. Natl. Acad. Sci. U. S. A. *86*, 114–118. https://doi.org/10.1073/pnas.86.1.114.

Shima, H. (1998). Disruption of the p70s6k/p85s6k gene reveals a small mouse phenotype and a new functional S6 kinase. EMBO J. *17*, 6649–6659. https://doi.org/10.1093/emboj/17.22.6649.

Shioi, T., Kang, P.M., Douglas, P.S., Hampe, J., Yballe, C.M., Lawitts, J., Cantley, L.C., and Izumo, S. (2000). The conserved phosphoinositide 3-kinase pathway determines heart size in mice. EMBO J. *19*, 2537–2548. https://doi.org/10.1093/emboj/19.11.2537.

da SILVA XAVIER, G., QIAN, Q., CULLEN, P.J., and RUTTER, G.A. (2004). Distinct roles for insulin and insulin-like growth factor-1 receptors in pancreatic beta-cell glucose sensing revealed by RNA silencing. Biochem. J. *377*, 149–158. https://doi.org/10.1042/bj20031260.

Stamateris, R.E., Sharma, R.B., Kong, Y., Ebrahimpour, P., Panday, D., Ranganath, P., Zou, B., Levitt, H., Parambil, N.A., O'Donnell, C.P., et al. (2016). Glucose Induces mouse β-cell proliferation via IRS2, MTOR, and cyclin D2 but Not the insulin receptor. Diabetes *65*, 981–995. https://doi.org/10.2337/db15-0529.

Steele-Perkins, G., Turner, J., Edman, J.C., Hari, J., Pierce, S.B., Stover, C., Rutter, W.J., and Roth, R.A. (1988). Expression and characterization of a functional human insulin-like growth factor I receptor. J. Biol. Chem. *263*, 11486–11492. https://doi.org/10.1016/s0021-9258(18)37983-3.

Stewart, A.F., Hussain, M.A., García-Ocaña, A., Vasavada, R.C., Bhushan, A., Bernal-Mizrachi, E., and Kulkarni, R.N. (2015). Human β-Cell Proliferation and Intracellular Signaling: Part 3. Diabetes *64*, 1872–1885. https://doi.org/10.2337/db14-1843.

Sturgill, T.W. (2008). MAP kinase: It's been longer than fifteen minutes. Biochem. Biophys. Res. Commun. *371*, 1–4. https://doi.org/10.1016/j.bbrc.2008.04.002.

Suckale, J., and Solimena, M. (2008). Pancreas islets in metabolic signaling - focus on the β-cell. Nat. Preced. https://doi.org/10.1038/npre.2008.1724.2.

Swenne, I. (1982). The role of glucose on the in vitro regulation of cell cycle kinetics and proliferation of fetal pancreatic B-cells. Diabetes *31*, 754–760. https://doi.org/10.2337/diab.31.9.754.

Swenne, I. (1992a). Pancreatic Beta-cell growth and diabetes mellitus. Diabetologia *35*, 193–201. https://doi.org/10.1007/BF00400917.

Tamarina, N.A., Roe, M.W., and Philipson, L.H. (2014a). Characterization of mice expressing Ins1 gene promoter driven CreERT recombinase for conditional gene deletion in pancreatic β-cells. Islets *6*. https://doi.org/10.4161/isl.27685.

Taylor, S.I., Grunberger, G., Marcus-Samuels, B., Underhill, L.H., Dons, R.F., Ryan, J., Roddam, R.F., Rupe, C.E., and Gorden, P. (1982). Hypoglycemia Associated with Antibodies to the Insulin Receptor. N. Engl. J. Med. *307*, 1422–1426. https://doi.org/10.1056/NEJM198212023072303.

Testa, G., Schaft, J., van der Hoeven, F., Glaser, S., Anastassiadis, K., Zhang, Y., Hermann, T., Stremmel, W., and Stewart, A.F. (2004). A reliable lacZ expression reporter cassette for multipurpose, knockout-first alleles. Genesis *38*, 151–158. https://doi.org/10.1002/gene.20012.

Teta, M., Long, S.Y., Wartschow, L.M., Rankin, M.M., and Kushner, J.A. (2005). Very Slow Turnover of β-Cells in Aged Adult Mice. Diabetes *54*. https://doi.org/10.2337/diabetes.54.9.2557.

Teta, M., Rankin, M.M., Long, S.Y., Stein, G.M., and Kushner, J.A. (2007). Growth and Regeneration of Adult β Cells Does Not Involve Specialized Progenitors. Dev. Cell *12*, 817–826. https://doi.org/10.1016/j.devcel.2007.04.011.

Thorens, B., Weir, G.C., Leahy, J.L., Lodish, H.F., and Bonner-Weir, S. (1990). Reduced expression of the liver/beta-cell glucose transporter isoform in glucose-insensitive pancreatic beta cells of diabetic rats. Proc. Natl. Acad. Sci. *87*, 6492–6496. https://doi.org/10.1073/pnas.87.17.6492.

Tschen, S.-I., Dhawan, S., Gurlo, T., and Bhushan, A. (2009). Age-Dependent Decline in β-Cell Proliferation Restricts the Capacity of β-Cell Regeneration in Mice. Diabetes *58*. https://doi.org/10.2337/db08-1651.

Tuttle, R.L., Gill, N.S., Pugh, W., Lee, J.P., Koeberlein, B., Furth, E.E., Polonsky, K.S., Naji, A., and Birnbaum, M.J. (2001). Regulation of pancreatic β-cell growth and survival by the serine/threonine protein kinase Akt1/PKBα. Nat. Med. *7*, 1133–1137. https://doi.org/10.1038/nm1001-1133.

Uchida, T., Nakamura, T., Hashimoto, N., Matsuda, T., Kotani, K., Sakaue, H., Kido, Y., Hayashi, Y., Nakayama, K.I., White, M.F., et al. (2005). Deletion of Cdkn1b ameliorates hyperglycemia by maintaining compensatory hyperinsulinemia in diabetic mice. Nat. Med. *11*. https://doi.org/10.1038/nm1187.

Uchizono, Y., Alarcón, C., Wicksteed, B.L., Marsh, B.J., and Rhodes, C.J. (2007a). The balance between proinsulin biosynthesis and insulin secretion: Where can imbalance lead? In Diabetes, Obesity and Metabolism, pp. 56–66.

Ueki, K., Okada, T., Hu, J., Chong, W.L., Assmann, A., Dahlgren, G.M., Peters, J.L., Shackman, J.G., Zhang, M., Artner, I., et al. (2006a). Total insulin and IGF-I resistance in pancreatic β cells causes overt diabetes. Nat. Genet. *38*, 583–588. https://doi.org/10.1038/ng1787.

Vasudevan, K.M., and Garraway, L.A. (2010). AKT Signaling in Physiology and Disease. pp. 105–133.

Vatamaniuk, M.Z., Gupta, R.K., Lantz, K.A., Doliba, N.M., Matschinsky, F.M., and Kaestner, K.H. (2006). *Foxa1* -Deficient Mice Exhibit Impaired Insulin Secretion due to Uncoupled Oxidative Phosphorylation. Diabetes *55*. https://doi.org/10.2337/db05-0470.

Verspohl, E.J., and Ammon, H.P.T. (1980). Evidence for presence of insulin receptors in rat islets of Langerhans. J. Clin. Invest. *65*, 1230–1237. https://doi.org/10.1172/JCI109778.

Wang, H., Brun, T., Kataoka, K., Sharma, A.J., and Wollheim, C.B. (2007). MAFA controls genes implicated in insulin biosynthesis and secretion. Diabetologia *50*. https://doi.org/10.1007/s00125-

006-0490-2.

Wang, L., Liu, Y., Yan Lu, S., Nguyen, K.-T.T., Schroer, S.A., Suzuki, A., Mak, T.W., Gaisano, H., and Woo, M. (2010). Deletion of *Pten* in Pancreatic β-Cells Protects Against Deficient β-Cell Mass and Function in Mouse Models of Type 2 Diabetes. Diabetes *59*. https://doi.org/10.2337/db09-1805.

Wang, Z.-Q., Fung, M.R., Barlow, D.P., and Wagner, E.F. (1994). Regulation of embryonic growth and lysosomal targeting by the imprintedIgf2/Mpr gene. Nature *372*, 464–467. https://doi.org/10.1038/372464a0.

Weng, J., Macfarlane, W.M., Lehto, M., Gu, H.F., Shepherd, L.M., Ivarsson, S.A., Wibell, L., Smith, T., and Groop, L.C. (2001). Functional consequences of mutations in the MODY4 gene (IPF1) and coexistence with MODY3 mutations. Diabetologia *44*, 249–258. https://doi.org/10.1007/s001250051608.

Whim, M.D. (2011). Pancreatic Beta Cells Synthesize Neuropeptide Y and Can Rapidly Release Peptide Co-Transmitters. PLoS One *6*. https://doi.org/10.1371/journal.pone.0019478.

Wicksteed, B., Alarcon, C., Briaud, I., Lingohr, M.K., and Rhodes, C.J. (2003). Glucose-induced Translational Control of Proinsulin Biosynthesis Is Proportional to Preproinsulin mRNA Levels in Islet β-Cells but Not Regulated via a Positive Feedback of Secreted Insulin. J. Biol. Chem. *278*, 42080–42090. https://doi.org/10.1074/jbc.M303509200.

Wicksteed, B., Uchizono, Y., Alarcon, C., McCuaig, J.F., Shalev, A., and Rhodes, C.J. (2007). A cis-Element in the 5′ Untranslated Region of the Preproinsulin mRNA (ppIGE) Is Required for Glucose Regulation of Proinsulin Translation. Cell Metab. *5*. https://doi.org/10.1016/j.cmet.2007.02.007.

Wicksteed, B., Brissova, M., Yan, W., Opland, D.M., Plank, J.L., Reinert, R.B., Dickson, L.M., Tamarina, N.A., Philipson, L.H., Shostak, A., et al. (2010). Conditional Gene Targeting in Mouse Pancreatic β-Cells. Diabetes *59*, 3090–3098. https://doi.org/10.2337/db10-0624.

Withers, D.J., Gutierrez, J.S., Towery, H., Burks, D.J., Ren, J.-M., Previs, S., Zhang, Y., Bernal, D., Pons, S., Shulman, G.I., et al. (1998a). Disruption of IRS-2 causes type 2 diabetes in mice. Nature *391*, 900–904. https://doi.org/10.1038/36116.

Withers, D.J., Burks, D.J., Towery, H.H., Altamuro, S.L., Flint, C.L., and White, M.F. (1999). Irs-2 coordinates Igf-1 receptor-mediated β-cell development and peripheral insulin signalling. Nat. Genet. *23*, 32–40. https://doi.org/10.1038/12631.

Xu, G.G., and Rothenberg, P.L. (1998). Insulin Receptor Signaling in the β-Cell Influences Insulin Gene Expression and Insulin Content: Evidence for Autocrine β-Cell Regulation. Diabetes *47*, 1243–1252. https://doi.org/10.2337/diab.47.8.1243.

Xuan, S., Kitamura, T., Nakae, J., Politi, K., Kido, Y., Fisher, P.E., Morroni, M., Cinti, S., White, M.F., Herrera, P.L., et al. (2002). Defective insulin secretion in pancreatic β cells lacking type 1 IGF receptor. J. Clin. Invest. *110*, 1011–1019. https://doi.org/10.1172/JCI15276.

Yoshinari, M., and Daikoku, S. (1982). Ontogenetic appearance of immunoreactive endocrine cells in rat pancreatic islets. Anat. Embryol. (Berl). *165*, 63–70. https://doi.org/10.1007/BF00304583.

Zhang, C., Moriguchi, T., Kajihara, M., Esaki, R., Harada, A., Shimohata, H., Oishi, H., Hamada, M., Morito, N., Hasegawa, K., et al. (2005). MafA Is a Key Regulator of Glucose-Stimulated Insulin Secretion. Mol. Cell. Biol. *25*. https://doi.org/10.1128/MCB.25.12.4969-4976.2005.

Zhao, A.Z., Zhao, H., Teague, J., Fujimoto, W., and Beavo, J.A. (1997). Attenuation of insulin

secretion by insulin-like growth factor 1 is mediated through activation of phosphodiesterase 3B. Proc. Natl. Acad. Sci. *94*, 3223–3228. https://doi.org/10.1073/pnas.94.7.3223.

Zhou, Q., Law, A.C., Rajagopal, J., Anderson, W.J., Gray, P.A., and Melton, D.A. (2007). A Multipotent Progenitor Domain Guides Pancreatic Organogenesis. Dev. Cell *13*. https://doi.org/10.1016/j.devcel.2007.06.001.

Zick, Y. (2005). Ser/Thr phosphorylation of IRS proteins: a molecular basis for insulin resistance. Sci. STKE *2005*. https://doi.org/10.1126/stke.2682005pe4.

9 Acknowledgments

In den nächsten Zeilen möchte ich all jenen danken, die es mir ermöglicht haben, meine Promotion erfolgreich abzuschließen. Die vorliegende Arbeit wurde unter der Leitung von Prof. Dr. Heiko Lickert am Institut für Diabetes und Regenerationsforschung des Helmholtz Zentrums München durchgeführt. Herr Prof. Dr. Heiko Lickert hat die dortige Betreuung übernommen, während Herr Prof. Dr. Micheal W. Pfaffl die Betreuung des Fachbereiches Biologie übernommen hat.

Zuallererst möchte ich mich bei Prof. Dr. Heiko Lickert für die Möglichkeit, meine Arbeit in seiner Arbeitsgruppe anfertigen zu können und die Übernahme des Zweitreferats bedanken. Danke für das Korrekturlesen dieser Arbeit.

Mein Dank gilt auch meinem Doktorvater Herr Prof. Dr. Micheal W. Pfaffl der es mir ermöglichte meine Doktorarbeit am GZW anzufertigen und für die Übernahme des Hauptreferats.

Herrn Prof. Dr. Ralph Kühn danke ich herzlich für die Übernahme des Vorsitzes der Prüfungskommission.

Ganz besonderen Dank gilt Dr. Aurelia Raducanu für die Einführung in sämtliche Techniken, Etablierung von Methoden und Fragestellungen für Rezeptor Projekt.

Mein herzlicher Dank gehört Dr. Ansarullah und Dr. Felizitas Gräfin von Hahn für die ausgezeichnete Betreuung, die ständige Hilfe und Diskussionsbereitschaft und die Unterstützung bei dem nicht einfachen Rezeptor Projekt. Feli danke ich für die liebevolle Aufnahme in die AG Lickert und der daraus resultierenden Freundschaft.

Danke möchte ich außerdem Dr. Aimée Bastidas-Ponce und Dr. Mostafa Bakhti. Danke, dass ihr alle meine Texte durchgelesen habt und mich mit neuen Ideen und Verbesserungsvorschläge unterstutzt habt.

Ein ganz herzliches Dankeschön gilt den Kollegen aus Rezeptor-Gruppe, Dr. Katharina Wißmiller, Dr. Amir Morshedi, Dr.Silvia Schirge, Dr. Chirag Jain, Robert Fimmen und Jürgen Schultheiß, die immer ein offenes Ohr für meine Fragen hatten und mir bei Problemen geholfen haben.

Des Weiteren danke ich Dr. Anika Böttcher, Dr. Ingo Burtscher und der gesamten AG Lickert für die Hilfe im Labor. Es hat mich sehr gefreut, in so einem netten Team gearbeitet zu haben.

Allergrößter Dank gilt meinen Eltern, die mir mein Studium ermöglicht, mich immer unterstützt und mir das kostspielige Leben in Deutschland mitfinanziert haben. Danke für alles.

Meinen Ehemann, Sam danke ich auch herzlich für seine volle Unterstützung. Ohne deine Hilfe wäre das Phd-Studium für mich nicht möglich gewesen. Du hast mir in allen Situationen geholfen und bist immer hinter mir gestanden, damit mein Traum in Erfüllung geht. Ich liebe dich.

10 List of Publications

Ansarullah, Chirag Jain, **Fataneh Fathi Far**, Sarah Homberg, Katharina Wißmiller, Felizitas Gräfin von Hahn, Aurelia Raducanu, Silvia Schirge, Michael Sterr, Sara Bilekova, Johanna Siehler, Julius Wiener, Lena Oppenländer, Amir Morshedi, Aimée Bastidas-Ponce, Gustav Collden, Martin Irmler, Johannes Beckers, Annette Feuchtinger, Michal Grzybek, Christin Ahlbrecht, Regina Feederle, Oliver Plettenburg, Timo D. Müller, Matthias Meier, Matthias H. Tschöp, Ünal Coskun & Heiko Lickert (2021). Inceptor counteracts insulin signalling in β-cells to control glycaemia. Nature volume 590, pages326–331. doi.org/10.1038/s41586-021-03225-8

Gerald Grandl, Gustav Colldén, Ansarullah Ansarullah, Weiwei Xu, **Fataneh Fathi Far**, Tim Gruber, Aimée Bastidas-Ponce, Qian Zhang, Aaron Novikoff, Cristina Garcia-Caceres, Matthias Tschöp, Heiko Lickert, Timo Müller. (2022). Global, neuronal, and beta-cell specific deletion of insulin inhibitory receptor (incep-tor) improves glucose homeostasis in diet-induced obese mice. Preprint. doi.org/10.21203/rs.3.rs-1497073/v1

11 Contributions

My own contributions to the experiments and figures are as follows:

Figure 4.1: mRNA expression profile of *Iir* in various mouse tissues.

- Dissection of the tissues of P0 WT mice.

Figure 4.2: Inceptor antibody specificity in immunocytochemistry in WT pancreas

- Dissecting of the pancreas of E19.5 WT mice. Performing the immunostaining and execution of the imaging using confocal microscope.

Figure 4.3: Inceptor is widely expressed in mouse tissues.

- Dissection of the pancreas of P0 WT mice. Performing the immunostaining and execution of the imaging using confocal microscope.

Figure 4.4: Inceptor is highly expressed in the brain.

- Performing the immunostaining.

Figure 4.5: Inceptor expression during pancreas development.

- Dissection of the pancreas of E14.5, E16.5 and E18.5 WT mice. Performing the immunostaining and execution of the imaging using a confocal microscope.

Figure 4.6: Inceptor expression in different endocrine cell types.

- Dissection of the pancreas of WT mice. Performing the immunostaining and execution of the imaging using a confocal microscope.

Figure 4.8: Generation and genotyping of full body *Iir*$^{-/-}$ mice.

- Execution of mouse mating and weaning. Breeding the intercrosses. Performing the genotyping of mice using PCR. Design of the primers.

Figure 4.10: Confirmation of KO efficiency in vivo.

- Dissection of the pancreas of E19.5 WT and *Iir* KO mice. Performing the immunostaining and execution of the imaging using a confocal microscope. Performing WB.

Figure 4.11: No morphological differences in *Iir*$^{-/-}$ organs in E19.5 animals.

- Dissection of the tissues of E19.5 WT mice. Performing the H&E staining.

Figure 4.12: Morphology, body weight and mendelian ratio of *Iir*$^{-/-}$ mice.

- Measurement of the body weight of E19.5 E19.5 WT and *Iir* KO mice. Monitoring WT and *Iir* KO mice at embryonic stages E7.5-E19.5 or 1-7 days after birth (P1-7) for mendelian ratio.

Figure 4.13: *Iir*$^{-/-}$ new born mice show hypoglycemia and hyperinsulinemia phenotype.

- Collecting blood E19.5 E19.5 WT and *Iir* KO mice and performing the Mutarotase-GOD method and ELISA. Analyzing the data.
- Dissection of the pancreas of E19.5 WT and *Iir* KO mice. Preparation of the pancreas and performing the ELISA. Analyzing the data.

Figure 4.14: Elevated β-cell area in *Iir*$^{-/-}$ pups.

- Dissection of the pancreas of E19.5 WT and *Iir* KO mice. Sectioning the whole pancreas and performing the immunostaining.
- Collecting blood of E19.5 WT and *Iir* KO mice and performing ELISA. Analyzing the data.

Figure 4.15: Increased in endocrine cell proliferation in *Iir*$^{-/-}$ mice.

- Injection of pregnant WT and *Iir* KO mice. Dissection of the pancreas and performing immunostaining. Execution of the imaging using a confocal microscope and counting the cells using IMARIS.

Figure 4.16: Effect of Inceptor deletion on the proliferation of β-, α-, δ- and PP-cells.

- Injection of pregnant WT and *Iir* KO mice. Dissection of the pancreas and performing immunostaining. Execution of the imaging using a confocal microscope and counting the cells using IMARIS.

Figure 4.17: *Iir*$^{-/-}$ activates IR/IGF-IR signaling during nutritional starvation.

- Dissection of the pancreas of E19.5 WT and *Iir* KO mice. Performing the WB and analyzing the data.

Figure 4.18: *Iir*$^{-/-}$ activates phosphorylation of AKT upon glucose induction.

- Injection of E19.5 WT and *Iir* KO mice. Dissection of the pancreas and performing DAB staining. Execution of the imaging.

Figure 4.19: *Iir*$^{-/-}$ newborn mice could be rescued from death by glucose injection.

- Injection of E19.5 WT and *Iir* KO mice. Collecting blood and measurement of blood glucose. Analyzing the data.

Figure 4.20: Dynamic glucose induced insulin secretion in E19.5 pancreata.

- Dissection of the pancreas of E19.5 WT and *Iir* KO mice.

Figure 4.21: Increased glycogen accumulation in liver of *Iir*$^{-/-}$ mice.

- Dissection of the liver of E19.5 WT and *Iir* KO mice. Processing the liver and performing the colorimetric assay. Analyzing the data.

Figure 4.22: Differential gene expression changes in control vs *Iir*$^{-/-}$ P0 pups.

- Dissection of the pancreas WT and *Iir* KO mice at E18.5 and P0. Isolation of RNA. Determination of RNA concentration and integrity.

Figure 4.26: Deletion efficiency in vivo with tamoxifen in control and CKO mice.

- Set up the Cohort. Injection of the CKO and Control mice with Tamoxifen. Dissection of the pancreas and performing the immunostaining and execution of the imaging using a confocal microscope.

Figure 4.27: Body weight, fasting blood glucose and fasting serum insulin of CKO mice.

- Set up the Cohort. Injection of the CKO and Control mice with Tamoxifen. Monitoring the body weight. Measurement of the blood glucose, collecting blood and performing EISA. Analyzing the data.

Figure 4.28: CKO male mice showed improved glucose tolerance.

- Set up the Cohort. Injection of the CKO and Control mice with Tamoxifen. Organization and performing the ip-GTT and ip-GSIS. Collecting blood and performing ELISA. Analyzing the data.

Figure 4.29: β-cell specific inceptor CKO mice display an increase in β-cell mass.

- Dissection of the pancreas and performing the immunostaining. Analyzing the data.

Figure 4.30: β-cell specific deletion of inceptor increases proliferation in β-cells.

- Dissection of the pancreas and performing the immunostaining.

Figure 4.31: Islet cyto-architecture analysis in CKO mice. Figure 4.32: Expression of maturity markers in CKO mice.

- Dissection of the pancreas and performing the immunostaining. Execution of the imaging using a confocal microscope.

Figure 4.33: β-cell specific deletion of inceptor causes increased IR/IGF-IR signaling.

- Set up the Cohort. Injection of the CKO and Control mice with Tamoxifen. Isolation of islets. Performing the Western blot.

Figure 4.34: Increased protein expression of inceptor in islets of adult WT mice upon HFD.

- Dissection of the pancreas and performing the immunostaining. Execution of the imaging using a confocal microscope. Quantification of images using IMARIS. Analyzing the data.
- Isolation of islets and performing the WB. Analyzing the data.